

UNIVERSITY OF NOVA GORICA
GRADUATE SCHOOL

**NOVEL METHODS FOR THE DETECTION AND REMOVAL OF
CYANOBACTERIA AND CYANOTOXINS**

DISSERTATION

Ambra Delneri

Mentor: prof. dr. Mladen Franko

Nova Gorica, 2014

UNIVERZA V NOVI GORICI
FAKULTETA ZA PODIPLOMSKI ŠTUDIJ

**NOVE METODE ZA DETEKCIJO IN ODSTRANJEVANJE
CIANOBAKTERIJ IN CIANOTOKSINOV**

DISERTACIJA

Ambra Delneri

Mentor: prof. dr. Mladen Franko

Nova Gorica, 2014

Alla mia famiglia

(To my family)

ACKNOWLEDGEMENTS

During my years as a PhD student I had the chance to meet a lot of special people that deserve a big thank. First of all, I want to thank my supervisor prof. dr. Mladen Franko for his patience and for being always there for me when I needed his help. There is a comic that describes how most professors see their PhD students: a brain on a stick (<http://www.phdcomics.com/comics/archive.php?comid=1126>). I'm grateful to prof. Franko, not only for his guidance in the laser lab, but also for not seeing me in such a way.

Moreover I want to thank dr. Chieu Tran that gave me the great opportunity to work in his lab at Marquette University (and that, while I was flying to U.S.A., explained to the U.S. Homeland Security that the toxin I sent him was intended only for research use, not for a terroristic attack). I must thank also dr. Tran's PhD students, Simon and Mowen, two of the most kind and motivated researchers I ever met. They helped me in everything for my whole staying at Marquette University, till the very last minute, I will never forget it. In addition I want to thank prof. dr. Aurelia Tubaro from University of Trieste for hosting me in her lab and for sharing her knowledge about toxins detection. I want to thank dr. Silvio Sosa as well for his kind help in developing the experiments. Furthermore I must thank also prof. dr Mira Terzic from University of Novi Sad for her precious collaboration and for being always so warm towards me. I use this occasion also to thank the committee that revised and improved my thesis.

I am grateful to AD FUTURA, for the financial support I received in my last two years of doctoral studies and in particular to Miss Doris Sattler that has always been really kind and understanding. A special thank goes to Miss Tea Stibilj Nemeč that hosted me in Nova Gorica and that was my lifeline in the sea of Slovenian bureaucracy, I don't know what I would have done without her.

I must thank in particular other two persons that took care of me during my years at UNG, Nadja Lovec Santaniello and Marina Artico. In more than one occasion Nadja helped me before I even knew I needed help and I'm really grateful to her for this and for her constant support. Marina will never stop surprising me for her calm and her ability to eliminate my stress in the very first moment I step in her office.

And of course, I must thank my colleagues, especially Dorota Korte, Mingqiang Liu and my Persian black sheep, Minoo Tasbihi. They are not just colleagues, they are

friends and in these years we shared much more than the office or the lab. You can't imagine to which kind of friendship a post Monday meeting, a late afternoon talk or an evening spent writing on a white-board can lead.

Other people to whom I must say *thank you* are popping out in my mind: Maja Wagner that with her open and friendly smile made me feel welcome on my first day at UNG. Vesna Lavtižar for her energy and enthusiasm. Sabina Zelinšček that was always so nice, starting from my first travel as a PhD student. Olga Malev that I'll always remember introducing herself while sitting in front of the building of Stara Gorica, waiting for our first seminar. Tatjana Radovanović and Franja Prosenec for sharing good and bad moments in the laser lab. Romina Žabar that always made me look at the light at the end of the tunnel (still have to understand if it is a train though). I want to acknowledge also prof. dr. Sabina Passamonti for introducing me to prof. Franko and my friends, Špela Može and Lovro Žiberna, for introducing me to Slovenia (a special thank to Lovro for improvising himself a good Italian speaker when I needed it). Thank also to all my other colleagues that gave me science and life teachings in many different and unexpected ways. Thanks to all my friends for listening about my life as a PhD student (special mention to Raffi and Lalli), especially to those who don't even have a clue of what a lab and a PhD are.

Finally I want to thank my family; I don't have words to express how much I love them and how grateful am I for their unconditioned support.

I apologize if I forgot to thank someone but, if this is the case, I'm quite sure he or she won't be surprised, knowing that I'm finishing to write these acknowledgements almost on my way to the copy shop.

POVZETEK

Cvetenje cianobakterij predstavlja nevarnost za okolje in zdravje ljudi zaradi sproščanja velikih količin toksičnih sekundarnih metabolitov - cianotoksinov, ki nastajajo v procesu staranja in odmiranja cianobakterij. Te spojine so dermatotoksične, hepatotoksične, delujejo kot promotorji tumorjev, v zadnjem času pa jih povezujejo tudi z neurodegenerativnimi obolenji kot sta Alzheimerjeva bolezen ali amiotrofična lateralna skleroza. Eden najresnejših primerov toksičnega delovanja tovrstnih spojin je poznan iz Brazilije leta 1996, ko je zaradi onesnaženja vode v vodovodnem omrežju hemodializnega centra prišlo do smrti šestindvajsetih pacientov zaradi odpovedi jeter. Zaradi nevarnosti za zdravje povezane s cianotoksini je svetovna zdravstvena organizacija WHO priporočila vrednost 1 µg/L kot mejno koncentracijo mikrocistina-LR (MC-LR) - najbolj nevarnega doslej poznega cianotoksina – v pitnih in rekreacijskih vodah. Možno pa je, da bo ta vrednost v prihodnosti še znižana, če bodo ugotovljeni novi toksični učinki tega toksina. V tej luči WHO in druge javne agencije v različnih državah močno priporočajo nadaljnje raziskave cianobakterij in cianotoksinov ter razvoj sistemov za njihovo zgodnje odkrivanje in odstranjevanje.

Ta disertacija se osredotoča na razvoj novih metod za detekcijo cianopigmentov in mikrocistina LR ter njegovo odstranjevanje iz sladkih vod. V prvem delu smo uporabili visoko občutljivo spektrometrijo na toplotne leče (TLS) za detekcijo dveh cianopigmentov: zamreženega alofikocianina (CL-APC) in Cr-fikoeritrina (Cr-PE). Oba pigmenta smo uspešno detektirali s tehniko TLS v sistemu, ki je bil v nadaljevanju optimiziran za detekcijo Cr-PE. Za Cr-PE smo s kombinacijo TLS in pretočne injekcijske analize (FIA) dosegli spodnjo mejo detekcije 13 µg/L. Pri tem smo lahko uporabljali manjše količine vzorcev, zaradi pretočnega sistema pa je bila tudi zmanjšana fotorazgradnja tega fotolabilnega pigmenta. Dosežena spodnja meja detekcije je le štirikrat višja od koncentracije fikoeritrina 3.16 µg/L, ki jo po konzervativni oceni sprosti enaka količina cianobakterij, kot lahko povzroči nastanek 1 µg/L mikrocistina-LR. Glede na to, da realno pričakujemo dodatno znižanje spodnje meje detekcije za fikoeritrin z optimizacijo eksperimentalnih pogojev, navedeni rezultati kažejo, da lahko TLS uporabimo kot učinkovito metodo za detekcijo cianobakterijskih pigmentov in kot metodo za zgodnje odkrivanje prisotnosti cianotoksinov.

Cr-PE smo detektirali tudi na mikrofluidnem čipu pri čemer smo uporabili mikroskop na termične leče. Ob dodatku 30% etanola, ki zaradi ugodnejših optotermičnih lastnosti (višji temperaturni koeficient lomnega količnika, nižja toplotna prevodnost) v primerjavi z vodo izboljša občutljivost tehnike TLS, smo dosegli spodnjo mejo detekcije 51 $\mu\text{g/L}$, ki jo z dodatno optimizacijo instrumenta lahko še izboljšamo.

V drugem delu disertacije je predstavljen detekcija MC-LR s sistemom, ki deluje an osnovi kombinacije TLS in FIA ter inhibicije proteinske fosfataze PP2A. MC-LR inhibira proteinsko fosfatazo, zato lahko določimo koncentracijo toksina na osnovi TLS meritve zmanjšanja koncentracije produkta reakcije med PP2A in substratom (p-nitrofenilfosfatom), ki je sorazmerna zmanjšanju aktivnosti encima. Z opisano metodo smo dosegli spodnjo mejo detekcije 0.64 $\mu\text{g/L}$, ki je 1.6 krat nižja od dopustne koncentracije za MC-LR v pitni vodi po priporočilu WHO.

V zaključnem delu disertacije je predstavljena metoda za odstranjevanje MC-LR iz vode, ki temelji na adsorpciji toksina na novem kompozitnem materialu iz hitosana in celuloze. Naše raziskave so pokazale, da so tovrstni materiali sposobni vezati 96 mg mikrocistina na gram adsorbenta, kar je 4.8 krat več od najbolj učinkovitega materiala doslej opisanega v literaturi. Poleg visoke adsorpcijske sposobnosti so materiali na osnovi celuloze in hitosana okolju bolj prijazni, saj sta hitosan in celuloza biokompatibilna in biorazgradljiva, kompozitni material pa je sintetiziran z uporabo ionskih tekočin, ki jih po izpiranju z materiala lahko recikliramo z destilacijo.

Ključne besede: cianobakterija, cvetenje cianobakterij, cianopigmenti, mikrocistina LR, toplotne leče, kompozitni material iz hitosana in celuloze.

SUMMARY

Cyanobacteria blooms represent a threat to environment and human health due to the huge release of toxic secondary metabolites during their senescence and death. These compounds are dermatotoxic, hepatotoxic, tumor promoters and recently they have been related to neurodegenerative diseases such as Alzheimer and Lateral Amyotrophic Sclerosis. The most serious case occurred in Brazil in 1996 when the contamination of the water supplies of a hemodialysis centre caused the death of 26 patients following liver failure. The health's risk associated to these contaminants lead the World Health Organization (WHO) to set provisional guidelines for the presence of microcystin-LR (MC-LR) – so far, the most harmful cyanotoxin known - in drinking and recreational waters. The maximum allowed concentration of this toxin in drinking water was set to 1 µg/L but it is possible that in the future this limit will be further decreased if new toxic effects will be discovered. In this perspective, WHO and other public agencies of different countries strongly recommend further studies on cyanobacteria, cyanotoxins and on the development of early warning detection and removal systems of cyanobacteria and cyanotoxins.

This work is focused on the development of novel methods for the detection of cyanopigments and for the detection and removal of MC-LR from freshwater. In the first part of this thesis the highly sensitive thermal lens (TL) techniques were applied to the detection of two cyanopigments, namely cross linked allophycocyanin (CL-APC) and Cr-phycoerythrin (Cr-PE). Both pigments were successfully detected in a thermal lens spectrometric (TLS) system which was further optimized for Cr-PE. For Cr-PE a limit of detection (LOD) of 13 µg/L was achieved by coupling TLS with flow injection analysis (FIA), a technique that allowed to use smaller sample volumes and to reduce pigment photodegradation.

The achieved LOD is close to the value of 3.16 µg/L which is the average estimated concentration of PE that can be related to the presence of an amount of cyanobacteria that could result in formation of 1 µg/L of MC-LR. Given the fact that a further decrease in the LOD is expected to be achieved by optimization of the experimental conditions, results indicates that TLS can be a powerful tool for the detection of cyanobacteria pigments and hence an effective early warning system for the presence

of cyanotoxins. Cr-PE was also successfully detected on a microfluidic chip by a thermal lens microscope. In this system the lowest LOD was equal to 51 µg/L and it was achieved in the presence of 30% ethanol that, as other organic solvents, is known to improve the sensitivity of the TLS technique. As in the case of TLS system it is expected that lower LODs will be reached by further optimization of the experimental conditions.

In the second part of this thesis a detection system for MC-LR based on the coupling of TLS with FIA and the protein phosphatase inhibition assay (PPIA) is presented. MC-LR inhibits the protein phosphatase and the concentration of the toxin is extrapolated from the decrease of the enzymatic activity which is related to concentration of the reaction product detected by TLS. The LOD achieved with this system was 0.64 µg/L, i.e. 1.6 times lower than the limit set by WHO for drinking water.

In the final part of this work a method for the removal of MC-LR based on the adsorption on chitosan-cellulose novel composite materials is presented. The maximum adsorption efficiency of these materials, in the given experimental conditions, was equal to 96 mg per gram of adsorbent material i.e. 4.8 times higher than the best adsorber found in literature. Besides the high adsorption efficiency, these composite materials have also the advantage of being completely green. Indeed, chitosan and cellulose are biocompatible and biodegradable. Moreover the ionic liquid that is used to prepare them can be washed away and recovered by distillation.

Keywords: *cyanobacteria blooms, cyanobacteria, cyanopigments, microcystin-LR, thermal lens techniques, chitosan-cellulose composite materials.*

TABLE OF CONTENTS

ACKNOWLEDGEMENTS.....	I
POVZETEK.....	III
SUMMARY.....	V
TABLE OF CONTENTS.....	VII
LIST OF FIGURES.....	XI
LIST OF TABLES.....	XIV
LIST OF ABBREVIATIONS AND ACRONYMS.....	XV
LIST OF SYMBOLS.....	XVIII
1-INTRODUCTION.....	1
2-AIMS OF THE THESIS.....	3
3-THEORETICAL BACKGROUND.....	4
3.1 Harmful algal blooms.....	4
3.1.1 Cyanobacteria harmful algal blooms formation.....	4
3.1.2 Harmful algal blooms management.....	6
3.1.3 Guidelines and policies.....	7
3.2 Detection of cyanobacteria.....	10
3.2.1 State of the art in the detection of cyanobacteria.....	10
3.2.2 Cyanobacteria pigments.....	11
3.3 Detection of cyanobacteria toxins.....	11
3.3.1 Cyanobacteria toxins.....	11
3.3.2 Microcystins.....	12
3.3.3 State of the art in the detection of MC-LR.....	13
3.4 Protein phosphatase inhibition assay.....	15
3.5 Thermal lens spectrometry.....	15
3.6 Thermal lens microscopy.....	18
3.7 TLM combined with microfluidics chips.....	19
3.8 TL coupled with FIA.....	21
3.9 Removal of MC-LR from fresh water.....	24
3.9.1 State of the art in the removal of cyanotoxins from drinking water.....	24
3.9.2 Novel polysaccharide composite materials for the removal of MC-LR.....	25

4-EXPERIMENTAL.....	29
4.1 Chemicals and reagents.....	29
4.2 Buffers and solutions.....	29
4.3 Thermal lens manifold.....	30
4.3.1 Conventional TLS system.....	30
4.3.2 Commercial thermal lens microscope.....	31
4.3.3 Built in house thermal lens microscope.....	32
4.3.4 Thermal lens signal, calibration curves and LOD calculation.....	33
4.4 Absorbance measurements.....	34
4.5 Fluorescence measurements.....	34
4.6 Protein phosphatase inhibition assay.....	35
4.6.1 Colorimetric reaction in a 96-multiwell plate.....	35
4.6.2 Protein phosphatase inhibition assay in a 96 multiwell plate.....	36
4.6.3 Colorimetric reaction in a spectrophotometric cell.....	36
4.6.4 Colorimetric reaction in a FIA-TLS system.....	36
4.6.4.1 System set up.....	37
4.6.4.2 Colorimetric reaction.....	38
4.6.4.3 Protein phosphatase inhibition assay.....	38
4.7 Adsorption of MC-LR on composite materials.....	38
4.7.1 Composite materials.....	38
4.7.2 Experimental set up.....	39
4.7.3 Kinetic of adsorption.....	42
5-RESULTS AND DISCUSSION.....	44
5.1 DETECTION OF CYANOBACTERIAL PIGMENTS.....	44
5.1.1 Preliminary experiments in a TLS-batch mode system.....	44
5.1.1.1 Batch mode experiments on CL-APC in a conventional TL system.....	44
5.1.1.2 Batch mode experiments on Cr-PE in a conventional TL system.....	45
5.1.1.3 Batch mode experiments on Cr-PE by TLM.....	45
5.1.2 Improvement of the TL detection by quenching.....	47
5.1.2.1 Quenching effect of KI on CL-APC.....	47
5.1.2.2 Quenching effect of KI on Cr-PE.....	48
5.1.2.3 Quenching effect of KI on the TL signal.....	49
5.1.3 Improvement of the TL detection by the use of ethanol.....	50

5.1.3.1	Fluorescence spectra of Cr-PE in the presence of ethanol.....	50
5.1.3.2	Absorbance spectra of Cr-PE in the presence of ethanol.....	51
5.1.3.3	Comparison between fluorescence and absorbance spectra of Cr-PE in the presence of ethanol.....	52
5.1.3.4	Ethanol effect on the sensitivity of a TL-batch mode detection system.....	53
5.1.4	Improvement of the TLS system by coupling with FIA.....	54
5.1.4.1	Detection of Cr-PE in a FIA-TLS system.....	54
5.1.4.2	Effect of ethanol on the sensitivity of a FIA-TLS detection of Cr-PE.....	56
5.1.5	Detection of Cr-PE in a microfluidic chip by a thermal lens microscope.....	59
5.1.5.1	Set up of the microfluidic chip-TLM system.....	59
5.1.5.2	Improvement of the TLM-microfluidic system by addition of ethanol.....	62
5.2	DETECTION OF MC-LR.....	65
5.2.1	Set up of the PPIA in a 96 multiwell plate.....	65
5.2.1.1	Protein phosphatase 2A activity.....	65
5.2.1.2	PP2A inhibition by MC-LR.....	66
5.2.2	Set up of the PPIA in a FIA-TL system.....	67
5.2.2.1	Preliminary tests on the absorbance spectra of the reagents and the product.....	67
5.2.2.2	Set up of the colorimetric reaction.....	70
5.2.2.3	Effects of increased concentrations of reagents and decreased flow rate on the colorimetric reaction in the FIA-TLS system.....	71
5.2.2.4	Effect of sample volumes and flow rate on the colorimetric reaction in the FIA-TLS system.....	72
5.2.2.5	Development of the PPIA in a FIA-TLS system.....	73
5.2.2.6	Calibration curve and estimation of LOD for MC-LR.....	74
5.3	REMOVAL OF MC-LR BY ADSORPTION ON COMPOSITE MATERIALS.....	78
5.3.1	Preliminary experiments.....	78
5.3.1.1	Screening of the adsorption of MC-LR on the chitosan-tricyclodextrins composite materials.....	78
5.3.1.2	Screening of the adsorption of MC-LR on the cellulose-tricyclodextrins composite materials.....	79
5.3.1.3	Adsorption of MC-LR on the chitosan-cellulose composite materials.....	80
5.3.1.4	Influence of the pH on the adsorption of MC-LR on composite materials.....	81
5.3.2	Mechanism of adsorption.....	82

6-CONCLUSIONS.....	87
7-REFERENCES.....	90

LIST OF FIGURES

Figure 3.1 Massive algal blooms in lakes.....	4
Figure 3.2 HABs and their negative effects on environment.....	5
Figure 3.3 Absorbance spectra of photosynthetic pigments.....	10
Figure 3.4 Structure of MC-LR.....	12
Figure 3.5 Colorimetric reaction catalyzed by protein phosphatases.....	15
Figure 3.6 Scheme of the propagation of the beams in a thermal lens microscope...19	
Figure 3.7 Scheme of a flow injection system.....	22
Figure 3.8 Structure of cellulose.....	26
Figure 3.9 Structure of chitosan.....	26
Figure 3.10 Structure of butylmethyl imidazolium chloride.....	28
Figure 4.1 Scheme of a conventional thermal lens system.....	31
Figure 4.2 Commercial Y chip and H interface.....	32
Figure 4.3 Scheme of the built in house thermal lens microscope.....	33
Figure 4.4 Scheme of the tubing connections to the chip.....	33
Figure 4.5 System set up for the detection of MC-LR.....	37
Figure 4.6 Composite materials.....	40
Figure 4.7 Support developed for washing the films.....	41
Figure 4.8 Scheme of the mesh-film-mesh sandwich.....	42
Figure 5.1 TL signal of CL-APC in a conventional TL system.....	44
Figure 5.2 TL signal of Cr-PE in a conventional TL system.....	45
Figure 5.3 Photodegradation of Cr-PE in a TLM system.....	46
Figure 5.4 Fluorescence spectra of CL-APC in KPi and CL-APC in the presence of 1 M KI and 2.5 M KI.....	48
Figure 5.5 Fluorescence spectra of Cr-PE in KPi and Cr-PE in the presence of 1 M KI and 2.5 M KI.....	48
Figure 5.6 Calibration curves of Cr-PE in 0.1 M KPi and Cr-PE in 1 M KI.....	49
Figure 5.7 Fluorescence spectra of Cr-PE in KPi and Cr-PE in KPi, 0.5%, 2.5%, 5%, 10% and 50% ethanol.....	51
Figure 5.8 Absorbance spectra of Cr-PE in KPi and Cr-PE in KPi, 0.5%, 2.5%, 5%, 10% ethanol.....	52

Figure 5.9 Calibration curve of Cr-PE in in ethanol 10% in a conventional TL system.....	54
Figure 5.10 TL signals of Cr-PE in a FIA-TLS system.....	55
Figure 5.11 Calibration curve of Cr-PE in KPi in a FIA-TLS system.....	56
Figure 5.12 Absorbance spectra of Cr-PE in KPi and Cr-PE in 30% and 40% ethanol.....	57
Figure 5.13 Fluorescence spectra of Cr-PE in KPi and Cr-PE in 30% and 40% ethanol.....	57
Figure 5.14 Calibration curve of Cr-PE in 40% ethanol in a FIA-TLS system.....	58
Figure 5.15 TL signals of Cr-PE in KPi in a TLM system.....	60
Figure 5.16 TL signals of different injection volumes of Cr-PE in a TLM-gravity driven flow system.....	61
Figure 5.17 TL signals of Cr-PE in a TLM-gravity driven flow system at different flow rates.....	61
Figure 5.18 Calibration curves of Cr-PE in KPi and Cr-PE in 30% ethanol in a TLM-gravity driven flow system.....	62
Figure 5.19 TL signals of Cr-PE in 30% ethanol in a TLM- gravity driven flow system.....	63
Figure 5.20 PP2A activity in a 96-well plate.....	66
Figure 5.21 Inhibition of PP2A by MC-LR in a 96-well plate.....	66
Figure 5.22 Absorbance spectra of 20 mM pNPP and pNP.....	68
Figure 5.23 Absorbance spectra of different concentrations of pNPP.....	69
Figure 5.24 TL signal of pNP after the injection of the second solution.....	71
Figure 5.25 TL signal of pNP. 32 and 17 minutes reaction time.....	72
Figure 5.26 TL signal of pNP after a 50 μ L injection containing 0.1 mU of PP2A..	73
Figure 5.27 Inhibition of PP2A by MC-LR in a FIA-PPIA-TLS system.....	74
Figure 5.28 Calibration curve of MC-LR in a FIA-PPIA-TLS system.....	76
Figure 5.29 Absorbance measurements of solutions of MC-LR in the presence of a 100% CS and a 50% CS-50% TCD composite material.....	78
Figure 5.30 Absorbance measurements of MC-LR solutions in the absence and in the presence of a 50% CEL-50% TCD and 75% CEL-25% TCD composite materials..	79

Figure 5.31 Absorbance measurements of a solution of MC-LR in the presence of a 100% CEL composite material.....	80
Figure 5.32 Absorbance measurements of a solution of MC-LR in the presence of a 50% CS-50% CEL composite material.....	80
Figure 5.33 Absorbance measurements of a solution of MC-LR in the presence of a 100% CS material at pH 5 and pH 7.....	81
Figure 5.34 Q_t as a function of time for different concentrations of chitosan in the chitosan-cellulose composite materials.....	83

LIST OF TABLES

Table 3.1 Guidelines for drinking waters in different countries.....	8
Table 3.2 WHO guidelines for recreational waters.....	9
Table 3.3 Guidelines for recreational waters in Australia and Europe.....	9
Table 3.4 Methods developed for the detection of MC-LR.....	14
Table 3.5 Some of the recent analytical applications of TLS.....	18
Table 3.6 Examples of the application of TLM combined with microfluidics.....	21
Table 3.7 Examples of analytical applications of flow injection analysis.....	23
Table 4.1 Reagents and chemicals used.....	29
Table 4.2 Buffers.....	30
Table 4.3 List of the tested composite materials.....	39
Table 5.1 Fluorescence –absorbance ratios of Cr-PE in the presence of different ethanol concentrations.....	53
Table 5.2 Analytical performances of TL systems and conventional spectrometry...	64
Table 5.3 Comparison of analytical performances obtained in this work and in literature.....	77
Table 5.4 Fitting of the data to the pseudo first and pseudo second order models....	84
Table 5.5 Adsorbent materials already developed for the removal of MC-LR.....	85

LIST OF ABBREVIATIONS AND ACRONYMS

[BMIm+Cl-]	butyl methylimidazolium chloride
μ-TAS	micro-total analysis systems
ACF	activated carbon fibers
ADDA	3-amino-9-methoxy-2,6,8-trimethyl-10-phenyldeca-4-6-dienoic acid
APC	allophycocyanin
APCI	Atmospheric Pressure Chemical Ionization
BA	bioanalytical assay
BSA	bovine serum albumin
CCL	Contaminant Candidate List
CE	Capillary Electrophoresis
CEL	cellulose
CL-APC	cross-linked allophycocyanin
Cr-PE	Cr-Phycoerythrin
CS	chitosan
DB18C6	dibenzo-18-crown-6
DTT	dithiothreitol
EDTA	ethylenediaminetetraacetic acid
ELISA	Enzyme-Linked Immunosorbent Assay
EPA	Environmental Protection Agency
ESI	Electron Spray Ionization
EWMI	Evanescence Wave Multi-Channel Immunosensor system
FIA	Flow Injection Analysis
FRET	Förster Resonance Energy Transfer
HABs	harmful algal blooms
HPLC	High Performance Liquid Chromatography
IARC	International Agency for the Research on Cancer
IC	Ion Chromatography
IL	ionic liquid
ISO	International Organization for the Standardization

KPi	potassium phosphate buffer
LC	Liquid Chromatography
LDTD	Laser Diode Thermal Desorption
LOD	limit of detection
MAC	maximum allowed concentration
MALDI	Matrix-Assisted Laser Desorption/Ionization
MC-LR	microcystin-LR
MCL	maximum contaminant level
MCs	microcystins
MS	Mass Spectrometry
MS/MS	Tandem Mass Spectrometry
MSC	model selection criteria
NHMRC	National Health and Medical Research Council
OATP	organic anion transporting polypeptides
PAC	powdered activated carbon
PC	phycocyanin
PDA	Photodiode Array
PDVF	polyvinylidene fluoride
PE	phycoerythrin
p-NP	<i>para</i> -nitrophenolate
p-NPP	<i>para</i> -nitrophenylphosphate
PP	protein phosphatase
PP2A	protein phosphatase 2A
PPIA	Protein Phosphatase Inhibition Assay
PTFE	polytetrafluoroethylene
QD	Quantum Dot
QPCR	Quantitative Polymerase Chain Reaction
SELDI	Surface-Enhanced Laser Desorption/Ionization
SIR	Selected Ion Recording
SPE	Solid Phase Extraction
SPM	Suspended Particulate Matter
SPR	Surface Plasmon Resonance
TCD	tricyclodextrins
TL	Thermal Lens

TLC	Thin Layer Chromatography
TLM	Thermal Lens Microscopy
TLS	Thermal Lens Spectrometry
TOF	Time Of Flight
TRFIA	Time-Resolved Fluorescence
UF	ultrafiltration
UPLC	Ultra Performance Liquid Chromatography
UV	ultraviolet
VIS	visible
WHO	World Health Organization

LIST OF SYMBOLS

A: absorbance

dn/dT : sample's temperature coefficient of refractive index

E: thermal lens enhancement factor

k : thermal conductivity

k_1 : pseudo-first order rate constant of sorption

k_2 : pseudo-second order rate constant of sorption

λ : wavelength

P: laser power

q_e : amount of analyte adsorbed at equilibrium

q_t : amount of analyte adsorbed at any time

R^2 : coefficient of determination

s: slope

σ_{blank} : standard deviation of the blank

t: time

1-INTRODUCTION

During the last decades *harmful algal blooms* (HABs) phenomenon in fresh water has increased in seriousness and occurrence. The reason for this worsening is probably due to the global warming¹, to eutrophication² and dissemination of bacteria cells that are transported in ship ballast³.

Cyanobacteria are among the principle microorganisms involved in HABs. These blooms can pose a serious threaten to the environment and human health for two reasons. The first is that these blooms can cause an oxygen depletion in water with consequences on the aquatic ecosystem⁴. The second is that cyanobacteria during their senescence and death release secondary metabolites among which there are compounds (cyanotoxins) that are toxic to both animals and humans. Contamination occurs by direct contact, ingestion and inhalation; their effects are acute and chronic and in at least one case they had fatal consequences on humans. Since these toxins are quite stable they can effect the environment and human health at different levels. They can directly poison aquatic animals and mammals, birds, cattle, livestock and pets that drink from befouled reservoirs^{5,6}. They can scale up the food chain by accumulation in predators⁷. Food can be a source of intoxication as well: crops can be irrigated with contaminated water⁸, cattle fed with polluted forage and aquaculture products⁹ can be infected through water. Humans can enter in contact with cyanotoxins also trough recreational and occupational waters by breathing aerosols or by accidental swallow of water. In addition to health issues it must be mentioned that cyanotoxins have also an economic impact. Farmers and fish farmers can lose their products. Recreational waters tourism can be effected as well. Beaches and recreational boating areas can not be frequented during the occurrence of HABs. Moreover also sport fish is effected by HABs that brake the ecosystem and release algal toxins that poison the fish. However the main concern about freshwaters cyanotoxins derives from the fact that they can be found in drinking water supplies. Not all the traditional water treatments are successful in the removal of these harmful compounds. Moreover a single treatment is not enough to get rid of all the contaminants from water hence the complete removal of this toxic compounds can be very expensive. Furthermore there is a lack of an official regulation regarding

cyanotoxins treatment in drinking water plants. The absence of legislation is due to the fact that there are no standardized methods for the identification and quantification of these harmful chemicals in the samples. Given the different types of existing cyanotoxins, the variability among the same groups and the fact that in a sample more than one of these compounds can be present, a single method is not enough for an accurate analysis. Often it is required to concentrate the toxins and separate them from matrix contaminants and this makes the analysis expensive and time consuming. Moreover there is a lack of standard reference materials for the majority of the known cyanotoxins. The *World Health Organization* (WHO) has released a guideline for drinking water quality¹⁰ but only MC-LR has been taken in consideration due to the fact that, so far, it is the most noxious and better known cyanotoxin among all the others.

More than one method has been developed to detect cyanobacteria and cyanotoxins but there is a lack of a unique and standardized method for all of these compounds. Moreover, due to the seriousness of the public health and environmental issues world organizations such as WHO and public agencies of different countries such as the U.S. and Australia Environmental protection agency (EPA), strongly recommend further studies on the biology of cyanobacteria, on the structures and effects of cyanotoxins and on the development of early warning detection and removal systems of cyanobacteria and cyanotoxins in fresh waters. Indeed, the effects of these toxins are not completely known and only in recent years they have been found to play a role in neurodegenerative diseases^{11,12,13}. It is likely that further studies will unearth new cyanotoxins effects and therefore it can be expected that the guidelines will be revised and that the acceptable limit for the presence of these toxic compounds in drinking and recreational waters will be decreased. Consequently more powerful tools to detect and remove these toxins will be required.

2- AIMS OF THE THESIS

This work is focused on the developing of novel tools to face the threat represented by the cyanobacterial blooms at three different levels: 1) the detection of cyanobacteria pigments as early warning systems for the presence of microcystins, 2) the detection of MC-LR and 3) the removal of this toxin from water.

The amount of pigments in water can be correlated with the relative amount of microcystins and hence their detection represent an early warning tool for the presence of these toxic compounds. In order to be effective, the detected amount has to be in the order of few micrograms per liter, hence really sensitive detection techniques are required. Given their high sensitivity, thermal lens techniques are particularly suitable for this purpose. Indeed thermal lens spectrometry (TLS) can indirectly detect samples absorbances down to 10^{-7} while thermal lens microscopy (TLM) in combination with microfluidics was reported to being able to detect subyoctomoles of analyte¹⁴. In the first part of this thesis the development of novel tools for the detection of cyanopigments based on thermal lens techniques are presented.

It is worth mentioning that, even though thermal lens techniques are affected by fluorescence and cyanobacteria pigments are highly fluorescent, there are some advantages that compensate for this drawback. Indeed, combining TLM with microfluidics allows to downscale the analysis on a chip. Taking in consideration that the lasers required for this detection method are expected to become cheaper and portable, it looks worth to perform preliminary experiments on this cyanopigments. Moreover, as shown in the second part of this thesis, these techniques can be applied also to the detection of cyanotoxins, meaning that in a laboratory (or directly on field if portable systems will be developed) only one type of instrumentation is required for the two different kinds of analytes.

In the second part of this thesis a novel MC-LR detection method, based on the combination of FIA with PPIA and the TLS is presented.

Finally, in the last part of this thesis, a novel method for the removal of MC-LR based on the adsorption on completely green composite materials is presented.

3-THEORETICAL BACKGROUND

3.1 Harmful algal blooms

3.1.1 Cyanobacteria harmful algal blooms formation

Fresh water cyanobacteria together with marine cyanobacteria are the oldest photosynthetic organisms on Earth¹⁵. During their evolution they developed numerous adaptive mechanism that confer them a high tolerance to extreme environmental conditions such as very high and low light, desiccation, high temperatures and nutrient deprivation. This explains their distribution all over the globe where fresh water cyanobacteria can be found in lakes, ponds and rivers. Some species are able to fix the atmospheric nitrogen and to store phosphorus allowing them to exploit both deficiencies and overabundance of nutrients. The great capability of exploiting nutrients enriched environments together with favorable climate conditions such as very high/low light, high temperatures, low water turbulence and long water residence time can lead to a massive proliferation of these microorganisms (Fig.3.1).



Figure 3.1 Massive algal blooms in lakes. Left panel: cyanobacteria bloom (in turquoise) in the lakes Osterseen, Bavaria, Germany (Courtesy: Michael Knall). Right panel: Microcystis bloom in Lake Erie , USA (Courtesy: NASA Earth Observatory).

The high density of the cells can cause foul odor, bad taste and water toxicity. Moreover it can cause a loss in water transparency and a fast depletion of nutrients, inorganic carbon and other important resources, resulting in a decline of biomass. This decline is usually associated with the formation of decaying scum that are foul smelling and unsightly. The scum can host microbial pathogens and deprive the water layers beneath it causing hypoxia and anoxia (Fig.3.2). In addition there can be

a release of hydrogen sulfide that is toxic and the release of nutrients from sediments that increases eutrophication thus stimulating the growth of the bloom. Furthermore some species of cyanobacteria release secondary metabolites (cyanotoxins) that are toxic to the environment, animals and humans.

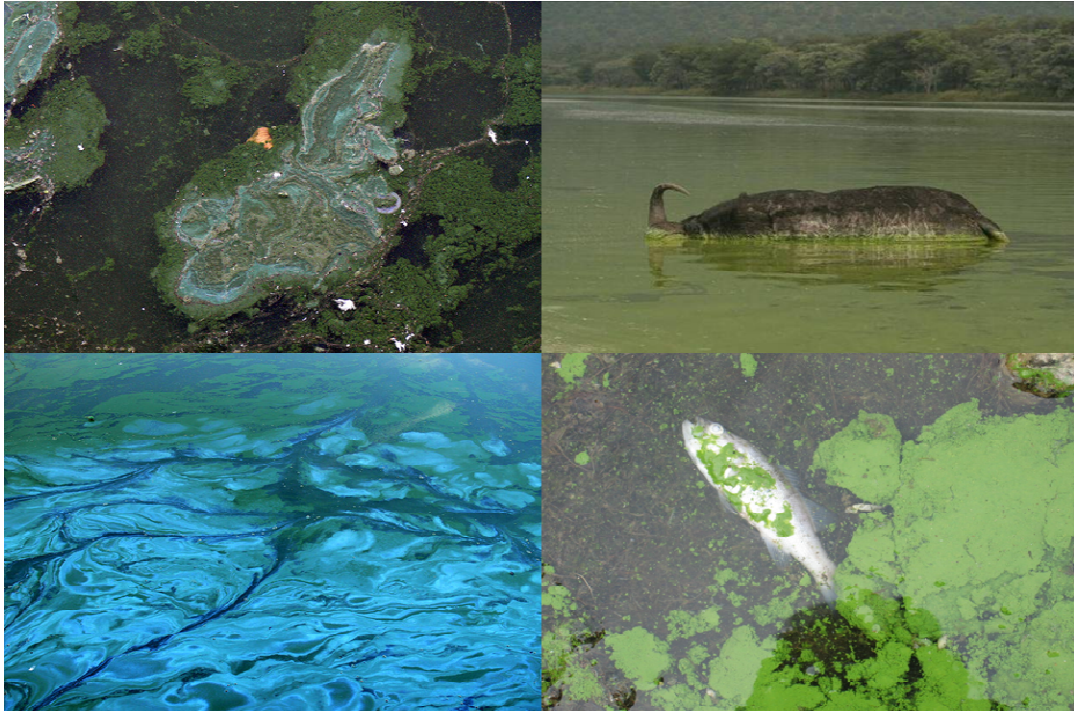


Figure 3.2 HABs and their negative effect on the environment. Upper and lower left panels: cyanobacteria blooms in a Deûle channel, Lille, France (Courtesy: Lamiot). The scums were emitting a strong odor, probably due to the presence of *Spirulina*. The blue color is given by the release of pigments from dead cyanobacteria. Upper right panel: a dead buffalo found in a reservoir with a dense bloom of *Microcystis* in South Africa (Courtesy: Jannie Coetz). Lower right panel: a dead fish found in Binder Lake, IA, USA, stricken by a cyanobacteria bloom (USGS).

Algal blooms are an increasing environmental concern. Lake Erie in 2011 experienced the largest algal bloom peak of any time¹⁶. New blooms appear where they have never been observed in the past¹⁷. Eutrophication¹⁸ and climate change¹⁹ are considered to be the main reasons for the growth of the number and severity of the HABs. Eutrophication is mainly due to anthropogenic activities. Nutrients from farms and yards, urban runoff, faulty septic systems, and the burning of fossil fuels are all contributing to the overload of nutrients in the environment²⁰. Climate change with the increase of temperature favors the spread of cyanobacteria. They grow better than other species at higher temperatures. Moreover, the surface warming causes a stratification of water layers in lakes thus reducing the vertical mixing and favoring the bloom formation.

3.1.2 Harmful algal blooms management

The management of HABs is a complex issue. Possible approaches are numerous but not adequate and/or too costly. Retention time can be shortened by flushing water²¹. Water stratification can be avoided by mixing^{22,23} or bubbling²⁴ but these methods are not always effective²⁵ and they can be very expensive. Algaecide can be used²⁶ but they can be noxious to the environment and to humans and moreover they could enhance the fast release of huge amounts of toxins^{27,28}. Another method that has been suggested to lower the amount of cyanobacteria mass is biomanipulation i.e. a controlled alteration of a food web in order to restore the ecosystem health²⁹. This can be done introducing planktivorous species³⁰ or by removing zooplanktivorous species thus increasing the herbivorous zooplankton³¹. It has to be pointed out anyway that biomanipulation does not lead to a long term effect on an ecosystem, that is not easy to carry it out on a large scale system and that is effected by the availability of phosphorous and nitrogen³². One more possible approach in HABs management is to reduce the load of nitrogen and phosphorous compounds deriving from anthropogenic activities by the application of a more wise management of farming and industrial activities. This strategy anyway can be difficult and costly and the positive effects can be seen on a long-term scale. Moreover even though it is possible to decrease the external loading of nutrients their internal load in the sediment as well as the climate change³³ can make ineffective this reduction³⁴.

At the present time there is no strategy to prevent the occurrence of HABs given the complexity and the extent of this phenomenon. It is expected, instead, that their occurrence will increase due to climate change and eutrophication. This scenario makes largely relevant the development of early warning detection systems for cyanobacteria and their cyanotoxins and of methods for the removal of harmful cyanobacterial secondary metabolites from water. In fact it is unlikely that it will be possible to avoid the formation of HABs and the consequent release of toxic compounds in water in the near future. However, if detected on time, it could be possible to avoid at least the exposure of humans to toxins that are present in drinking and recreational waters.

3.1.3 Guidelines and policies

The threat to human health represented by cyanotoxins lead to the release of a provisional guideline for drinking water by the World Health Organization in 1998. The guideline (that was confirmed in 2011 and is still valid) determines 1 µg/L as the maximum concentration of MC-LR allowed in drinking water, considering a daily intake of 2 liters of water¹⁰. Due to the lack of sufficient data regarding other cyanotoxins the guideline was restricted only to this type of cyanotoxin. Many countries including many European states, China, Korea, Japan and others adhered to it. The U.S.A. did not release federal guidelines (www.glerl.noaa.gov/res/Centers/HABS/guidelines.html) but the U.S. EPA included MC-LR (and some cyanotoxins) in the Contaminant Candidate List (CCL) (<http://water.epa.gov/scitech/drinkingwater/dws/ccl/>) in 1998, 2005 and 2009. Canada has fixed the *maximum acceptable concentration* (MAC) for MC-LR in drinking water at 1.5 µg/L³⁵ while Australia set the maximum allowed concentration of microcystin in drinking water at 1.3 µg/L³⁶. An overview of drinking water guidelines in other countries is given in table 2.1.

Regarding the recreational waters the WHO adopted guidelines³⁷ based on the risks associated with different types of exposure (Tab. 3.2). According to this guidelines at low risk concentrations the major threat is represented mainly by irritative and allergenic effects caused by skin exposure to the cyanotoxin. It is unlikely that an accidental swallow of contaminated water at this concentration could pose a serious hazard to humans but it has to be noted that the exposure could be harmful for people with a particular sensitivity to allergens. Microcystins at concentration between 10 and 20 µg/L represent a hepatotoxic risk. The guideline takes in consideration the tolerable daily intake and the assumption of an adult (60 kg) ingesting 100 mL of water. It must be taken in consideration that the seriousness of this risk increases in the case of children (because they weight less and it is likely that they swallow larger volumes of water) and of people with liver dysfunctions. At higher concentrations even a small volume of water if ingested can cause serious health problems. In the U.S.A. different states have set different guidelines, Australia and other countries have suggested a limit of 20 µg/L for recreational activities that entail a high risk of exposure (like swimming) while a 100 µg/L limit was suggested for other

recreational activities such as fishing and boating³⁸. Some other countries have set multilevel guidelines for recreational waters that are resumed in the table 3.3.

Table 3.1 Guidelines for drinking water in different countries (adapted from Burch 2008 and updated where possible)

COUNTRY	µg/L	Source
Australia	1.3	NHMRC Drinking Water guidelines 2011 (updated in December 2013) ³⁶
Brazil	1	From Burch 2008 ³⁹
Canada	1.5	Health Canada 2012 ⁴⁰
Czech Republic	1	From Burch 2008 ³⁹
China	1	From Burch 2008 ³⁹
France	1	From Burch 2008 ³⁹
Italy	1	Lucentini and Ottaviani 2011 ⁴¹
Japan	1	From Burch 2008 ³⁹
Korea	1	From Burch 2008 ³⁹
New Zealand	1	Drinking Water Standards for New Zealand 2008 ⁴²
Norway	1	From Burch 2008 ³⁹
Poland	1	From Burch 2008 ³⁹
South Africa	0-0.8 (acceptable range)	From Burch 2008 ³⁹
Spain	1	From Burch 2008 ³⁹
U.S.A.	NO LIMIT but in CCL	http://water.epa.gov/drink/ndwac/cclprocess/index.cfm
WHO	1	WHO Guidelines for Drinking Water Quality 2011 ¹⁰

Table 3.2 WHO guidelines for recreational waters

Probability of risk	Cyanobacteria (cells/mL)	MC concentration (µg/L)
Low	< 20,000	<10
Medium	20,000-100,000	10-20
High	100,000-10,000,000	20-2,000
Very high	> 10,000,000	>2,000

Table 3.3 Guidelines for recreational waters in Australia and Europe (adapted from Burch 2008).

Country	Level	Guideline	Provisions
Australia	1	10 µg/L of MCs or > 50,000 cells/mL of toxic <i>M. aeruginosa</i> or biovolume > 4 mm ³ /L of a mix of cyanobacteria where total biovolume of all cyanobacteria	Probability of adverse health effects due to known toxins => closure is recommended
	2	material > 10 mm ³ /L or scums are consistently present	Probability of adverse health effects due to high levels of cyanobacterial material where known toxins are not present => closure is
Germany	1	< 10 µg/L MCs	Monitor cyanobacteria in a routine surveillance program
	2	> 10 < 100 µg/L MCs	Publish warnings, discourage bathing, consider temporary closure
	3	> 100 µg/L MCs	Publish warnings, discourage bathing, temporary closure recommended
Netherlands	1	MC-LR > 10 µg/L or presence of scums	Issue warning
	2	MC-LR > 20 µg/L or presence of scums	Issue warning and continue monitoring; if levels are persistently high => closure of bathing facilities
France	1	20,000 cyanobacterial cells/mL	Monitoring intensified to fortnightly
	2	> 20,000 < 100,000 cyanobacterial cells/mL	Analysis of MCs. If MC-LR eq' > 25 µg/L => prohibition of swimming
	3	Scums	All activities are prohibited

3.2 Detection of cyanobacteria

3.2.1 State of the art in the detection of cyanobacteria

Monitoring the cyanobacterial concentrations in water can be a useful tool in order to assess the possible incoming of harmful blooming. This kind of approach nowadays is based on the measurement of the fluorescence of cyanobacteria given by their pigments^{43,44}. While total phytoplankton content is usually detected by the measurement of chlorophylls fluorescence, cyanobacteria can be detected separately because their photosynthesis accessory pigments absorb in a different range of the visible spectrum (Fig. 3.3). Moreover from the amount of cyanopigments detected, the concentration of cyanotoxins can be estimated⁴⁵.

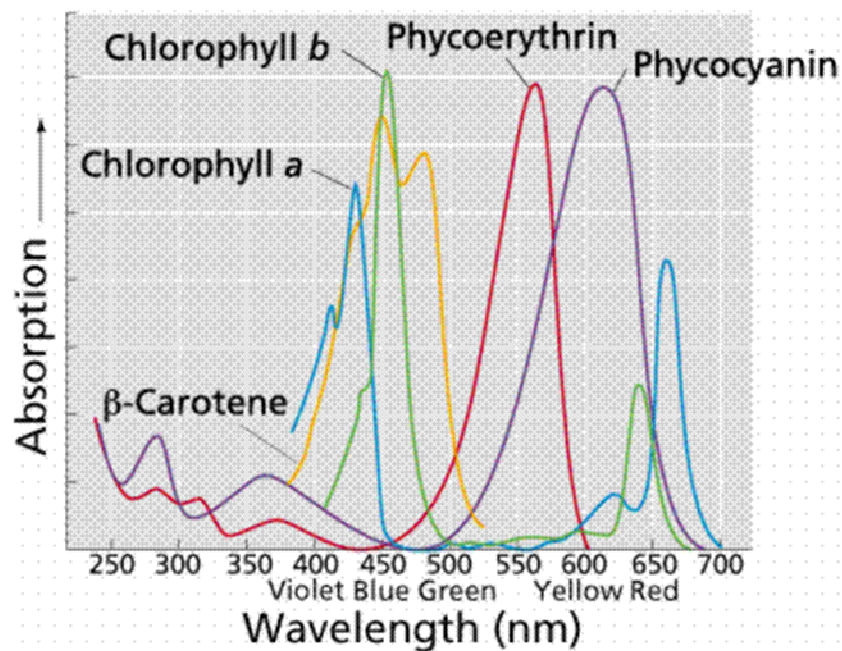


Figure 3.3 Absorbance spectra of photosynthetic pigments (Courtesy: Purves et al.).

Despite the doubts that have been risen about the validity of this approach, due to the fact that not all the cyanobacteria produce toxins, and hence it does not assess the real danger, the lack of a method suitable for the detection of a particular kind of these harmful metabolites still makes this approach a good tool as an early warning detection system. Frequent analysis can be performed to assess the presence of

potentially toxic cyanobacteria not only in the environment but also in water plants were an early and sensitive detection system is of extreme importance.

3.2.2 Cyanobacteria pigments

In comparison to plants cyanobacteria are able to use a broader part of the visible spectrum for photosynthesis. This capability derives from the fact that, besides chlorophylls, they have accessories pigments - *phycobiliproteins* - that absorbs at different wavelengths and that transfer the energy to chlorophyll. Phycobiliproteins can constitute up to 60% of the soluble protein content of cyanobacteria⁴⁶ and allow them to survive in severe conditions of dim light even in polar regions⁴⁷. The main groups of these pigments are phycocyanin (PC), allophycocyanin (APC) and phycoerythrin (PE). PC is purple to dark cobalt blue with an absorption maximum at 610-620 nm; APC is bright greenish or aqua-blue with an absorption maximum at 650-655 nm and PE is bright pink with an absorption maximum at 540-570 nm. The most largely expressed phycobiliproteins in cyanobacteria are phycocyanin and allophycocyanin while phycoerythrin is present in a small amount and not in all types of cyanobacteria⁴⁸. Besides their primary function of photosynthetic pigments it has also been suggested that they could have a role as microcystin carriers in the gut of grazers⁴⁹. Furthermore, given their highly fluorescence, they are used as fluorophores in immunofluorescence.

3.3 Detection of cyanobacteria toxins

3.3.1 Cyanobacteria toxins

Three are the main structures of cyanotoxins: cyclic peptides (that comprehends the families of microcystins and nodularins), alkaloids (including anatoxins, cylindrospermopsins, lyngbyatoxins and saxitoxins) and poyketides (aplysiatoxins)⁵⁰. Given the higher toxicity and the lack of guidelines for the other cyanotoxins, this work is focused on MC-LR. Therefore only the family of microcystins will be described.

3.3.2 Microcystins

The main species of cyanobacteria that contain microcystins are *Microcystis*, *Planktothrix* and *Anabaena*. Microcystins (MCs) are cyclic heptapeptides with a molecular mass between 500 and 4000 Da⁵¹. Their general structure is composed by the aromatic amino acid Adda (3-amino-9-methoxy-2,6,8-trimethyl-10-phenyl-4,6-dienoic acid) and two variable amino acids that are the main responsible for the diversity of more than 80 different analogues of this cyanotoxin.

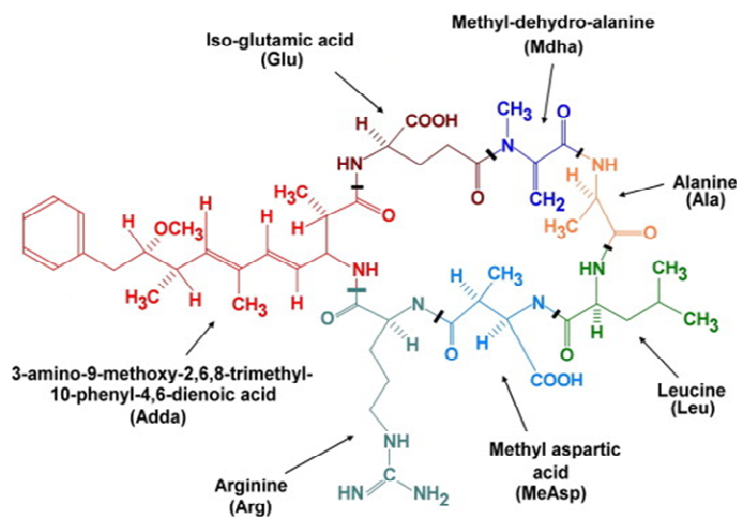


Figure 3.4 Structure of microcystin-LR

Different types of MCs differ in their lipophilicities and polarities and this could explain the differences in toxicities among the members of the same family of cyanotoxins. The most toxic one is MC-LR⁵² that is also the one that has been associated to the majority of the cases of cyanotoxin intoxication in most of the countries.

In humans the symptoms of microcystin poisoning differ depending on the way of exposure. Direct contact with the skin can cause rash, hives, or skin blisters (especially on the lips and under swimsuits). If contaminated water is swallowed the toxin can cause gastrointestinal symptoms such as stomach pain, nausea, vomiting, diarrhea, severe headaches, and fever. The inhalation of polluted water droplets can cause runny eyes and nose, cough, and sore throat, chest pain, asthma-like symptoms, or allergic reactions.

Moreover the exposure to large amount of microcystin can cause liver damage⁵³. Although it can affect also the kidney and the lungs and remain in small amounts in the blood stream thus contaminating other tissues, the main target organ of this class of cyanotoxin is the liver where it is mostly stored⁵¹. The toxin in fact is actively transported inside this organ via organic anion transporting polypeptides OATP1B1, OATP1B3 and OATP1A2 that are expressed only in the liver⁵⁴.

The mechanism of toxicity of the microcystins is based on the inhibition of type 1 and 2A protein phosphatases (PP) activity^{55,56}. The ADDA portion has an important role for the interaction with the PP⁵⁷. The toxin binds to the phosphatases present in the cytoplasm inducing an increase in phosphorylated proteins in the liver. The excessive phosphorylation of the cytoskeletal proteins causes the hypertrophy of the organ, the disruption of liver tissue with a consequent massive hepatic hemorrhage⁵⁸. Therefore microcystin intoxication in some cases can represent an indirect cause of death for example in patients with hepatic diseases⁵⁹. Moreover, microcystin is a possible carcinogenic compound to humans and it is likely that it has a tumor promoter activity⁶⁰. Indeed, the disequilibrium in the phosphorylation of tumor suppressor target proteins can cause tumor proliferation.

3.3.3 State of the art in the detection of MC-LR

A variety of methods have been developed to detect low concentrations of MC-LR and they can greatly differ in complexity and in the kind of information they provide. The only one that is officially recognized by ISO is the HPLC/PDA analysis (ISO 20179:2005, confirmed in 2009). In addition to this method that is the most used, other common analytical methods are ELISA immunoassays⁶¹ and the PPIA⁶². The advantage of these methods is that they are fast and sensitive and can be used for a large scale screening since they can be easily performed on 96-well plates. Anyhow they have some drawbacks such as the lack of selectivity for different analogues of microcystin and the predisposition to give false positive results. In the table 2.4 some of the numerous methods that have been developed for the detection of MCs are listed.

Table 3.4 Methods developed for the detection of MC-LR

Chromatographic methods	HPLC/UV	0.2 µg/L	Spoof et al. 2003 ⁶³
	LC-MS-SIR	0.2 µg/L	Spoof et al. 2003 ⁶³
	SPE/HPLC/PDA	0.25 µg/L	Lawton et al. 1994 ⁶⁴
	SELDI-TOF-MS	1.2 µg/L	Yuan and Charmichael 2004 ⁶⁵
	TLC	1 µg/L	Pelander et al. 2000 ⁶⁶
	SPE/UPLC/MS/MS	2.5 ng/L	Wang et al. 2007 ⁶⁷
	LC/ESI/MS	0.05 µg/L	Yu et al. 2009 ⁶⁸
	LC/MS/MS	0.025 µg/L	Zhang et al. and Thermoscientific 2012 ⁶⁹
	LDTD-APCI-MS/MS	0.2 µg/L	Roy-Lachapelle et al. 2014 ⁷⁰
	SPR	0.5 ng/ml extracellular 0.05 ng/ml intracellular	Devlin et al. 2014 ⁷¹
	MALDI-MS	6.5 µg/L	Roegner et al. 2014 ⁷²
	QD-FRET	0.03 µg/L	Feng et al. 2014 ⁷³
	Biological methods	PPIA	1 µg/L
ELISA		0.05 µg/L	Ueno et al. 1996 ⁶¹
TRFIA		0.01 ng/mL	Lei et al. 2004 ⁷⁴
Immuno-electrode		0.01 ng/L	Lebogang et al. 2014 ⁷⁵
Photoelectrochemical immunosensor		0.055 µg/L	Tian et al. 2014 ⁷⁶
EWMI		0.10 µg/L to 3.6 µg/L	Xiao-Hong et al. 2014 ⁷⁷
Q-PCR		7.2 ng/L	Fortin et al. 2010 ⁷⁸
Commercial kits	Microcystins/Nodularin PP2A Microtiter plate	0.25 µg/L	Abraxis
	QuantaPlate kit for Microcystins	0.147 µg/L	Envirologix
	Microcystins-DM ELISA (Microtiter Plate)	0.1 µg/L	Abraxis

3.4 Protein phosphatase inhibition assay

The PPIA is one of the methods in use for the detection of microcystins⁷⁹. It is based on the inhibition of protein phosphatase 1 or 2A by microcystins and the toxin concentration is therefore measured in terms of loss of enzymatic activity. In the colorimetric PPIA a protein phosphatase removes the phosphate group from the colorless substrate *para*-nitrophenylphosphate (p-NPP) leading to the formation of *para*-nitrophenol. In basic conditions the *para*-nitrophenol loses a proton and the resulting p-NP (yellow) can be detected at 405 nm. The concentration of microcystins is therefore extrapolated from the decrease in the formation of the reaction product pNP.

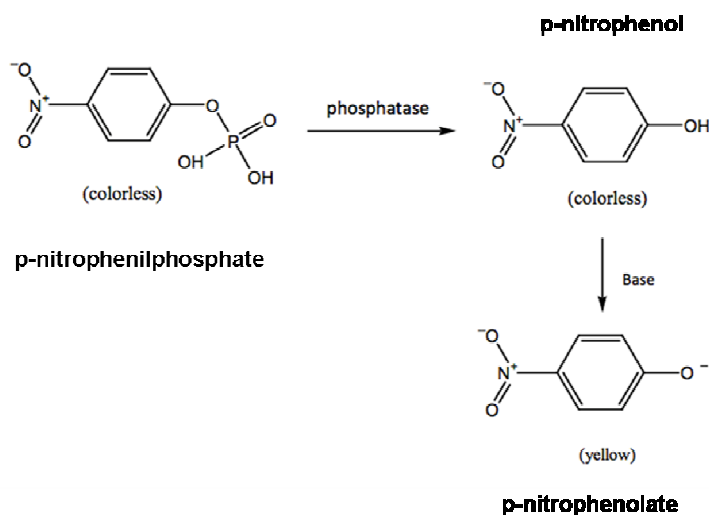


Figure 3.6 Colorimetric reaction catalyzed by protein phosphatases

3.5 Thermal lens spectrometry

The TLS is a photothermal technique that relies on the *thermal lens effect*. When a sample is irradiated by a laser (pump beam) and the excited species releases the energy via non radiative relaxation processes an increase of the sample temperature (between 10^{-4} and 10^{-3} K) occurs. If a laser beam with a Gaussian intensity profile is used for excitation a temperature gradient is generated in the sample, and this causes formation of a refractive index gradient that acts as a lens. This refractive index gradient causes in fact defocusing of the probe beam with a consequent change of its

radius and its intensity at the beam axis. In the TLS the changing of the refractive index is monitored by a probe beam and the relative change of intensity on the axis of the probe beam is converted into an electronic signal which is proportional to the concentration of the analyte in the sample. The amplitude of the thermal lens effect is proportional to the heat generated in the irradiated sample and therefore it depends on the power of excitation laser and the absorbance of the sample. The fluorescence efficiency of the sample has to be taken into account as well since the relaxation via radiative processes decreases the heating of the sample, thus decreasing the thermal lens effect. Also the thermo-optical properties of the medium such as the temperature coefficient of refractive index and the thermal conductivity play a role on the amplitude of the thermal lens effect. In a simplified model where it is assumed that the released heat is equal to the energy absorbed by the sample the relative change in the probe beam intensity is described by the equation

$$\frac{\Delta I}{I} = \frac{2.303P(-dn/dT)A}{\lambda k} \arctg\left(1/\sqrt{3}\right) = 2.303EA$$

Where $\Delta I/I$ is the relative change of the intensity in the centre of the beam, P is the excitation laser power, dn/dT is the sample's temperature coefficient of refractive index, A is the absorbance of the sample, λ is the wavelength of the probe beam and k is the thermal conductivity of the sample. E is the thermal lens enhancement factor and represents the increase in sensitivity depending from the laser power and the thermo-optical properties of the solvent. The advantage of TLS is that thermal lens effect can be observed already when applying a laser power on the order of milliwatts even in the case of samples that are considered transparent. From the equation it is evident that the sensitivity of the technique can be enhanced by increasing the power of the excitation laser and by improving the thermo optical properties of the sample medium. This enables measurements of optical absorbencies as low as 10^{-7} against the 10^{-4} usually reached by conventional transmission-mode spectrophotometric techniques. Moreover the TLS allows to perform measurements on non fluorescing samples. Another advantage of this technique is that very small amount of sample is required to perform a measurement. This makes it

possible to perform measurements in volumes down to sub pL. Furthermore the signal response is relatively fast (millisecond time scale for measurements in liquids). In addition detection on flowing samples can be performed.

Besides the great advantages of TLS some drawbacks must be mentioned. The sensitivity achieved in water samples is low due to the high k values and low dn/dT of this solvent but it can be improved by modifying the solvents in order to improve the thermo-optical properties of the sample. A higher laser power can be used but could represent a problem if a sample is photo-labile. Flow injection analysis, where the resident time of the sample under the intensive laser light is short, can be a solution. Another problem is that there are limited lasers sources thus in some cases the TLS has to be coupled to coloring reactions in order to enable excitation of the analyte with the available excitation laser (indirect detection). Furthermore this technique has a poor selectivity and it can not discriminate different compounds that are absorbing at the same wavelength. Therefore TLS has to be coupled with separation techniques like HPLC, IC, CE or with bioanalytical assays (BA), where it acts as a highly sensitive detector.

The coupling of TLS with other techniques such as BA and FIA enables to reach high sensitivity and increases selectivity in the determination of various analytes^{80, 81}. One example of the successful use of these hyphenated techniques are studies on bilirubin uptake in the hepatic cells⁸². In this experiment, a novel bilirubin detection method, based on TLS-FIA combination, was developed. Under physiological conditions, bilirubin has a very low solubility and it can not be detected by common spectrophotometry. TLS allowed the bilirubin detection under physiological conditions and was further used with FIA to avoid losing the sensitivity due to bilirubin photolability⁸³. Furthermore, recently the direct analysis of bilirubin in human and animal serum was reported for the first time⁸⁴. Other successful recent analytical applications of the TLS are listed in table 3.5.

Table 3.5 Some of the recent analytical applications of TLS

Determination of Hg ²⁺ in water and drug samples	Shokoufi et al 2014 ⁸⁵
Determination of carotenoids in food	Luterotti et al 2013 ⁸⁶
Determination of Lead (II) in ethanolic buffer	Saavedra and Gomez 2013 ⁸⁷
Study of Eosin Y Photobleaching	Herculano 2013 ⁸⁸
β- lactoglobulin detection on solid support	Cevdek and Franko 2010 ⁸⁹
Determination of colloidal silver in drinking water	Korte-Kobylinska et al 2010 ⁹⁰
Determination of Ag concentration in drinking water for space aircrafts	Bruzzoniti et al 2010 ⁹¹
Detection of thiono-organophosphorous pesticides	Boskin et al. 2009 ⁹²
Quality certification of biodiesels	Lima et al 2009 ⁹³
Study of vegetable edible oils characteristics	Jimenez-Perez 2009 ⁹⁴

3.6 Thermal lens microscopy

In 2000 Takehiko Kitamori's group discovered that thermal lens measurements were possible under optical microscope⁸⁵ and in 2001 they designed a large and complex thermal lens microscope that could detect 1 ymole of sample¹⁴. Later they developed a more user friendly microscope that is now commercially available (<https://www.i-mt.co.jp/e02tech/thrmlens.html>).

In the thermal lens microscopy the pump and the probe beam are aligned coaxially under the microscope and focused with a single chromatic lens (Fig. 3.6). The resulting chromatic aberration for wavelengths of probe and pump beam is of a few μm thus enabling the detection of analytes in microwells and microchannels. The combination of TLM with microchip technology was suggested as a novel powerful tool for a variety of research fields⁸⁶.

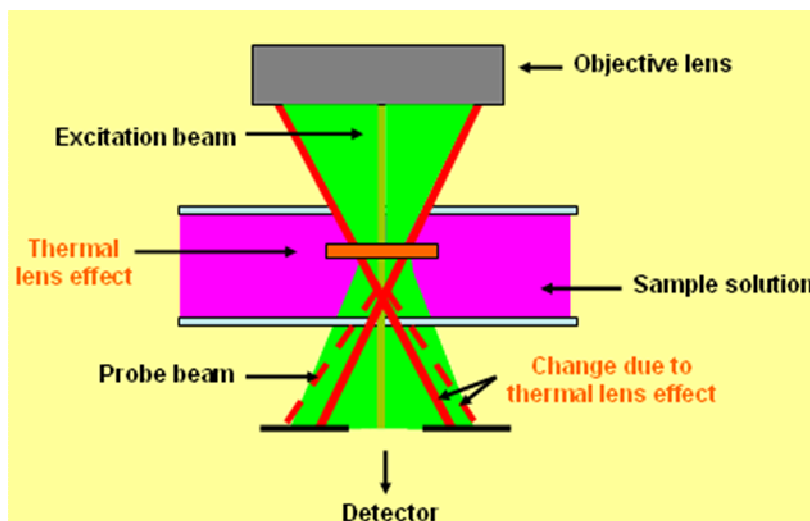


Figure 3.6 Scheme of the propagation of the beams in a thermal lens microscope

3.7 TLM combined with microfluidics chips

In microfluidics small amounts of fluids on the order of 10^{-8} 10^{-9} L are processed in a system basically consisting of a chip containing microchannels with dimensions in the range of 10-100 μm . A microfluidic system is generally composed of a device for introducing the liquid and the reagents into the system, a device to make the liquids flow in the system and mix them, and of a detection system. Other accessories are required for the specific type of experiment that will be performed on the chip.

The advantages of using a microfluidic chip are numerous. Physics of fluids differs from macro to micro-scale and this represents a big advantage in terms of reduced diffusion time for processes that are downscaled to a microfluidic chip. The diffusion time at microfluidics scale is reduced due to the fact that in the microchannels there is a high interface-to-volume ratio and a short diffusion distance, and the diffusion time decreases with the second power of distance. Analysis with multiple steps can be performed in a continuous flow on the same microchip, thus highly reducing operation time. The amount of reagents and power used is low, thus reducing the exposure of the operators to chemical hazards, decreasing the impact on the environment and the costs. Thanks to the improvement of the manufacturing

technologies^{87,88} of the accessories (for example micropumps) and materials^{89, 90}, a variety of microfluidics systems can be designed. For not elaborate systems basic chips are commercially available and are ready-to-use or can be customized by the distributors. The small dimension of a chip makes it suitable for in situ measurements and to perform reactions in parallel. Moreover microfluidic systems can be automated⁹¹.

Being the working volumes and related optical interaction lengths of a microfluidic chip so small, really sensitive detection systems are required. So far the most widely used methods of detection are based on fluorescence^{92,93,94,95,96}. Some other methods are based on electrochemistry^{97,98,99} and MS^{100,101}.

As for the already cited TL techniques in macroscale systems, TLM represent a powerful detection technique that complements the other fluorescence techniques in microfluidics systems. Both the time for the detection by TLM and for the reaction in a microfluidics chip are fast. Therefore, the time required for an analysis performed in such a kind of system can be really short. One significant example is represented by the time required for the antigen-antibody reaction to occur in the case of Immunoglobulin A that was reduced from 15 hours to 15 minutes downscaling the analytical system from a commercial microtiter plate for ELISA tests to a microchip-TLS system¹⁰². Some other applications of TLM for detection on microfluidic chips are described in the table 3.6.

Table 3.6 Examples of the application of TLM combined with microfluidics

Electrochemical valence control of uranium	Tsukahara et al. 2013 ¹⁰³
Detection of C reactive protein by micro-ELISA	Ohashi et al. 2010 ¹⁰⁴
Detection of thyroxine from serum sample	Islam et al. 2010 ¹⁰⁵
Detection of amino acids in buffers containing gold nano particles	Kitagawa et al. 2008 ¹⁰⁶
Detection of carbamate pesticides azo-derivatives in tetraborate buffer	Smirnova et al. 2008 ¹⁰⁷
Simultaneous detection of IgG from human, goat and chicken by using capillary-assembled microchip	Henares et al. 2007 ¹⁰⁸
Quantitative detection and fixation of gold nanoparticles on the wall of a microchannel	Mawatari et al. 2006 ¹⁰⁹
Cytochrome c monitoring in apoptotic cells	Tamaki et al. 2002 ¹¹⁰
Determinaiton of Co(II) in m-xylene	Minagawa et al. 2001 ¹¹¹
Subsingle-molecule determination of non fluorescent samples	Tokeshi et al. 2001 ¹⁴

3.8 TL coupled with FIA

In the flow injection analysis the samples and the reagents are injected into a flowing carrier stream. A FIA manifold is generally composed of a pump, an injection valve, a flow through detector and tubing that connects all the parts of the system. The pump propels the stream towards the flow through cell of the detection system via narrow tubing (usually with a diameter between 0.5 and 0.8 mm). The injection valve is used to inject a precise volume of the sample that in general is in the range of few μL up to few mL. The reaction takes place while the sample and the reagent run through the system and are mixed due to the fluid dynamics of flow through narrow-bore tubing. The product of the reaction is then detected as a transient peak with its height and area proportional to the concentration of the analyte. A schematic representation of a possible FIA system is represented in figure 3.7.

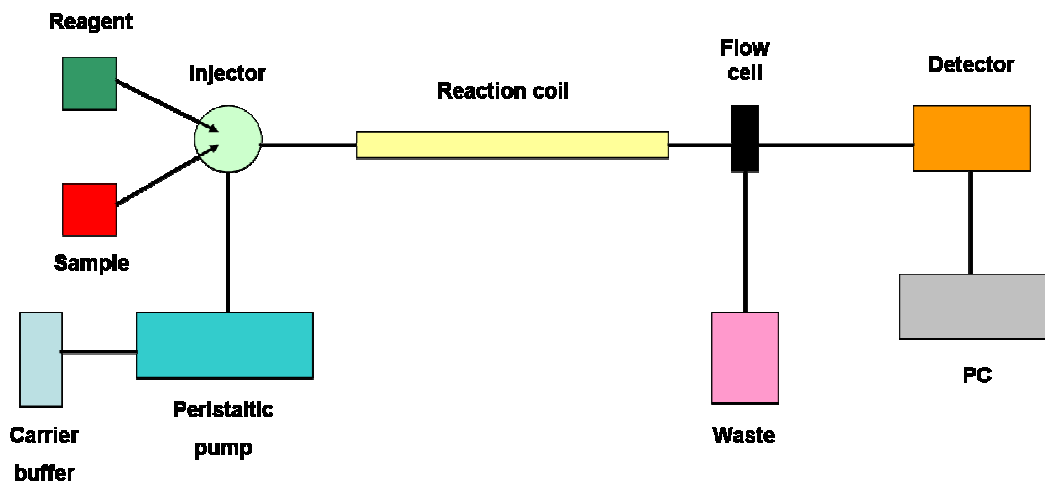


Figure 3.7 Scheme of a flow Injection system. The carrier buffer runs in the system driven by a peristaltic pump. The sample and the reagent are introduced in the flowing stream by an injector. The reaction occurs in a reaction coil and the product is detected while running in the flow cell. The signal recorded by the detector is then converted in numeric values by a PC software.

The advantages of FIA are many. It allows to increase the sample throughputs: only small amounts of sample are required and the time for the analysis in a flowing system is reduced. Moreover this technique has high versatility, robustness and reproducibility. New analytical improvements based on operating modes under non-stationary conditions have been made. FIA is simple, rapid and can be automated. Moreover the exposure of the operator under hazardous chemical and physical sample pre treatments is decreased. This technique is more environmentally friendly due to the downscaling of the processes and it allows the use of alternative detection systems with the concomitant simplification of the operating conditions (namely chemiluminescent detection). Furthermore flow analysis techniques are well-established tools for the automation and miniaturization of analytical methodologies and new applications have been used in the field of environmental analysis carried out by means of micro-total analysis systems (μ TAS)¹¹². In the table 3.7 some of the recent applications of FIA are listed.

Besides the already mentioned advantages the combination of FIA with TLS allows to avoid photodegradation of the analyte by the reduction of its exposure time to the laser. Moreover it allows the use of higher laser powers in order to improve the sensitivity of the system.

Table 3.7 Examples of analytical applications of flow injection analysis

Analysis of estrogenic compounds in methanolic solutions	Brocenschi et al. 2014 ¹¹³
Detection of human prealbumin in aqueous solutions	Ma et al. 2014 ¹¹⁴
Detection of highly polar pesticides in food	Mol and van Dam 2014 ¹¹⁵
Detection of aspartame in soft drinks and commercial pharmaceutical formulations	Radulescu et al. 2014 ¹¹⁶
Determination of guanine and adenine in beef	Thangaraj et al. 2014 ¹¹⁷
Determination of isoamyl nitrate in pharmaceuticals	Kishikawa et al. 2013 ¹¹⁸
Determination of protein content in dairy products	Liang and Li 2013 ¹¹⁹
Detection of pesticides in food, urine and blood plasma	Nanita and Padivitage 2013 ¹²⁰
Detection of acetaldehyde in saliva	Ramdzan et al. 2013 ¹²¹
Determination of titrable acidity and pH in wine	Vahl et al. 2013 ¹²²
Determination of hexavalent chromium in water	Madzgalj et. al 2008 ¹²³
Determination of hypochlorite in commercial products	Soto et al. 2008 ¹²⁴
Detection of Cu ²⁺ in wastewater	Tag et al. 2007 ⁹³
Determination of β -d-glucose in commercial medical solutions	Alvarez Romero et al. 2004 ¹²⁵

3.9 Removal of MC-LR from fresh water

3.9.1 State of the art in the removal of cyanotoxins from drinking water

Various water treatment processes have been suggested for the removal of intracellular or the inactivation of the extracellular cyanotoxins; some examples are coagulation¹²⁶, flocculation¹¹⁴, dissolved air flotation¹²⁷, microfiltration¹²⁸, ultrafiltration¹²⁹, adsorption on activated carbon¹³⁰, ultrasonication¹³¹ and photocatalytic degradation by TiO₂¹³². Oxidation processes have also been suggested but they can cause the lysis of the cells and thus toxins release in water, moreover the results about their efficacy are discordant. Ozonation was suggested to be a successful method to reduce MC-LR¹³³ but in a recent work it was reported that it increases the release of cyanotoxins from bacterial cells without being effective in their removal²⁶. The same group that reported the ineffectiveness of ozonation, found that chlorine, among the other tested chemicals, was the most effective in reducing the cyanotoxin. However this result is in contrast with previous reports where chlorination was found to cause a release of the toxin that was three time faster than its degradation by chlorine itself¹³⁴. Among the water treatment processes there is also the use of chlorine dioxide but in a recent study the formation of trihalometanes and haloacetic acids as disinfection by-products following the cell lysis of *Microcystis aeruginosa* by this chemical was reported¹³⁵. Furthermore the chlorine dioxide doses that can be used in a drinking water plant are not effective¹³⁶.

Apart from the discrepancies of the results, most of the aforementioned water treatments have the shortcoming of relying on the use of chemicals. In this work a novel, simple and green system for the removal of MC-LR from water based on polysaccharides composite materials is presented.

3.9.2 Novel polysaccharide composite materials for the removal of MC-LR

Polysaccharide composites are a category of materials with promising potential applications in the field of green chemistry¹³⁷. A composite is an engineered material made from two or more different constituents with different chemical and physical properties that are maintained separately in the finished material. Polysaccharide composites are of particular interest because they are environmentally friendly because of being degradable by microorganism without the need of other industrial processes. Furthermore, polysaccharides that are by-products of other processes could be used thus decreasing the impact on the environment and being more economically effective¹³⁸. Among the polysaccharides that are most commonly used in the preparation of these composite materials there are cellulose and chitosan.

Cellulose is the most common polysaccharide in nature and it is the main component of plants' cell wall and green algae. It is a polysaccharide consisting of a linear chain of several hundred to over ten thousand $\beta(1\rightarrow4)$ linked D-glucose units with a straight chain polymer organization that forms microfibrils. This structure confers to cellulose a high tensile strength. Cellulose is tasteless, odorless and biodegradable. Besides its traditional use in paper industry, new application of cellulose based materials have been developed. Cellulose has been used for microencapsulation, immunoisolation for allogenic or xenogenic implants¹³⁹, as wound dressing material¹⁴⁰ and tissue-engineered products for regeneration of damaged and diseased organs¹⁴¹. Cellulose beads have been used for protein immobilization, water treatment, and chromatographic material¹⁴². One drawback of cellulose as a constituent of composite materials is that it is insoluble in water and in most organic solvents due to its crystalline structure. High temperatures and concentrated acids are thus required to solubilize it¹⁴³. Moreover, these processes can involve side reactions¹⁴⁴ and the presence of impurities can be responsible for the modification of cellulose properties.

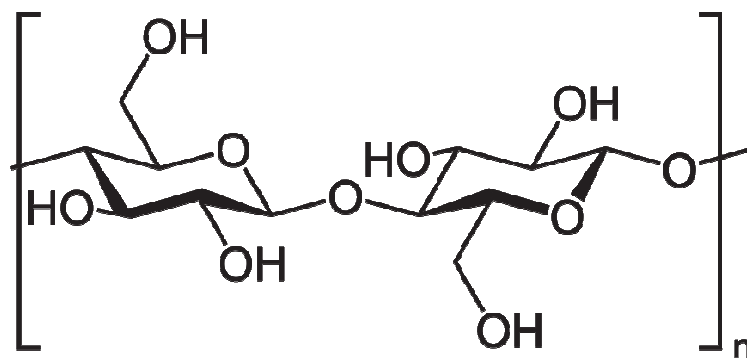


Figure 3.8 Structure of cellulose

Chitosan is a linear polysaccharide obtained upon partial deacetylation of chitin. Chitin is the second most abundant polysaccharide in nature after cellulose and it can be found in cell wall of fungi and in the exoskeleton of arthropods (where it represents the main component).

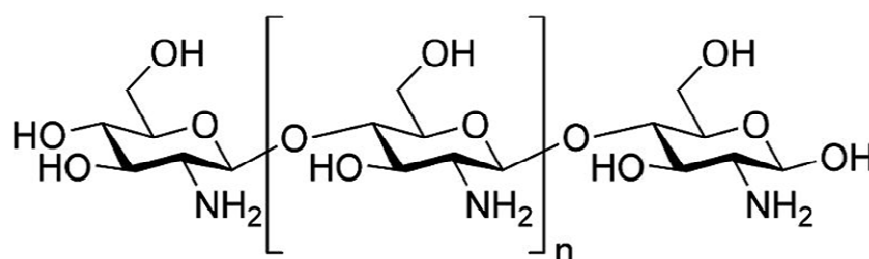


Figure 3.9 Structure of chitosan

Chitosan is a really versatile polysaccharide that has a variety of applications in many fields. The high number of N-groups makes chitosan a useful chelating agent and it makes it cost effective in comparison to cellulose that has a lower amount of N-groups and thus requires a synthetic substitution to functionalize it. Chitosan is biodegradable, relatively inert, non-toxic and biocompatible. Furthermore it has antibacterial¹⁴⁵ and wound healing properties¹⁴⁶ and it is easily processed into a variety of components such as gels¹⁴⁷, beads¹⁴⁸, scaffolds¹⁴⁹ etc. Structure and properties of chitosan have been exploited in medicine as a bactericide and fungicide

^{150,151}, hemostasis^{152,153}, drug delivery^{154,155}, cancer diagnosis^{156,157}, tumor treatment¹⁵⁸ and tissue regeneration^{159,160}. It has found application also in agriculture where it can be used for plant preservation¹⁶¹ and in winemaking for example to avoid the use of sulphur dioxide¹⁶². In food industry it has applications as a coating material to prolong the shelf-life of products¹⁶³, and its adsorbent properties have been exploited for water purification from metals¹⁶⁴, dyes^{165,166} and other water contaminants¹⁶⁷. Furthermore it has been reported that chitosan modified with fly ash or immobilized on clay, can adsorb and remove algae such as *Chlorella Pyrenoidosa*¹⁶⁸ or *Microcystis aeruginosa* from water¹⁶⁹.

Despite of its numerous useful properties, chitosan presents also some drawbacks. The intra and inter hydrogen bonds confer to this polysaccharide an ordered structure that is responsible for the previously described advantages but at the same time these bonds makes the chitosan poorly soluble in water as for cellulose¹⁷⁰. This implies that an acid is required to solubilize chitosan¹⁷¹. Furthermore chitosan swells in wet environments and this leads to weakening of its structure.

Recently it has been reported that an ionic liquid (IL), namely 1-butyl-3-methylimidazolium chloride ([BMIm⁺Cl⁻]), is able to dissolve both cellulose¹⁷² and chitosan¹⁷³. Ionic liquids are salts that are in the liquid state often up to 200 °C; they have many interesting properties such as chemical and thermal stability, high solubility power, non flammability, high ionic conductivity, and a wide electrochemical potential window¹⁷⁴. They are called *green solvents* because they differ from the traditional volatile compounds being their vapor pressure negligible and thus being recyclable¹⁷⁵. Their peculiar properties make IL good solvents and co-catalysts in many reactions including organic catalysis and inorganic synthesis¹⁷⁶.

The possibility to dissolve cellulose and chitosan in [BMIm⁺Cl⁻] at the same time brought to the development of a completely green composite material, being the IL recovered by distillation and hence recyclable¹⁷⁷.

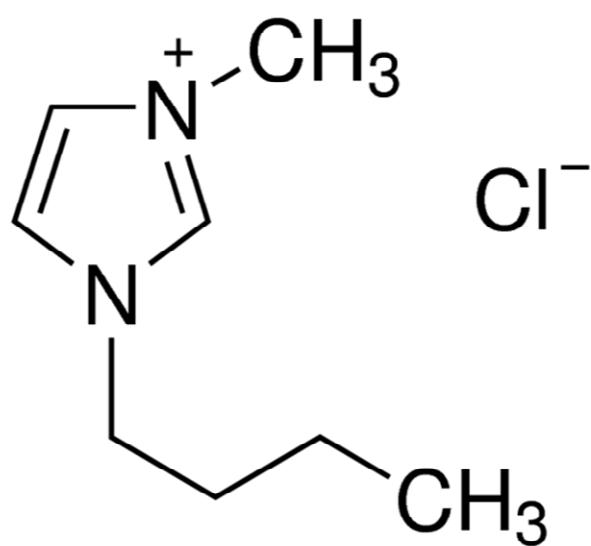


Figure 3.10 Structure of 1-butyl-3-methylimidazolium chloride

4-EXPERIMENTAL

4.1 Chemicals and reagents

Reagents and chemicals that were used in this work are listed in table 4.1

Table 4.1 Reagents and chemicals used

BSA	Sigma-Aldrich
Cross linked allophycocyanin (from cyanobacteria) Flogen®	FEBICO
Cr-phycoerythrin (from cyanobacteria) Flogen®	FEBICO
DTT	Sigma-Aldrich
EDTA	Sigma-Aldrich
Ethanol absolute	Sigma-Aldrich
K ₂ HPO ₄	Sigma-Aldrich
KH ₂ PO ₄	Sigma-Aldrich
MgCl ₂ •6H ₂ O	Fluka
Microcystin-LR (100% methanol solution)	DHI
Microcystin-LR (powder)	ENZO life sciences
Phosphatase 2A, C subunit, human recombinant, L309 deletion	Cayman chemical
p-NPP	Sigma-Aldrich
Potassium iodide	Fluka
TRIZMA base	Sigma-Aldrich

4.2 Buffers and solutions

All the water solutions were prepared using deionised water from a Milli-Q water purification system, MilliRO 5 PLUS (Merck Millipore, Merck KGaA, Darmstadt, Germany). A Potassium phosphate buffer (KPi) 0.1 M. pH 7 was used to dilute the cyanopigments. Other buffers that were used are listed in table 4.2.

Table 4.2 Buffers

Carrier buffer 1	Tris-HCl 40 mM pH 8.4, 34 mM MgCl ₂ , 4mM EDTA, 0.05mg/mL BSA, pNPP 1 mM
Carrier buffer 2	Tris-HCl 40 mM pH 8.4, 34 mM MgCl ₂ , 4mM EDTA, 0.05mg/mL BSA, pNPP 3 mM
Carrier buffer 3	Tris-HCl 40 mM pH 8.4, 34 mM MgCl ₂ , 4 mM EDTA, 0.05 mg/mL BSA, pNPP 20 mM
Enzyme buffer	Tris-HCl 40 mM pH 8.4, 34 mM MgCl ₂ , 4 mM EDTA, 0.05 mg/mL BSA, DTT 2mM

4.3 Thermal lens manifold

4.3.1 Conventional TLS system

The detector consisted of a dual-beam laser system. Depending from the experiments the excitation source (pump beam) was represented by an Argon-ion laser (Innova 90, Coherent Inc. Santa Clara CA, USA, operating at 514.5 nm or 457.9 nm) or by a Krypton laser (Innova 300 C Coherent) operating at 406.7 nm or 647 nm). The probe beam was represented by a Helium-neon laser (1103P, 632.8 nm, 2 mW JDS Uniphase Corporation, Milpitas CA, USA) or by a Helium-neon laser (25-LGR-393-230 533 nm, 4 mW Melles Griot, Carlsbad, CA, USA). The two beams were properly focused on the sample cell by a set of lenses while their collinear propagation was assured by a dichroic mirror (HR 514.5 nm or 457.9 nm/HT 632.8 nm/45 deg or HR533 nm/HT 47nm/45 deg and HR 632.8 nm/HT406.7 nm/45 deg Laser Components GmbH, Olching, Germany). The photothermal effect was induced by the pump laser that was modulated by a mechanical chopper (300 CD Scitec instruments Ltd, Trowbridge, U.K.) operating at 40 Hz. The consequent periodic changes in the refractive index gradient in the sample (related to the concentration of the sample) caused a defocusing of the probe beam resulting in a change of the probe beam intensity at its axis. This variation could be sensed by a PIN photodiode (Thorlabs Inc, Newton, NJ, USA) connected to a lock-in amplifier (SR830, Stanford

Research Systems Inc, Sunnyvale, CA, USA) and recorded, stored and later elaborated by a computer.

For batch mode measurements a 1 mL cell (1 cm pathlength) (101-QS Hellma Analytics GmbH & Co. KG, Müllheim, Germany) was used. For measurements performed in a FIA-TL system the cuvette was replaced by a 8 μ L flow-trough cell (Hellma 176.050-QS). The carrier buffer was pumped in the system by an HPLC pump (Smartline Pump 1000, Knauer, Berlin, Germany). The samples were injected in the system by a six port injector (A1358, Knauer) by means of microsyringes (Hamilton, Bonadutz AG, Switzerland).

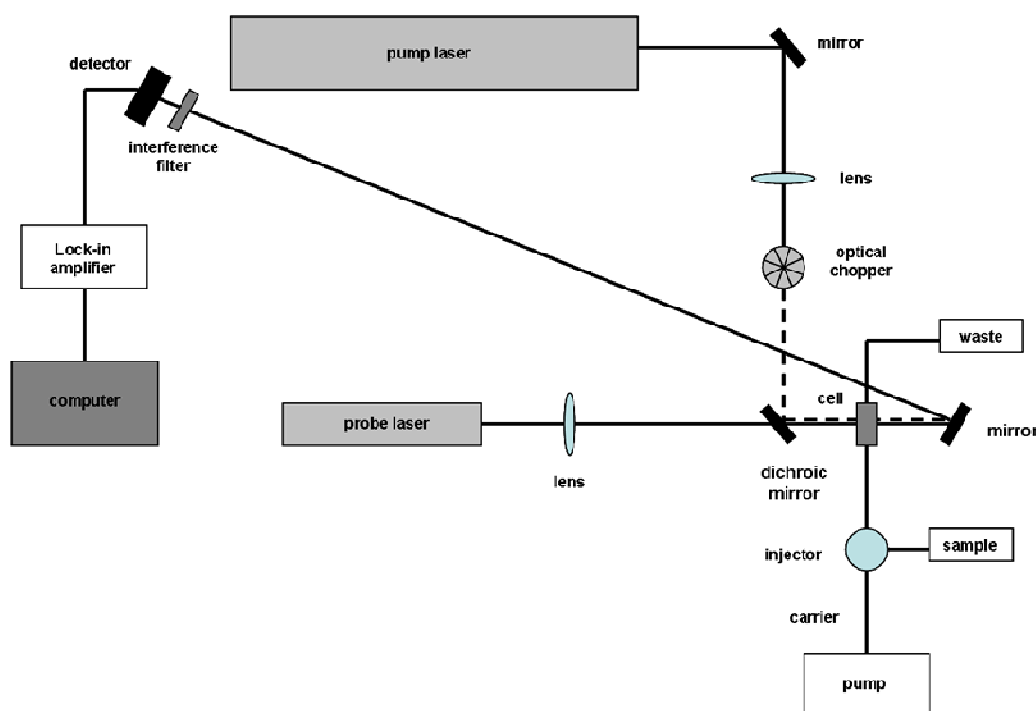


Figure 4.1 Scheme of a conventional TLS system

4.3.2 Commercial thermal lens microscope

A commercial thermal lens microscope (ITLM-10, IMT Co, Ltd, Sakado, Japan) operating with an excitation laser source of 532 nm and a probe laser source of 670 nm was used. The detector was composed of a silicon photodiode connected to a computer and the Cr-PE was detected in a 100 μ m capillary cell using an excitation

laser power of 20 mW. The position of the cell was changed at each measurement due to photodegradation of the sample.

4.3.3 Built in house thermal lens microscope

A thermal lens microscope built in house with an argon-ion laser as excitation source (wavelength = 514.5 nm, power = 85 mW) was exploited for the detection of Cr-phycoerythrin. For the experiments a commercial Y junction chip (part code No 3200008, Dolomite, Royston, UK) with an H interface (part code No 3200155, Dolomite) were used. The chip had microchannels 205 μm wide \times 100 μm deep, with one Y-junction channel and two straight channels.

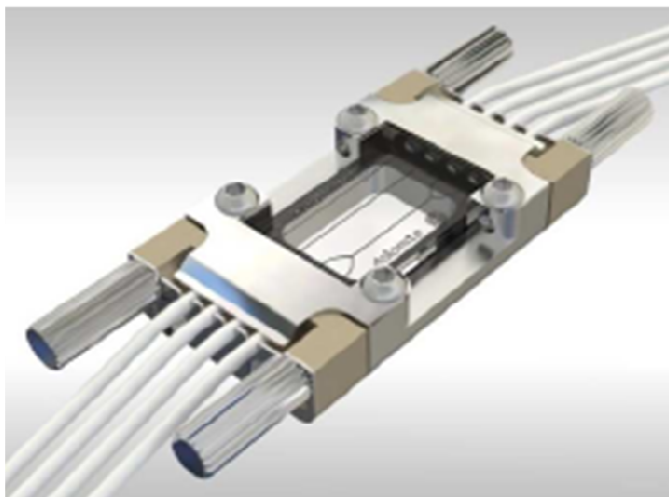


Figure 4.2 Commercial Y chip and H Interface

The Cr-PE solutions were injected by a microsyringe (Hamilton) in both settings and the pigment was detected directly on the microchip. The Cr-PE solutions were first detected in a static flow and in a gravity driven flow system. In the former, the buffer was not running in the system but only filling the microchip. In the latter, the pigment solutions were injected in a system where the flow was obtained by placing a syringe (filled with the carrier buffer and connected to the microchip by tubing) in a horizontal position and at different heights in order to obtain different flow rates (70 cm for the lowest 85 cm for the fastest).

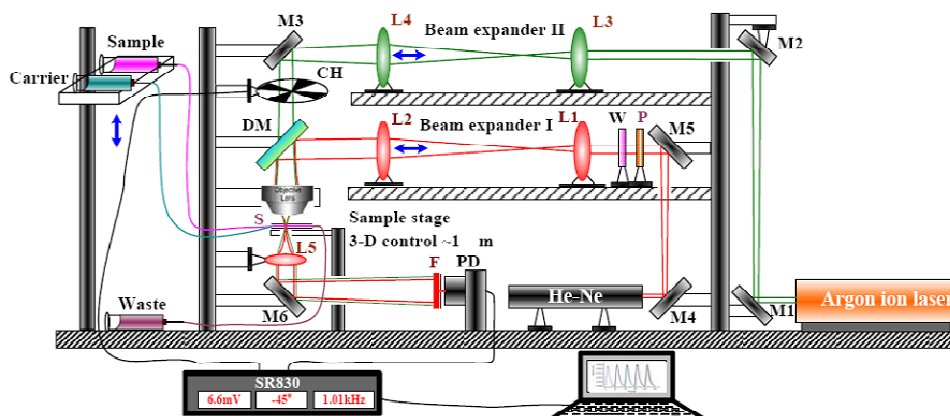


Figure 4.3 Scheme of the built in house TL microscope. A gravity driven flow system is shown. The pigment is detected directly in the chip that is placed under the thermal lens microscope [COURTESY: MingQiang Liu]

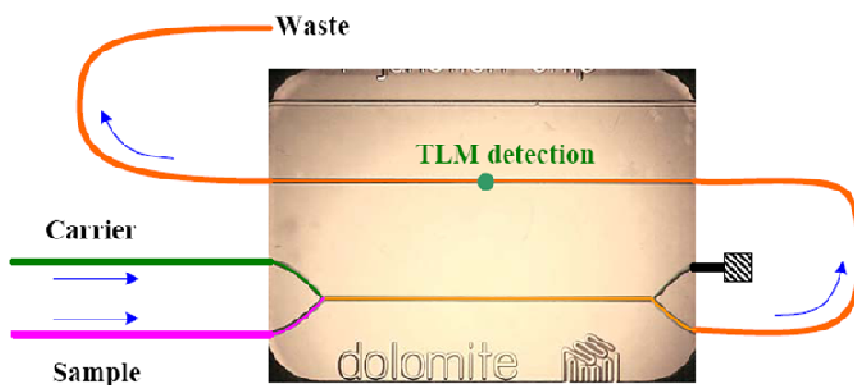


Figure 4.4 Scheme of the tubing connections to the chip [Courtesy MingQiang Liu]

4.3.4 Thermal lens signal, calibration curves and LOD calculation

In batch mode experiments the thermal lens signal (expressed in volts) was affected by photodegradation hence its strength was calculated taking in consideration the highest value obtained immediately after excitation of the samples. Since batch mode experiments were carried out just as preliminary tests, and were not foreseen in further experiments, only a single point calibration was performed at this stage.

The thermal lens signal obtained in a flow injection system is represented by peaks. In this work the height of the peaks was used to quantify the signal. In the case of

cyanopigments detection, the average heights of the peaks from three consecutive injections of the same sample solution were used. For most samples the differences between signals from consecutive injections were within 10% or less. In the rare cases where large differences were observed between replicates the, outliers were retained or rejected based on the Q test¹⁸⁷. In the case of MC-LR detection, only two peaks were measured. Indeed, in two parallel long runs, the difference in the height of the peaks were not larger than 10%. Hence, in order to avoid wasting of expensive reagents, all the experiments were performed in duplicates (in all the replicas the difference in the height of the peaks were never larger than 10%). The baseline, given by the noise of the system and the signal of the carrier buffer, was subtracted to obtain the final value of each peak. The points of a calibration curves were obtained by taking the average of three reliable measurements. The LODs were measured according to the formula:

$$\text{LOD} = (3.3 \times \sigma_{\text{blank}}) / s$$

Where σ_{blank} is the standard deviation of the blank and s is the slope of the calibration curve¹⁸⁸.

The raw data were elaborated using OriginPro8 and Microsoft Office Excel 2003 softwares.

4.4 Absorbance measurements

Absorbance measurements were recorded with a LAMBDA 650 UV/VIS spectrophotometer (Perkin-Helmer, Waltham, MA, USA) operating with a deuterium lamp. Data were acquired by the UV WinLab software (Perkin-Helmer). The samples were detected in a 3.5 mL spectrophotometric cell (100-OS, Hellma).

4.5 Fluorescence measurements

Fluorescence measurements were performed with a steady state fluorimeter (FS920, Edimburgh Instruments Ltd, Livingston, UK) with a 450 W Xenon lamp as the source of excitation. Emission spectra were obtained using an excitation wavelength of 540 nm for Cr-PE. The fluorimeter FS920 was controlled by an Edinburgh Instruments workstation on which the F900 spectrometer software was running. A daily stock solution 1 mg/mL of Cr-PE was prepared diluting the FEBICO commercial stock solution in KPi 0.1 M pH 7. Sample solutions were prepared in a 5 mL volumetric flask by pouring the ethanol or potassium iodide first, then the pigment and finally bringing to the final volume with phosphate buffer. A volume of 2.4 mL was used for each measurement; every solution was prepared just before recording the spectrum and always kept in the dark by covering the volumetric flask and the fluorescence cell (Hellma, 101-OS, 3.5 mL) with an aluminum foil.

4.6 Protein phosphatase inhibition assay

The PPIA was developed in two steps. Firstly, the best experimental conditions in order to obtain detectable amounts of para-nitrophenolate from the reaction of PP2A with pNPP were investigated. Then the assay was optimized for the use with protein phosphates 2A. Hereafter the reaction of PP2A with pNPP in the absence of MC-LR will be referred to as *colorimetric reaction*.

4.6.1 Colorimetric reaction in a 96-multiwell plate

Solutions of DTT 10 mM, pNPP 0.1 M and PP2A diluted in Tris-HCl buffer 40 mM pH 8.4 were prepared daily. Multiwell plates with flat bottom (Costar 3696, Corning, NY, USA) were used. The wells were filled with 150 and 100 μ L of Tris buffer in the case of the blank and the sample, respectively, 50 μ L of enzyme solution (sample), 50 μ L of DTT 10 mM (2 mM final concentration) and 50 μ L of pNPP 0.1 M (20 mM final concentration). The substrate was added after 5 minutes of incubation at 36 °C under gentle shaking in an incubating waving shaker (Talboys, Sigma-Aldrich, Saint Louis, MO, USA) . The first measurement was recorded immediately after adding the p-NPP and further measurements were taken every 10 minutes. The 96-microwell plate was kept at 36°C under gentle shaking between the measurements. Kinetic measurements were performed by recording the absorbances

at 405 nm by a TECAN multiwell plate reader (Spectra® photometer, TECAN, Milan, Italy) with a 492 nm filter as reference. No sample absorption is expected at the reference wavelength. The instrument measures the absorptions at both wavelengths and subtracts the values obtained at 492 nm (background) from the one obtained at 405 nm. This subtraction it is not strictly necessary but allows to obtain more accurate data when comparing different runs.

4.6.2 Protein phosphatase inhibition assay in a 96 multiwell plate

Solutions of p-NPP, PP2A and DTT were prepared daily as previously described. Microcystin solutions were prepared diluting a 100% methanol stock solution in Tris-HCl buffer. The wells were filled with 150, 100 and 50 μ L of TRIS buffer in the case of the blank, the control and the sample, respectively, 50 μ L of enzyme solution (control and samples), 50 μ L of DTT 10 mM (2 mM final concentration), 50 μ L of pNPP 0.1M (20 mM final concentration) and 50 μ L of microcystin solution. Measurements were performed as described previously.

4.6.3 Colorimetric reaction in a spectrophotometric cell

Solutions of p-NPP, and DTT were prepared as previously described for the experiments in the 96-multiwell plate. The enzyme (2 μ L i.e. final concentration of PP2A in the cell equal to 0.96 μ U/ μ L) was added directly in the cell containing 497 μ L of Tris buffer and 167 μ L of DTT 10 mM and incubated at 36 °C for 5 min in a thermostatic bath composed by a bath vessel and a immersion thermostat (EH 4 and EH 4.2, IKA, Staufen, Germany). The substrate (167 μ L p-NPP 10 mM) was added just prior the first measurement. Between the measurements (taken every 5 min) the cell was kept at 36 °C.

4.6.4 Colorimetric reaction in a FIA-TLS system

Since finding the optimal experimental conditions to perform the colorimetric and the protein phosphatase inhibition assays was one of the goals of this work, more details are given in the next chapter.

4.6.4.1 System set up

The detector consisted of a dual beam laser system. The pump beam was represented by an Argon-ion laser operating at 457.9 nm (P=100 and 10 mW) while the probe beam was a Helium-neon laser operating at 632.8 nm (P= 2 mW). The reaction occurred in a reaction coil connected by PDVF tubing to the injector and to the flow through cell. In order to keep the experimental conditions at 36°C, the coil was submerged in the bath vessel where the deionised water was heated by the immersion thermostat.

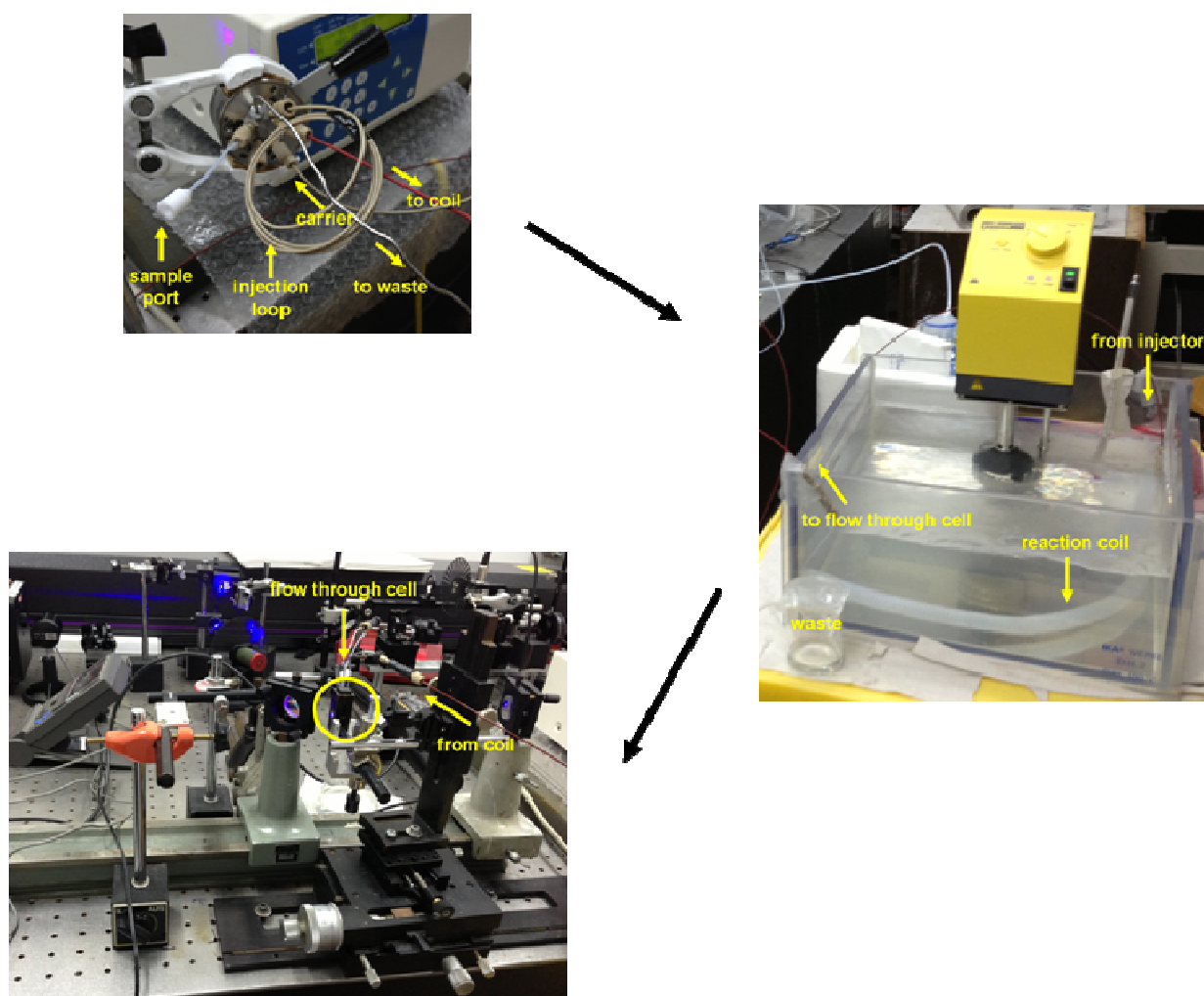


Figure 4.5 System set up for the detection of MC-LR

4.6.4.2 Colorimetric reaction

Depending on the different experiments the carrier buffer contained p-NPP in a concentration equal to 1, 3 or 20 mM. In the first experiment two different enzyme solutions were used. The first one was prepared by adding PP2A (0.2 mU/ μ L, glycerol 25%) to a Tris-HCl buffer solution containing 2 mM DTT (final concentration). The second enzyme solution was prepared by adding PP2A (0.2 mU/ μ L, glycerol 25%) to the carrier buffer solution. All the further experiments were carried out diluting the enzyme in the carrier buffer solution. Solutions were prepared fresh and filtered daily.

4.6.4.3 Protein phosphatase inhibition assay

Microcystin solutions were prepared as for the inhibition assay in a 96-multiwell plate but without the presence of DTT. Sample solutions were prepared by first diluting the enzyme in a Tris buffer without pNPP and subsequently adding the microcystin solution and the p-NPP solution. The extent of the inhibition was measured as the difference between the height of the peaks in the absence and in the presence of microcystin.

4.7 Adsorption of MC-LR on composite materials

4.7.1 Composite materials

Different composite materials (also referred to as *films* in this work) already prepared in the laboratory of Dr. Tran at Marquette University¹⁷⁷ were tested (see the table 4.2). The films were prepared dissolving different materials at different concentrations using the ionic liquid butyl methylimidazolium chloride ([BMIm⁺Cl⁻]) as solvent.

Table 4.3 List of the tested composite materials. Composition and relative percentage of the tested material are shown

Composite material	Abbreviation used in the text
50% chitosan 50% triciclodextrins	[50% CS-50% TCD]
50% chitosan 50% dibenzo-18-crown-6	[50% CS-50% DB18C6]
50% cellulose 50% dibenzo-18-crown-6	[50% CEL-50% DB18C6]
50% cellulose 50% triciclodextrins	[50% CEL-50% TCD]
60% cellulose 40% triciclodextrins	[50% CEL-40% TCD]
75% cellulose 25% triciclodextrins	[75% CEL-25% TCD]
100% cellulose	[100% CEL]
100% chitosan	[100% CS]
67% chitosan 33% cellulose	[67% CS-33% CEL]
50% chitosan 50% cellulose	[50% CS-50% CEL]
40% chitosan 60% cellulose	[40% CS-60% CEL]
29% chitosan 71% cellulose	[29% CS-71% CEL]
20% chitosan 80% cellulose	[20% CS-80% CEL]

4.7.2 Experimental set up

A daily stock solution of 3.7 mg/L of MC-LR diluted in deionised water was used for all the experiments. Dried materials (i.e. left for 2-3 days at room temperature in a 60% humidity controlled chamber after removal of the IL) were used to perform the kinetic experiments. Twenty mg of material (Fig. 4.6) were cut and washed before use in order to remove any preparation contaminant eventually present. The materials were stirred in de-ionized water for 24 hours at room temperature. Water was changed every 4 hours and each washing was done in 2 L of water. Spectrophotometric measurements at 214 and 293 (Lambda 35 UV/VIS spectrometer, Perkin Elmer, Waltham, MA, USA) were performed on the washing water in order to monitor the possible presence of contaminants and in particular of the ionic liquid [BMIm⁺ Cl⁻].

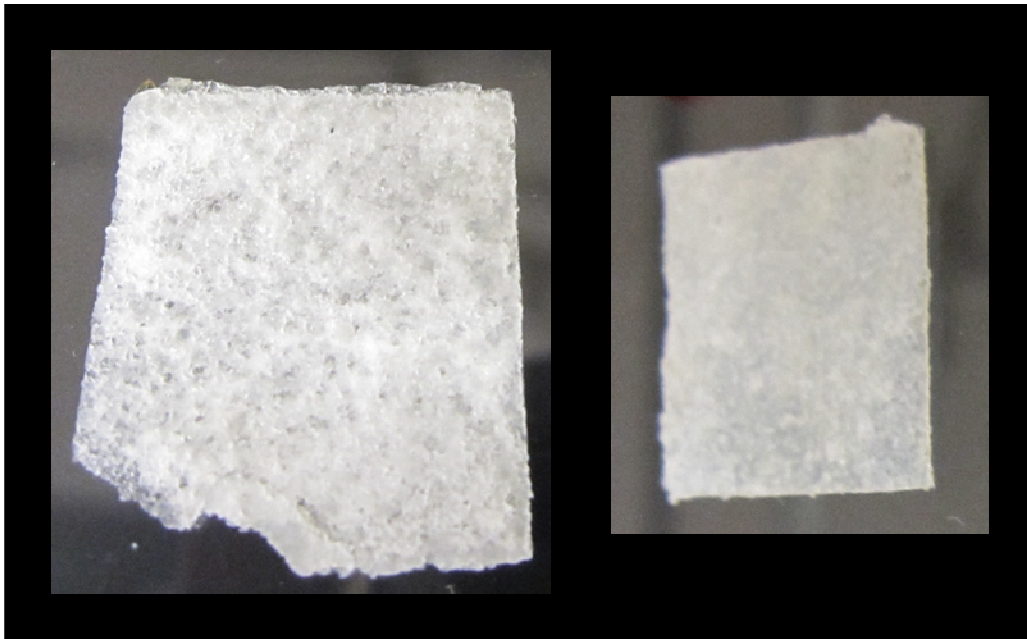


Figure 4.6 Composite materials. Two 20 mg pieces of composite materials are shown: [100% CS] (left) and [50% CS-50%CEL] (right). The difference in the dimensions (approximately 1.5 x 1.5 cm for [100% CS] and 1.0 x 1.3 cm for [50% CS-50%CEL]) are due to the different composition of the films.

In order to avoid the damage of the material during the washing a support was designed. The support was composed of a thin piece of PTFE rectangular shaped with 4 windows and two PTFE meshes. The samples were inserted in the windows, covered by the meshes and the three parts were fixed together by using plastic clips (Fig. 4.7). The support enabled to avoid the damage of the samples due to the turbulence of water under stirring while the meshes allowed the free circulation of water through the materials. The washed materials were placed in a spectrophotometric cell (1cmx1cm square spectrophotometric cell) that was then filled with 2.7 mL of a 3.7 mg/L MC-LR solution (and deionised water for the blank). Absorbance measurements (Perkin Elmer Lambda 35 UV/VIS spectrometer) were taken at 238 nm every 10 min in the first 2 hours and then every 20 min. In order to ensure a good circulation of the solution in the spectrophotometric cell a small magnetic spin bar was used and the solution was taken under stirring for the whole measurement.

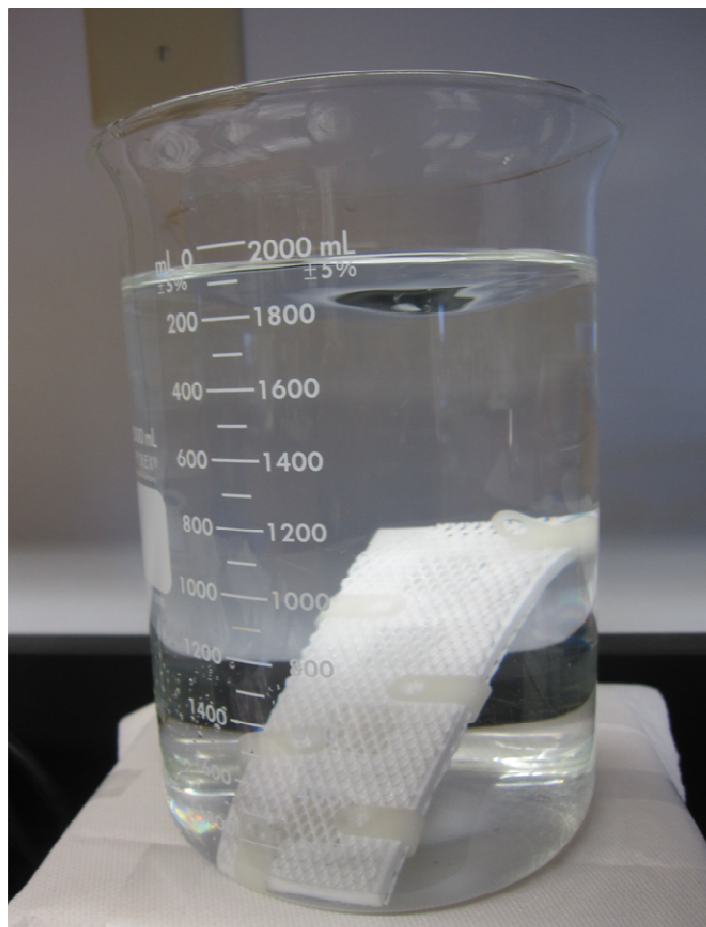


Figure 4.7 Support developed for washing the films

To avoid damaging from the magnetic bar the sample was inserted between two PTFE meshes and the spin bar positioned on the top of the mesh-composite-mesh sandwich (Fig. 4.8). If the sample was too big to lay down flat it was cut in small pieces in order to prevent an interference with the light beam of the spectrophotometer. Moreover cutting the bigger samples prevented a possible displacing of the spin bar resulting in the damaging of the sample or in an adequate mixing of the solution. The use of the meshes allowed the material to be protected from the stirrer but at the same time to have enough surface area in contact with the solution.

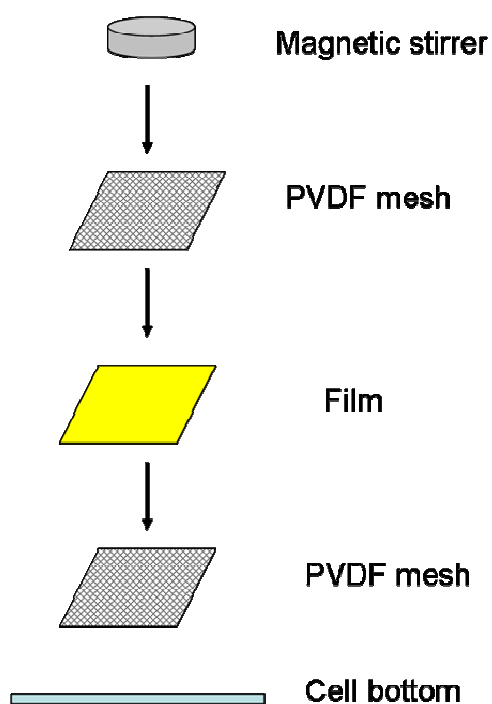


Figure 4.8 Scheme of the mesh-film-mesh sandwich.

4.7.3 Kinetics of adsorption

Adsorption of MC-LR on the films was observed as a time dependent decrease in the absorbance of microcystin solution at 238 nm. The percentage of adsorption of MC-LR on the films was calculated as the difference between the initial and the equilibrium concentration of the cyanotoxin solution. The concentration of MC-LR at $t=0$ and $t=\text{equilibrium}$ was extrapolated from calibration curves prepared by laboratory technicians on monthly basis from absorbance readings performed on the Perkin Elmer Lambda 35 UV/VIS spectrometer.

The mechanism of adsorption of MC-LR on the composite materials was investigated by fitting the kinetic data to the pseudo-first order and pseudo-second order models (described in the chapter 5). The best fitting model was chosen on the basis of the calculated coefficient of determination R^2 and the model selection criteria MSC:

$$\text{MSC} = \ln \left\{ \frac{\sum_{i=1}^n w_i (Y_{\text{obs}_i} - \bar{Y}_{\text{obs}})^2}{\sum_{i=1}^n w_i (Y_{\text{obs}_i} - Y_{\text{cal}_i})^2} \right\} - \frac{2p}{n}$$

Where Y_{obs_i} and Y_{cal_i} are observed and calculated values of i -th point respectively, w_i is the weight that is applied to the i -th point and that was considered 1 by default, n is the number of the points and p is the number of parameters.

R^2 and MSC were calculated from raw data elaborated by PSI-Plot software.

5-RESULTS AND DISCUSSION

5.1 DETECTION OF CYANOBACTERIAL PIGMENTS

In the first part of this work preliminary experiments were performed in order to investigate the possibility of using thermal lens spectrometry and thermal lens microscopy to detect cyanobacterial pigments.

5.1.1 Preliminary experiments in a TLS-batch mode system

5.1.1.1 Batch mode experiments on CL-APC in a conventional TL system

Preliminary experiments on CL-APC in batch mode were carried out in a dual beam thermal lens system where the pump beam was generated by a krypton laser (wavelength 647.1 nm, P=100 mW). A solution of CL-APC 10 $\mu\text{g/mL}$ in KPi pH 7 was measured. As it can be seen in figure 5.1 the TL signal showed a significant decrease with time meaning that under the given experimental conditions the pigment undergoes photodegradation processes. In particular the TL signal of CL-APC showed a decrease of 0.38 mV over a period of 180 s i.e. a drop of 30%. The high noise of the signal observed was due to a particularly high random fluctuation of the electricity in the system in the day of recording.

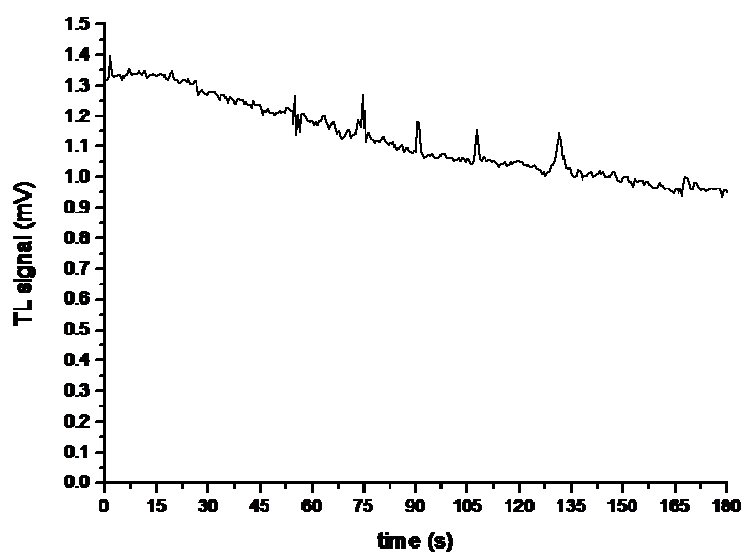


Figure 5.1 Photodegradation of CL-APC in a conventional TLS

5.1.1.2 Batch mode experiments on Cr-PE in a conventional TL system

Batch mode measurements of a solution of Cr-PE 10 $\mu\text{g/mL}$ in KPi pH 7 were performed in a thermal lens system where the pump beam was generated by an argon-ion laser (wavelength 514.5 nm, P=100 mW). Also in this case a considerable degree of photodegradation was observed (Fig. 5.2) with a decrease in the signal of 0.25 mV over a period of 180 s i.e. a drop of 68%, showing that Cr-PE TL signal is more affected by photodegradation than CL-APC. The noise observed in the case of CL-APC was not observed in the case of Cr-PE.

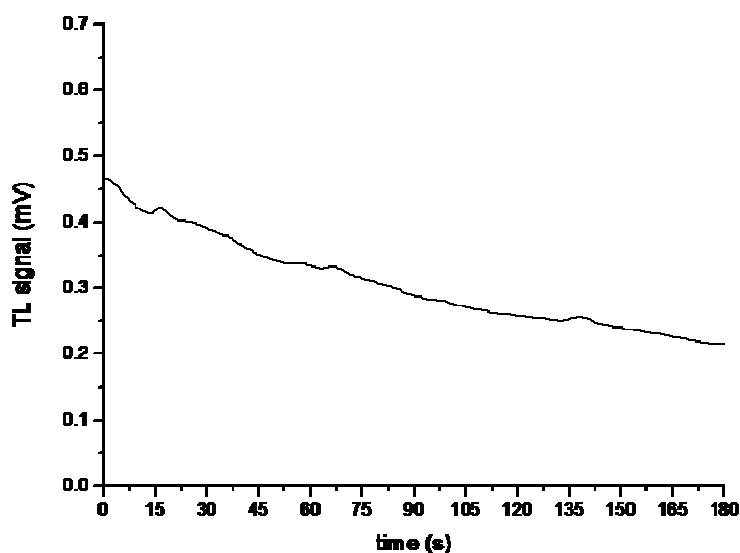


Figure 5.2 TL signal of Cr-PE in a conventional TL system

5.1.1.3 Batch mode experiments on Cr-PE by TLM

Preliminary experiments on Cr-PE were performed using a commercial thermal lens microscope (excitation wavelength 532 nm, laser power 20 mW). Solution of Cr-PE 1 mg/mL in KPi pH 7 was used. Higher concentration of cyanopigment, in comparison to the one used in the conventional TL system was chosen in order to demonstrate in the best possible way the expected photodegradation. Effectively, also in the case of TLM photodegradation of the pigment was observed (Fig. 5.3). The signal of Cr-PE decreased of 65%, i.e. 8.8 μV , in 3 minutes. The degradation rate was comparable to the one obtained in the conventional TL system even though the 5 times lower average power. This can be attributed to the much higher power

intensity due to tight focusing of excitation beam by microscopic objective lens and to the smaller irradiated volume of the sample.

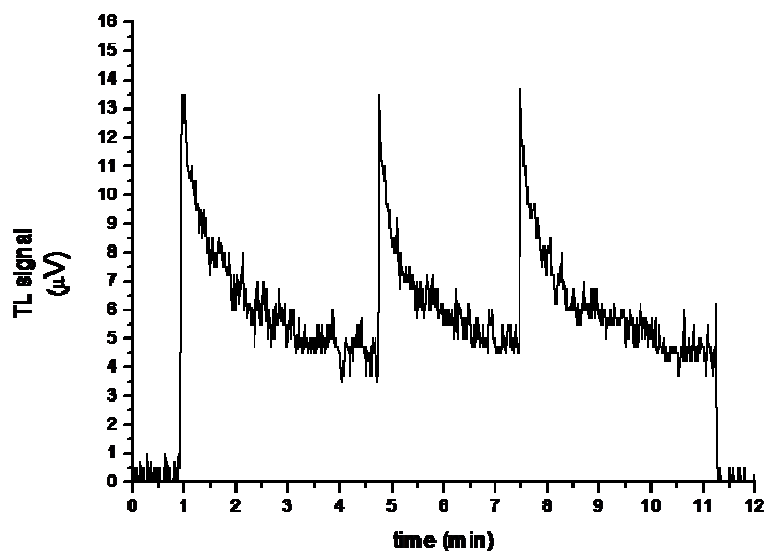


Figure 5.3 Photodegradation of Cr-PE in a TLM system

Figure 5.3 shows three measurements of the Cr-PE solution performed consecutively. Due to photodegradation, in order to repeat the measurements on the same sample the capillary cell was displaced after each recording. Both the height of the peaks and the degradation rate were the same for the three measurements proving that the signal was reproducible.

These preliminary results showed that both CL-APC and Cr-PE could be detected at a concentration of 10 $\mu\text{g}/\text{mL}$ by TLS. Moreover Cr-PE was successfully detected also by TLM at a concentration of 1 mg/mL . However the TL signal in both systems was highly affected by photodegradation processes and further improvements were needed in order to improve its stability.

5.1.2 Improvement of the TL detection by quenching

Another process that affects the efficiency of a thermal lens detection system is fluorescence which the absorbed energy is dissipated and is not available for generation of heat and temperature changes in the sample through non radiative de-excitation. Therefore the TL signal is decreased. Both cyanopigments are highly fluorescent (the quantum yield of CL-APC equals to 0.68 and it can be assumed that the quantum yield of Cr-PE is similar) therefore the possibility of further improving the detection sensitivity by fluorescence quenching was investigated. Preliminary experiments were performed in the presence of iodide (KI), a well known quencher which reduces the fluorescence quantum yield and should therefore increase the TL signal. Emission spectra of CL-APC and Cr-PE in the absence and in the presence of KI were recorded in order to evaluate if and how much the fluorescence of the two pigments was affected by the quencher.

5.1.2.1 Quenching effect of KI on CL-APC

Emission spectra (excitation wavelength = 600 nm) of 10 $\mu\text{g/mL}$ solutions of CL-APC in 0, 1 and 2.5 M KI were recorded by an Edinburgh Instruments Spectrophotometer F900. As expected, at increasing concentrations of KI decreasing fluorescence signals were recorded. In particular, in the presence of 1 M KI the decrease in intensity of emitted light at the fluorescence maximum of 650 nm was 37.7% while in the presence of 2.5 M KI the drop in the fluorescence signal was 60.7% (Fig. 5.4).

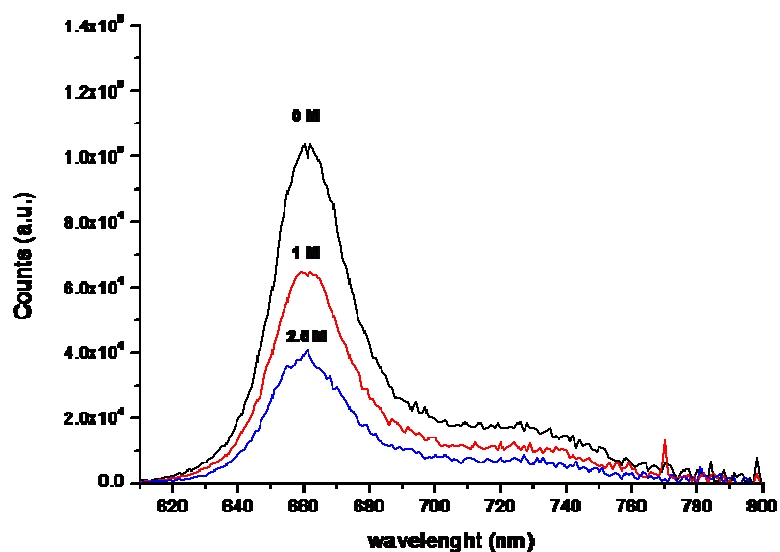


Figure 5.4 Fluorescence spectra of CL-APC in KPi (black line) and CL-APC in the presence of 1 M KI (red line) and 2.5 M KI (blue line).

5.1.2.2 Quenching effect of KI on Cr-PE

Emission spectra (excitation wavelength = 540 nm) of 20 $\mu\text{g/mL}$ solutions of Cr-PE in 0, 1 and 2.5 M KI were recorded (Fig. 5.5). Also in the case of Cr-PE at increasing concentrations of KI decreasing fluorescence signals were observed. In the presence of 1 M KI a fluorescence decrease at the fluorescence maximum of 43.5% was observed while in the presence of 2.5 M KI a decrease equal to 68.5% was observed.

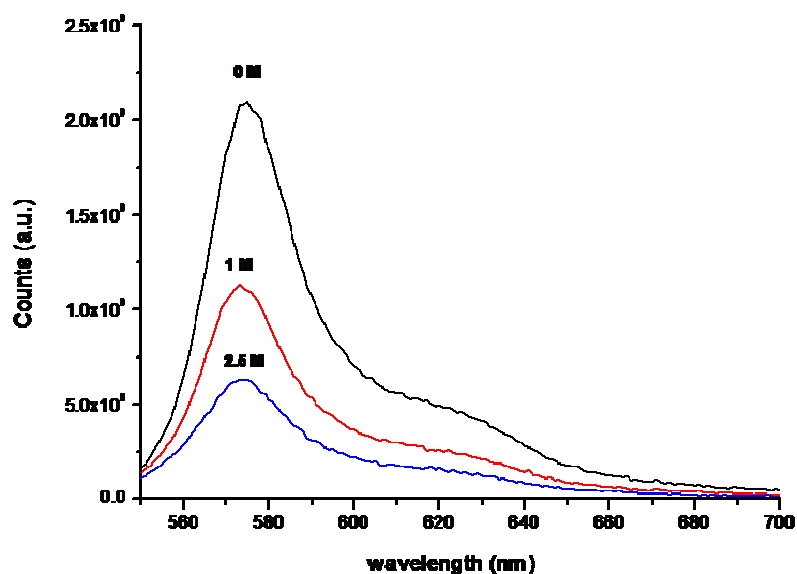


Figure 5.5 Fluorescence spectra of Cr-PE in KPi (black line) and Cr-PE in the presence of 1M KI (red line) and 2.5 M KI (blue line)

Results showed that potassium iodide is able to quench the fluorescence of both pigments but that Cr-PE fluorescence is more affected by this quencher. Under the given experimental conditions in fact the ratio of the fluorescence between CL-APC in KPi and CL-APC in KI was 1.6 and 2.5 for 1 M and 2.5 M KI, respectively. In the case of Cr-PE the ratio of the fluorescence in the absence and in the presence of 1 M and 2.5 M KI was 1.8 and 3.2 respectively.

Based on this further experiments were focused only on Cr-PE. Indeed this pigment looked more promising for the improvement of the TL systems, being Cr-PE more affected by quenching than CL-APC.

5.1.2.3 Quenching effect of KI on the TL signal

Once established that KI quenches the Cr-PE fluorescence, the effect of the presence of 1 M KI on the TL signal was tested on a solution of Cr-PE 10 $\mu\text{g/mL}$. In the presence of 1 M KI the observed TL signal of Cr-PE was 1.5 times higher than the one in KPi i.e. 0.69 mV and 0.46 mV respectively. The signals of Cr-PE solutions (5, 10, 15, and 20 $\mu\text{g/mL}$) in the presence and in the absence of 1 M KI were measured. The slopes of the calibration curves in the absence and in the presence of KI were $4.89 \times 10^{-2} \text{ mV } \mu\text{g}^{-1} \text{ mL}$ ($R^2=0.98384$, $\text{RSS}=2.35369 \times 10^{-8}$, $p=6.29713 \times 10^{-5}$) and $8.91 \times 10^{-2} \text{ mV } \mu\text{g}^{-1} \text{ mL}$ ($R^2=0.9895$, $\text{RSS}=5.05316 \times 10^{-8}$, $p=2.65504 \times 10^{-5}$) respectively (Fig. 5.6).

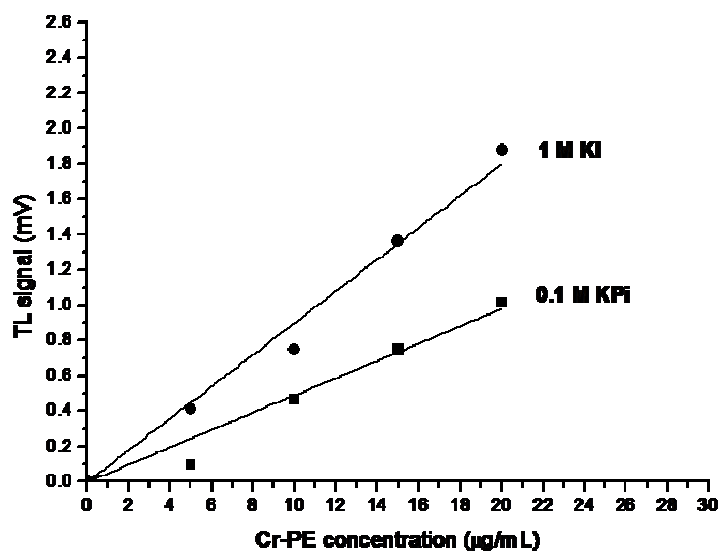


Figure 5.6 Calibration curves of Cr-PE in 0.1 M KPi and Cr-PE in 1 M KI

Assuming that the fluorescence quantum yield of Cr-PE is the same as the one of CL-APC (i.e. 0.68) it was calculated that in the presence of KI the decrease in fluorescence should have been around 40% and thus the absorbed energy that would have been converted to heat (that in the absence of quencher is the 32%) should have increased up to 59%. This value corresponds to an increase in sensitivity of 1.9 times in the presence of 1 M KI and it is consistent with the obtained slopes ratio that is equal to 1.82. Despite the increased sensitivity of the system in the presence of KI, the calculated LODs were almost the same i.e. 57 $\mu\text{g/mL}$ for Cr-PE in KPi and 56 $\mu\text{g/mL}$ for Cr-PE in 1 M KI. Due to this high noise problem, in this work no further experiments were carried out in the presence of KI. However it is expected that the noise could be reduced by purifying the quencher or by changing the quencher.

5.1.3 Improvement of the TL detection by the use of ethanol

Another possible way to improve the sensitivity of a thermal lens system is to use solvents that, due to their thermo-optical properties, enhance the thermal lens effect. Among these solvents, ethanol^{189,190} is one of the less expensive and less toxic. It was also demonstrated that it does not interfere with the stability of phycoerythrin¹⁹¹ and this represents an additional advantage in terms of sample preservation when working in a thermal lens system. Furthermore solvents as ethanol enhance the thermal stability of proteins¹⁹². For the aforementioned reasons, part of this work is focused on the study of the efficacy of using ethanol in order to improve the sensitivity of the TL system for the detection of Cr-PE. In the first step the effect of the presence of ethanol in Cr-PE solutions was investigated by recording the fluorescence and absorbance spectra of the pigment in the presence of different concentrations of the solvent. Once established the best range of solvent concentration to work with, the improvement in the sensitivity by the use of ethanol was investigated in TL and TLM systems.

5.1.3.1 Fluorescence spectra of Cr-PE in the presence of ethanol

Fluorescence spectra of solutions of Cr-PE 20 $\mu\text{g/mL}$ in the presence of different concentrations of EtOH (0, 0.5, 2.5, 5, 10 and 50% vol/vol) were recorded. A decrease of Cr-PE fluorescence signal (Fig. 5.7) that was dependent from the

increase of EtOH was observed for solvent concentrations in the range of 0-10%. In particular the losses were equal to 1.0, 11.8, 17.4, and 50.7% in the presence of 0.5, 2.5, 5 and 10% EtOH respectively. At the higher concentration of 50% the loss was equal to 81.3% moreover a shift in the emission maximum was observed.

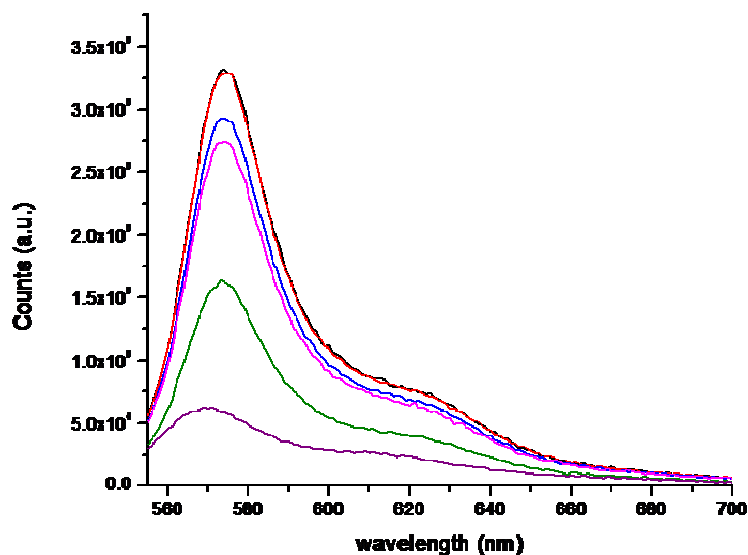


Figure 5.7 Fluorescence spectra of Cr-PE in KPI (black line) and of Cr-PE in KPI, 0.5% (red line), 2.5% (blue line), 5% (pink line), 10% (green line) and 50% (violet line) ethanol.

5.1.3.2 Absorbance spectra of Cr-PE in the presence of ethanol

Absorption spectra of Cr-PE 30 $\mu\text{g/mL}$ in EtOH 0, 0.5, 2.5, 5 and 10% vol/vol were recorded. As it can be seen in figure 5.8, for this range of EtOH concentrations the losses in absorbance are really modest being equal to 0.5, 3, 3.5 and 4.6% respectively.

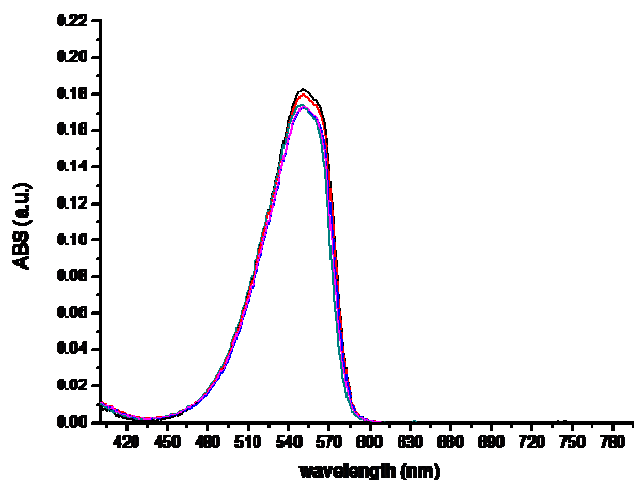


Figure 5.8 Absorbance spectra of Cr-PE in KPi (black line), and in 0.5% (red line), 2.5% (blue line), 5% (green line) and 10% (pink) ethanol.

5.1.3.3 Comparison between fluorescence and absorbance spectra of Cr-PE in the presence of ethanol

In order to understand if the drop of Cr-PE fluorescence in the presence of ethanol was due only to a loss in absorbance, the ratio between the maximum of fluorescence and the maximum of absorbance was calculated. As it can be seen from the table 5.1 the ratios between the fluorescence and the absorbance signals at different ethanol concentrations were not constant as it would be expected if the drop in fluorescence would be due only to a drop in absorbance. Therefore, it was reasonable to speculate that some solvent effect related to ethanol was involved in the loss of pigments fluorescence. This could represent an additional advantage, besides the already mentioned, in using ethanol for Cr-PE detection in a thermal lens system.

Table 5.1 Fluorescence –absorbance ratios of Cr-PE in the presence of different concentrations of ethanol

Ethanol % (vol/vol)	0%	0.5%	2.5%	5%	10%
Fluorescence intensity (counts)	3.323×10^5	3.290×10^5	2.928×10^5	2.746×10^5	1.640×10^5
Absorbance (a.u.)	0.18307	0.18224	0.17785	0.17663	0.17474
I_f/ABS	1.81×10^6	1.80×10^6	1.65×10^6	1.55×10^6	9.38×10^5

5.1.3.4 Ethanol effect on the sensitivity of a TL-batch mode detection of Cr-PE

Once established the effects of ethanol on the absorbance and fluorescence spectra of Cr-PE, the effect of this solvent on the sensitivity of a TLS system was investigated. A dual beam thermal lens system where the pump beam was generated by an argon-ion laser (wavelength 514.5 nm, P=100 mW) was used. A calibration curve was obtained from solutions at different concentrations (2, 4, 6, 8 and 10 $\mu\text{g/mL}$) of Cr-PE in KPi, EtOH 10% (Fig. 5.9). Ethanol addition resulted in higher background noise therefore the improvement in sensitivity was only slightly reflected in the improvement of Cr-PE detection. Indeed, the sensitivity of the system in 10% ethanol was 8 times higher than the one obtained previously in KPi (slope= 4.13×10^{-4} mV μg^{-1} , $R^2=0.99563$, RSS= 1.3754×10^{-7} , $p=2.72298 \times 10^{-7}$), while the calculated LOD in 10% ethanol was only 1.3 times lower than the one obtained in KPi, i.e. 43 $\mu\text{g/L}$.

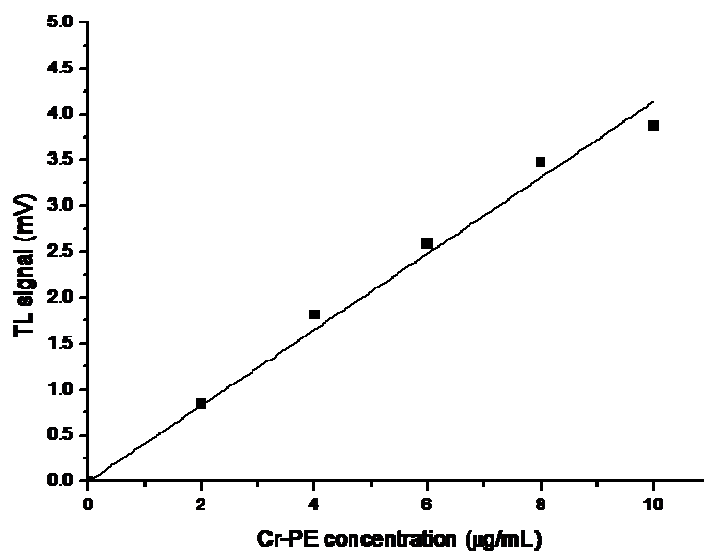


Figure 5.9 calibration curve of Cr-PE in EtOH 10% in a conventional TL system

5.1.4 Improvement of the TLS system by coupling with FIA

In order to reduce the exposure of the pigments to the intensive laser light, the thermal lens technique was coupled with the flow injection analysis.

5.1.4.1 Detection of Cr-PE in a FIA-TLS system

Experiments were performed in a system where the pump beam was given by an argon-ion laser ($\lambda=514.5$ nm, $P=100$ mW). Solutions of Cr-PE (5, 10, 15 $\mu\text{g/mL}$, 200 μL injection volume) in KPi pH 7 were injected into the carrier buffer (KPi pH 7) that was running in the system at a flow rate of 1 mL/min. The resident time of the sample in the flow through cell was 480 ms. Under the given experimental conditions reproducible peaks were obtained (Fig. 5.10).

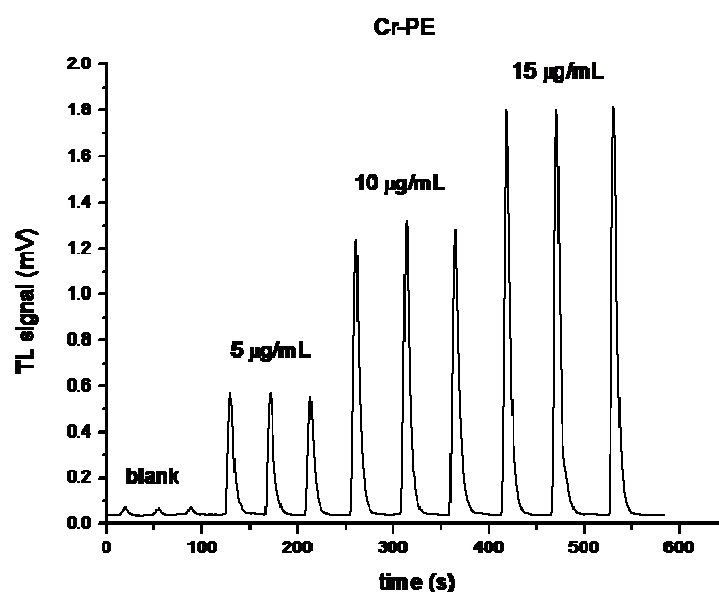


Figure 5.10 Signals of Cr-PE in a FIA-TLS system

Further measurements were carried out reducing the injection volume to 100 μL . Solutions of Cr-PE (0.05, 0.5, 2, 6, 10, 20 $\mu\text{g/mL}$) were injected in the carrier buffer (KPi pH 7) that was running at a flow rate of 1 mL/min. In the given experimental conditions the sensitivity of the system was equal to $1.5 \text{ mV } \mu\text{g}^{-1} \text{ mL}$ ($R^2=0.9999$) (Fig. 5.11) i.e. 31 times higher than the one obtained previously in batch mode. Despite this increase in sensitivity, the extrapolated LOD in the FIA-TLS system was only 4.35 times lower than the one obtained in batch mode i.e. 13 $\mu\text{g/L}$. This can be explained by a higher noise due to fluctuations in a flowing system where the carrier buffer is driven by a peristaltic pump. However the signals obtained in such a system are reproducible and calibration curves with regression coefficients higher than 0.99 can be obtained demonstrating that coupling the TLS system with FIA is a successful way to overcome the photodegradation of Cr-PE.

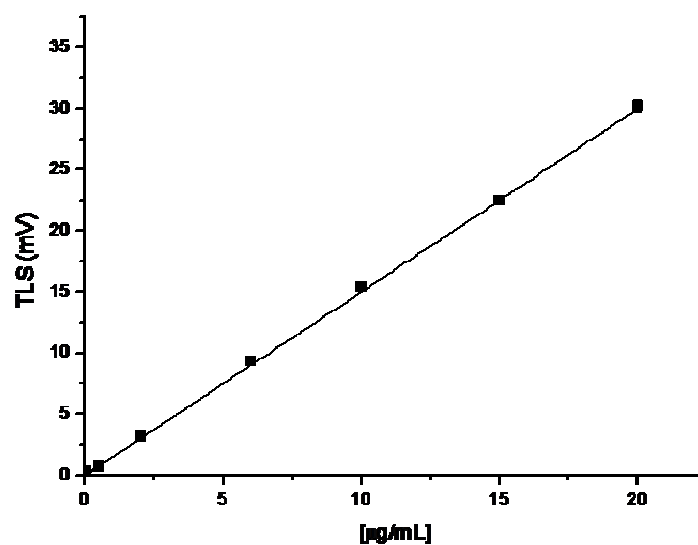


Figure 5.11 Calibration curve of Cr-PE in KPI in a FIA-TLS system. Slope=1.5 mV μg^{-1} mL, $R^2=0.99999$, RSS=77.67797, $p=0.00001$. For concentrations of 0.5 $\mu\text{g}/\text{mL}$ and higher the SD errors of 3 replicas were always between 0.02% and 5% while for the concentration of 0.05 $\mu\text{g}/\text{mL}$ the SD error was 10%.

5.1.4.2 Effect of ethanol on the sensitivity of a FIA-TLS detection of Cr-PE

The further step was to investigate the effect of ethanol on the sensitivity of a FIA-TLS system. Based on the preliminary test in batch mode and on additional recordings of the absorbance (Fig. 5.12) and fluorescence spectra (Fig. 5.13) of Cr-PE in the presence of 30% and 40% EtOH, a 40% concentration of the solvent was chosen to perform the experiment. Indeed, in these experimental conditions, there is a little loss of absorbance (7%) while the loss in fluorescence is around the 69%.

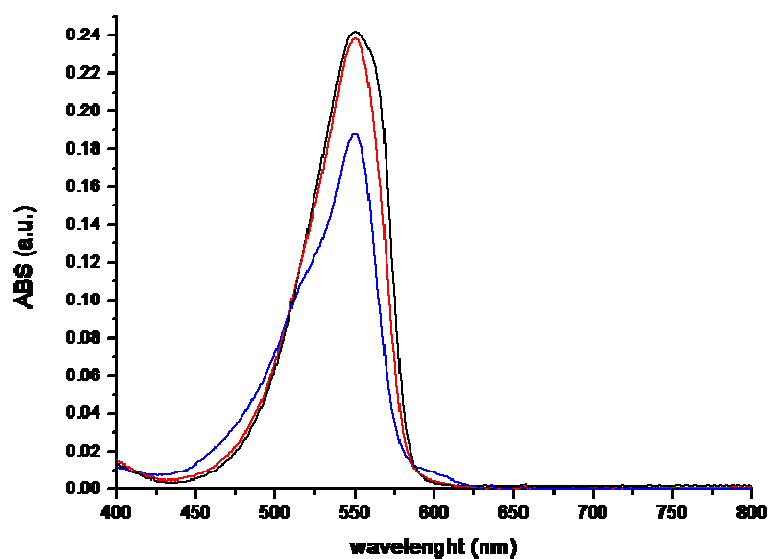


Figure 5.12 Absorbance spectra of Cr-PE in KPi (black line) and Cr-PE in 30% (red line) and 40% (blue line) ethanol.

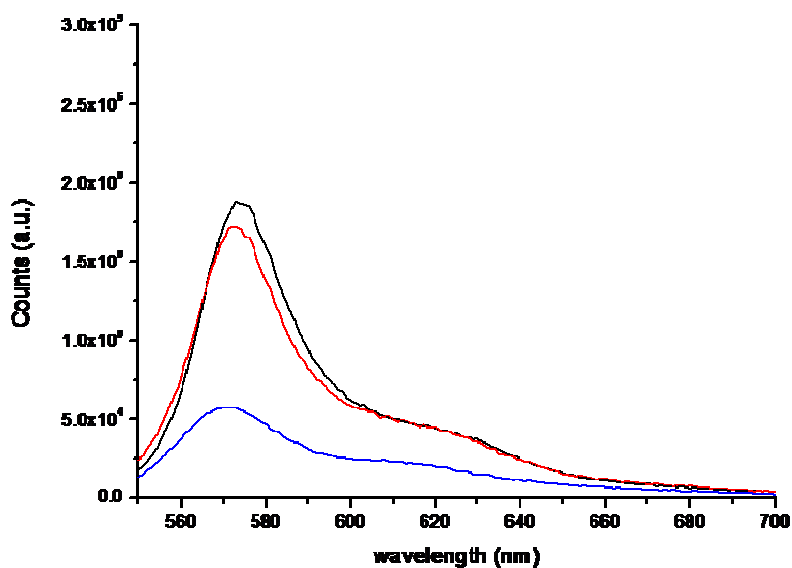


Figure 5.13 Fluorescence spectra of Cr-PE in KPi (black line) and Cr-PE in 30% (red line) and 40% ethanol (blue line)

A dual beam thermal lens system where the pump beam was generated by an argon-ion laser (wavelength 514.5 nm, P=100 mW) was used. The samples were injected with a 100 μ L loop in the carrier buffer (KPi, EtOH 40% pH 7) that was running at a flow rate of 1 mL/min. A calibration curve (Fig. 5.14) was obtained from solutions of Cr-PE in EtOH 40% (0.05, 0.5, 2, 6, 10 μ g/mL). The sensitivity of the system for Cr-

PE in the presence of EtOH 40% was 3.9 times higher than the one for Cr-PE in KPi, indeed the calculated slope was equal to $4.53 \text{ mV } \mu\text{g}^{-1} \text{ mL}$ ($R^2=0.99856$).

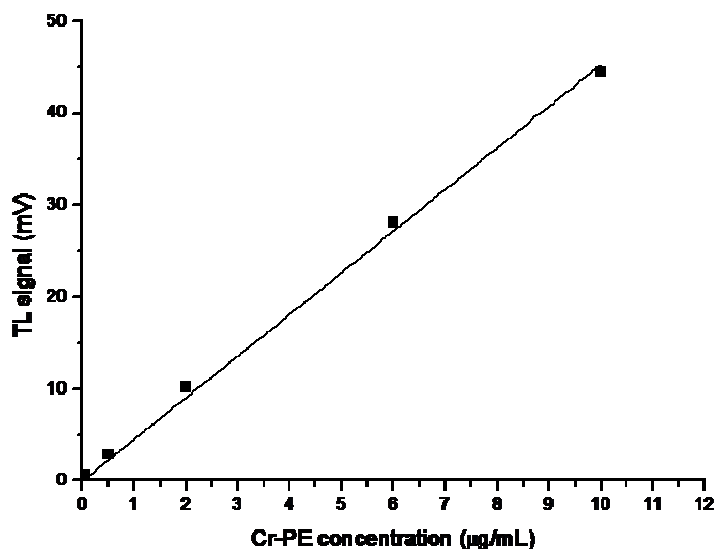


Figure 5.14 Calibration curve of Cr-PE in 40% EtOH in a FIA-TLS system. Slope= $4.53 \text{ mV } \mu\text{g}^{-1} \text{ mL}$, $R^2=0.99856$, $\text{RSS}=3.4662 \times 10^{-6}$, $p=1.71 \times 10^{-9}$. For concentrations of $0.5 \mu\text{g/mL}$ and higher the SD errors of 3 replicas were always between 0.1% and 3% while for the concentration of $0.05 \mu\text{g/mL}$ the SD error was 8%.

The extrapolated LODs were 40 and $22 \mu\text{g/mL}$. The former was obtained measuring the standard deviation of the heights of the peaks obtained after the blank injection (KPi, 40% EtOH) while the latter was obtained by taking in consideration the standard deviation of the baseline. The same calculations were performed in the previous experiment but the LODs in that case coincided. Probably the difference in the carrier buffer composition causes an increase of the noise. A possible solution for this problem could be achieved by reducing the pressure in the system by decreasing the flow rate.

Taking into account that on average one cyanobacterial cell ($60 \mu\text{m}^3$) produces about 0.2 pg of microcystins¹⁹³, than 5000 cells/mL are needed to reach the limit of $1 \mu\text{g/L}$ for microcystin in water. Considering that the average amount of PE in dry mass cyanobacterial cells is approximately around 4%, with the range between 1 and 8%¹⁹⁴, and by accepting that on average cyanobacteria contain $264 \text{ fg dry mass}/\mu\text{m}^3$

¹⁹⁵, than a comparable concentration of 3.2 µg/L PE corresponding to maximum contaminant level (MCL) for microcystin can be calculated. From the results that were obtained such low concentrations of PE are within reach of FIA-TLS. Indeed the lowest LOD that was obtained in this work is 13 µg/L in KPi i.e. only 4 times higher than the one calculated as the one corresponding to the MCL of microcystin. Further improvements in sensitivity of phycoerythrin detection by TLS can be achieved by reduction of the noise in the system, improvements in the thermo-optical properties of analyzed samples and by the use of appropriate quenchers. These further improvements are expected to make the FIA-TLS compares favorably to recently reported techniques which could be used as early warning systems for microcystins and are based on detection of cyanopigments⁴⁵. The achieved LODs already indicate that TLS could represent a powerful tool for the detection of cyanobacteria in water which can therefore detect early onsets of massive HABs in natural waters, where concentrations of cyanobacteria can peak up to 1000 times higher levels as needed to reach the MCL for microcystin.

5.1.5 Detection of Cr-PE in a microfluidic chip by a thermal lens microscope

In this work a further step in the exploitation of thermal lens techniques for the detection of Cr-PE was the downscaling of conventional FIA to a microfluidic system where the detection was performed by a thermal lens microscope built in house with an argon-ion laser ($\lambda_{exc}=514.5$ nm, P=85 mW) as excitation source.

5.1.5.1 Set up of the microfluidic chip-TLM system

A first set of experiments was performed in static flow in order to investigate whether the system was sensitive enough to detect Cr-PE. Different volumes (2 and 4 µL) of solutions of PE 15 and 45 µg/mL in KPi were injected manually into the system. As it can be seen in figure 4.15 it has been possible to obtain repeatable signals that were proportional with the injection volumes used.

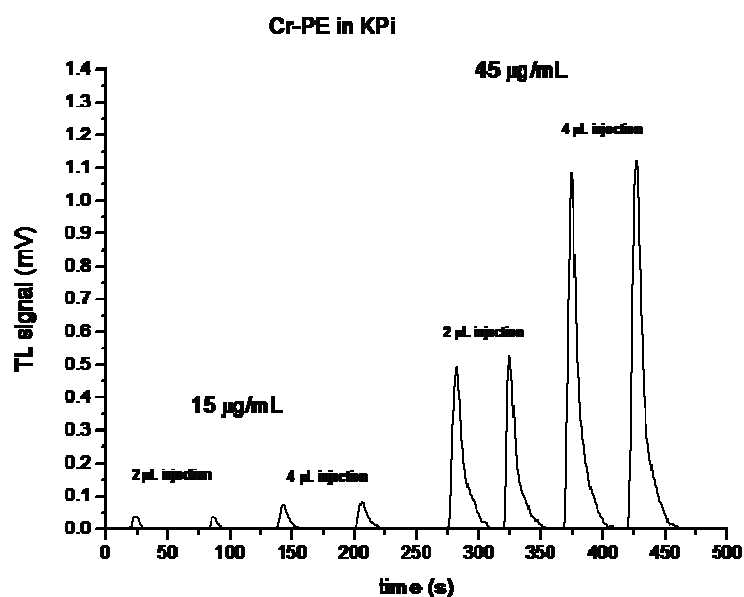


Figure 5.15 TL signals of Cr-PE in KPi in a TLM system

To further improve the system, different injection volumes were tested in order to gain a higher sensitivity. In addition a faster flow rate was tested in order to avoid the presence of the peak tails that have been observed previously. Experiments were performed at two different flow rates i.e. 0.625 and 0.91 $\mu\text{L/s}$ and injecting volumes of 4, 6, 8, 10 and 12 μL of 15 and 45 $\mu\text{g/mL}$ Cr-PE in KPi. Results showed that the optimal injection volume was 10 μL in both of the given experimental conditions. Indeed, when injection volumes larger than 10 μL were used, no significant increase of the TL signal was observed. Figure 5.16 shows TL signals obtained after the injection of 4, 6, 8, 10 and 12 μL of a 45 $\mu\text{g/mL}$ Cr-PE solution at a flow rate of 0.91 $\mu\text{L/s}$. The observed TL signals were equal to 0.22, 0.33, 0.39, 0.44 and 0.45 mV respectively, showing that the increase in the TL signal reaches a plateau at injection volumes equal to 12 μL . As expected, at a higher flow rate the tailing of the peaks was reduced (Fig. 5.17).

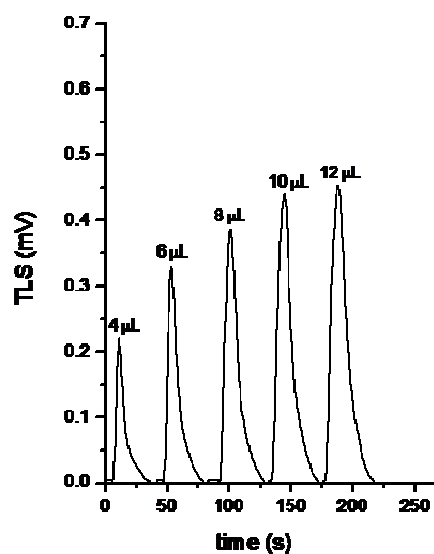


Figure 5.16 TL signals of different injection volumes of Cr-PE in a TLM-gravity driven flow system.

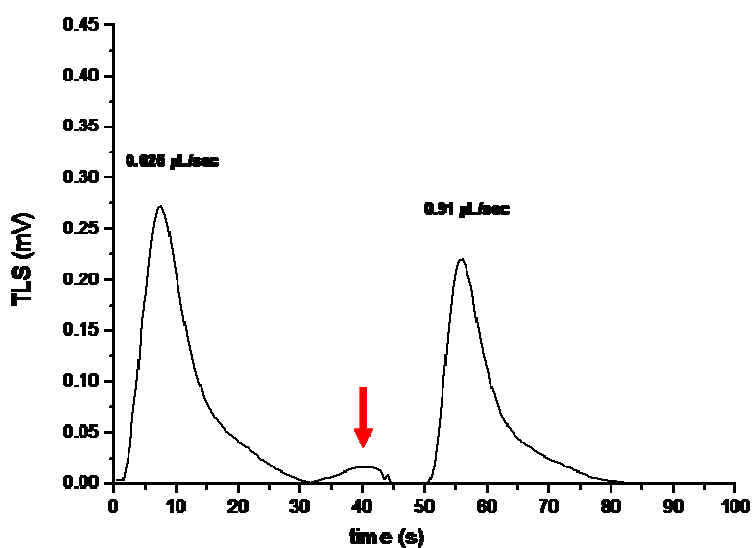


Figure 5.17 TL signals of Cr-PE in a TLM-gravity driven flow system at different flow rates. Peaks corresponding to 4 μL injections of Cr-PE 45 $\mu\text{g}/\mu\text{L}$ are shown. A peak tail (red arrow) is observed at the flow rate of 0.625 $\mu\text{L}/\text{sec}$ but not at the higher flow rate of 0.91 $\mu\text{L}/\text{sec}$.

5.1.5.2 Improvement of the TLM-microfluidic system by addition of ethanol

The improvement in the sensitivity by the use of ethanol was tested also in the microfluidic system. Experiments were performed by injecting volumes of 4, 6, 8, 10, and 12 μL of 15 and 45 $\mu\text{g}/\text{mL}$ Cr-PE in KPi containing 30% and 40% EtOH. Working with the same experimental set up as in previous experiments (performed in the absence of EtOH) the resulting flow rates were slower (i.e. 0.33 and 0.45 $\mu\text{L}/\text{s}$) due to the different densities of the solutions. Similarly to the experiment performed in the absence of ethanol the injection volume of 10 μL was proven to be the best option. A better repeatability of the peaks was achieved working at a flow rate of 0.45 $\mu\text{L}/\text{s}$. Anyhow, under these experimental conditions, reproducible peaks were obtained but only the signals of the solutions added with 30% EtOH resulted to be proportional with the injection volumes. Therefore calibration curves (0.5, 1, 2, 5 and 10 $\mu\text{g}/\text{mL}$) in the presence and in absence of EtOH 30% (Fig. 5.18) were recorded injecting 10 μL of the solutions in a flow rate of 0.45 $\mu\text{L}/\text{s}$. Figure 5.19 shows the reproducibility and coherence of the Cr-PE signals used to plot the calibration curve in EtOH.

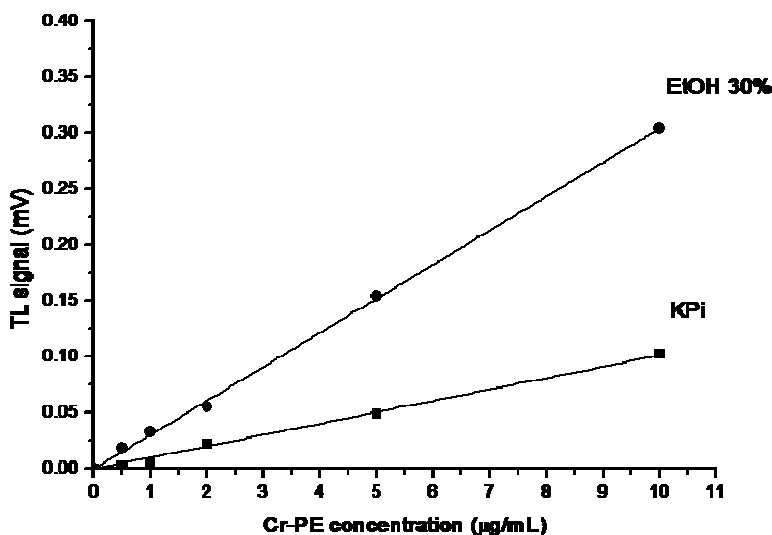


Figure 5.18 Calibration curves of Cr-PE in KPi and Cr-PE in 30% EtOH in a TLM-gravity driven flow system. Cr-PE in KPi: slope= 1.01×10^{-2} mV μg^{-1} mL, $R^2=0.99674$, RSS= 1.33512×10^{-9} , $p=2.55 \times 10^{-6}$. For concentrations of 1 $\mu\text{g}/\text{mL}$ and higher the SD errors of 3 replicas were always between 0.6% and 4% while for the concentration of 0.5 $\mu\text{g}/\text{mL}$ the SD error was 14%. Cr-PE in 30% EtOH: slope= 3.04×10^{-2} mV μg^{-1} mL, $R^2=0.99937$, RSS= 1.20647×10^{-7} , $p=9.60 \times 10^{-8}$. For concentrations of 1 $\mu\text{g}/\text{mL}$ and higher the SD errors of 3 replicas were always between 1% and 5% while for the concentration of 0.5 $\mu\text{g}/\text{mL}$ the SD error was 18%.

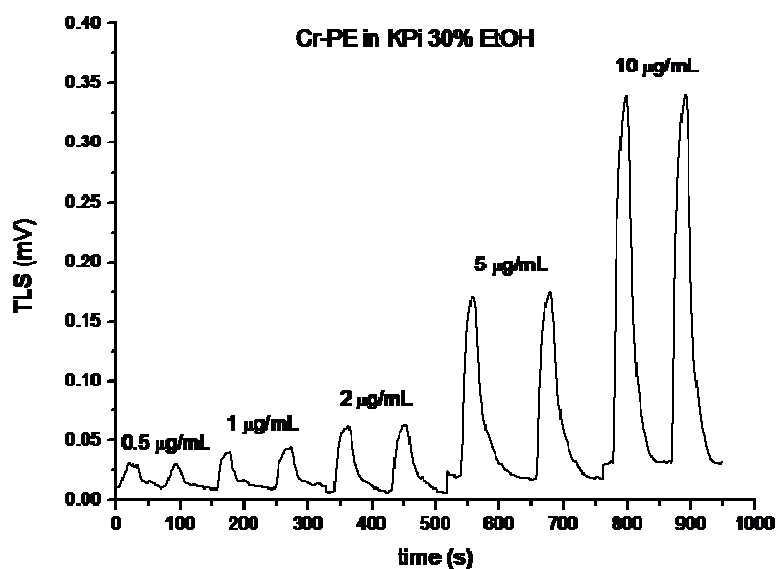


Figure 5.19 TL signals of Cr-PE in KPi 30% EtOH in a TLM-gravity driven flow system

The increase in the sensitivity of the system was by a factor of 3 in the case of 30% EtOH, since the slopes for Cr-PE in KPi and in 30% EtOH equal to $1.01 \times 10^{-3} \text{ mV } \mu\text{g}^{-1} \text{ mL}$ ($R^2=0.99674$) and $3.04 \times 10^{-3} \text{ mV } \mu\text{g}^{-1} \text{ mL}$ ($R^2= 0.99937$), respectively. The LODs extrapolated from the calibration curves were $119 \mu\text{g/L}$ in the case of KPi and $51 \mu\text{g/L}$ in the case of 30% EtOH. The LOD in the presence of ethanol was 2.3 times lower than the one in KPi, showing that under the given experimental conditions, the noise had a minor effect in comparison to the one observed in the FIA-TLS system.

Results showed that Cr-PE was successfully detected in a microchip-TLM system. Furthermore the LOD was reduced to $46 \mu\text{g/L}$ by addition of EtOH 30%. The sensitivity gained in the TLM system is comparable to the one obtained by classic TLS however further improvements can be achieved by the optimization of the experimental conditions and the automation of the system. Different solvents and quenchers can be exploited; moreover micropumps and microinjectors can be used for a better control of the flow rates and the accuracy of the injections.

The Table 5.2 resumes the analytical performances of the TL systems for the detection of Cr-PE together with the one of the traditional spectrometry found in the literature. Accuracy and precision, in terms of repeatability and reproducibility of the data, are shown. The accuracy was measured as the percentage mean recovery (mean

R%) of 3 replicates. The repeatability was determined as the percentage of the relative standard deviation (RSD) of 3 replicates while the reproducibility was determined as the percentage of the RSD of 2 sets of 3 replicates measured in different days. All the parameters were tested at two fortification levels i.e. 2 and 20 µg/mL. As it can be seen, the performances of TL system are comparable to the one of the traditional spectrometry.

Table 5.2 Analytical performances of TL systems and conventional spectrometry

Detection technique (this work)	Analyte	Analyte concentration (µg/mL)	Accuracy mean R (%)	Repeatability (n=3) RSD (%)	Reproducibility (n=2x3) RSD (%)
FIA-TLS	Cr-PE in KPi	2	95.1	2.92	3.12
		10	98.1	1.46	4.17
	Cr-PE in 40% EtOH	2	93	1.28	3.16
		10	106.4	0.13	1.77
FIA-TLM	Cr-PE in KPi	2	86.7	1.63	2.57
		10	93.7	1.55	2.31
	Cr-PE in 30% EtOH	2	112.7	1.01	5.31
		10	102	1.83	2.1
Detection technique (other works) ⁴⁴	Analyte	Analyte concentration (µg/mL)	Accuracy mean R (%)	Repeatability (n=3) RSD (%)	Reproducibility (n=5x3) RSD (%)
Absorbance	R-Phycoerythrin in aqueous buffer	1-10	93.7	0.5-34.7	4.9
Fluorescence	R-Phycoerythrin in aqueous buffer	0.001-1	98.9	0.15-4	4.9

5.2 DETECTION OF MC-LR

The protein phosphatase inhibition assay is a well known method for the detection of cyanotoxins. In literature many applications of PPIA to detect microcystins can be found but to our knowledge thermal lens techniques have never been used for this purpose. Moreover even if PPIA is based on a quite simple colorimetric reaction there are many different protocols that can be found in literature. Therefore the first step in the developing of a PPIA-TL detection system was to optimize a colorimetric assay of our own. For the preliminary experiments the PPIA assay was performed in a 96 multiwell plate, a well known method for the detection of microcystins.

5.2.1 Set up of the PPIA in a 96 multiwell plate

The enzymatic assay was performed following the protocol proposed for okadaic acid¹⁹⁶ and lately applied for the detection of microcystins^{178,179}.

5.2.1.1 Protein phosphatase 2A activity

A first set of experiments were carried out in order to find the optimal range of enzymatic units to work with i.e. the range at which the absorbance of the product pNP was high enough in order to be detected in a TL system. The activity of solutions containing 0.06, 0.12, 0.24 and 0.48 mU/well of PP2A (i.e. final concentrations of 0.24, 0.48, 0.96 and 1.92 $\mu\text{U}/\mu\text{L}$) were tested. As it can be seen in figure 5.20 at the given experimental conditions the colorimetric reaction occurred at a fast rate in the first 30 minutes and then it slowly reached a plateau. In the presence of 0.48 mU after 10 min the observed absorbance of the product was already around 0.75. The same value was obtained with 0.24 mU in 30 min while after 15 min the absorbance was almost 0.25. At lower enzymatic activity i.e. 0.12 and 0.06 mU the times required to reach an absorbance value equal to 0.25 were around 30 and 70 min respectively. Given the fact that in a TL system there is linearity between the TL signal and the concentration of the sample for absorbances up to 0.1 a.u, further experiments were carried out at an enzymatic activity equal to 0.24 mU. Indeed this enzymatic activity was a good compromise between the time to reach absorbances around 0.1 a.u. (10 min) and the amount of enzyme required (Fig. 5.20).

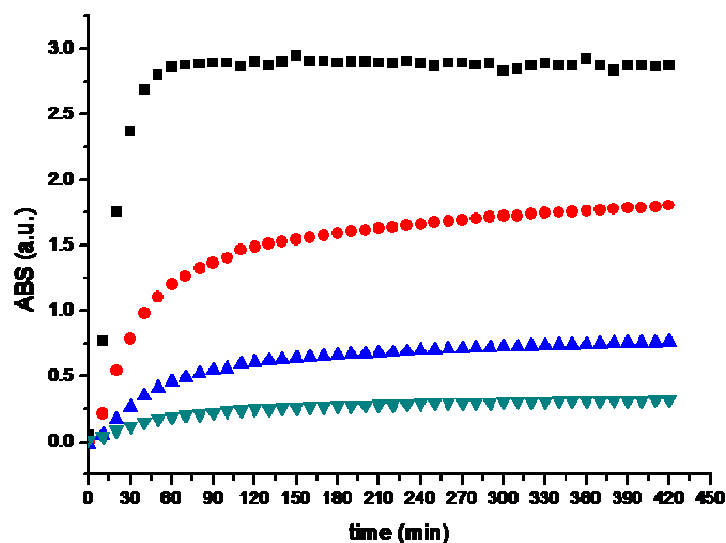


Figure 5.20 PP2A activity in a 96 multiwell plate. The activity of 0.06 (green triangles), 0.12 (blue triangles), 0.24 (red dots) and 0.48 mU/well of PP2A (black squares) are shown.

5.2.1.2 PP2A inhibition by MC-LR

The following step was to investigate the effect of MC-LR on the activity of PP2A. The enzyme (0.24 mU/well, final concentration 0.96 $\mu\text{U}/\mu\text{L}$) was incubated with different concentrations (0.2, 1, 5 $\mu\text{g}/\text{L}$) of MC-LR and absorbance measurements were taken every 5 minutes in order to determine the inhibition effect of the toxin on the enzyme (Fig. 5.21).

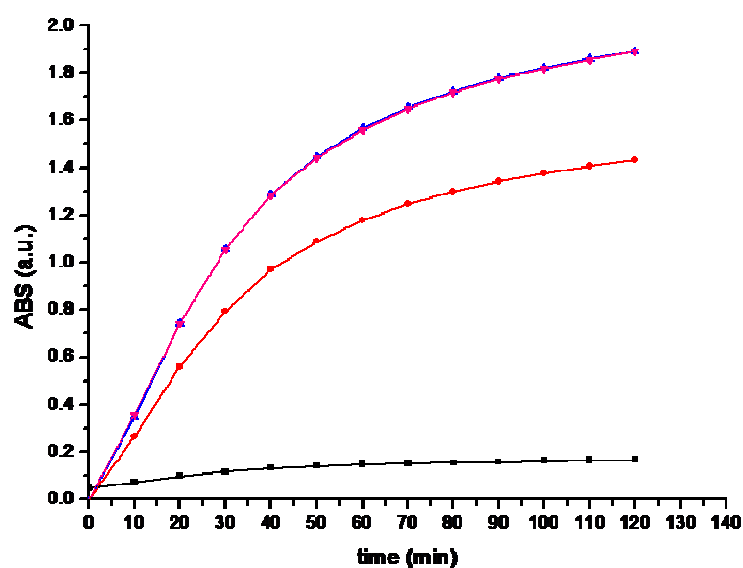


Figure 5.21 Inhibition of PP2A by MC-LR in a 96 multiwell plate. The activity of PP2A (pink line) and of PP2A in the presence of 0.2 (blue line), 1 (red line) and 5 $\mu\text{g}/\text{L}$ of MC-LR (black line) are shown.

At the given experimental conditions no inhibiting effect was observed after the incubation of PP2A with the lowest concentration of microcystin and as it can be seen in figure 5.24 the curves of the control (pink) and the one of 0.2 $\mu\text{g/L}$ microcystin (blue) are essentially indistinguishable. The incubation of PP2A with 1 $\mu\text{g/L}$ (the limit fixed by WHO for MC-LR in drinking water) caused a 25% loss of the enzymatic activity visible already after 10 minutes. The incubation with the highest concentration of the toxin caused an almost complete inactivation of the enzyme that showed a loss in activity equal to 91%. The absorbances recorded at 10 minutes were 0.35 a.u. for the control solution and 0.35, 0.26 and 0.07 a.u. for the 0.2, 1 and 5 $\mu\text{g/L}$ microcystin solutions.

Results showed that, under the given experimental conditions, a quite fast PPIA assay in a 96-multiwell plate is possible, with the total 15 min time required for the assay (5 for the incubation of the enzyme with the toxin plus 10 min for the measurement). Moreover the measured absorbances were high enough to perform the assay in a TL system where linearity between the TL signal and the sample concentration is expected for absorbances up to 0.1 a.u.

5.2.2 Set up of the PPIA in a FIA-TL system

5.2.2.1 Preliminary tests on the absorbance spectra of the reagents and the product

The thermal lens systems are highly sensitive and they allow to detect an analyte even by using excitation wavelengths different from the one of the absorbance maximum, where the extinction is the highest. This characteristic allows performing experiments even in cases where there is no laser line available at an optimal excitation wavelength or when there is an overlapping of the absorbance spectra of the analyte and reagents which requires excitation at the wavelength of the lowest absorbance of the reagent. Hence, in order to choose the appropriate laser line to be used in the TL-PPIA system, absorbance spectra of PP2A, pNPP and pNP were recorded. Measurements were performed in a 1 mL spectrophotometric cell under the same conditions of the colorimetric assay performed in the 96 multiwell plate (final concentration of PP2A in the cell 0.96 $\mu\text{U}/\mu\text{L}$, Tris buffer 40 mM, pNPP 20 mM,

DTT 20 mM). Absorbance spectra of pNP were recorded at different times from the start of the reaction (0, 5, 10, 15, 20 min). The maximum of absorbance of pNP is at 405 nm hence a krypton laser line operating at 406.7 nm would have seemed the best option as a pump beam. However, while the absorbance of PP2A was found to be negligible, the absorbance spectrum of 20 mM pNPP was in part overlapping with the spectrum of pNP (Fig. 5.22) contributing to relatively high background absorbance at 407 nm.

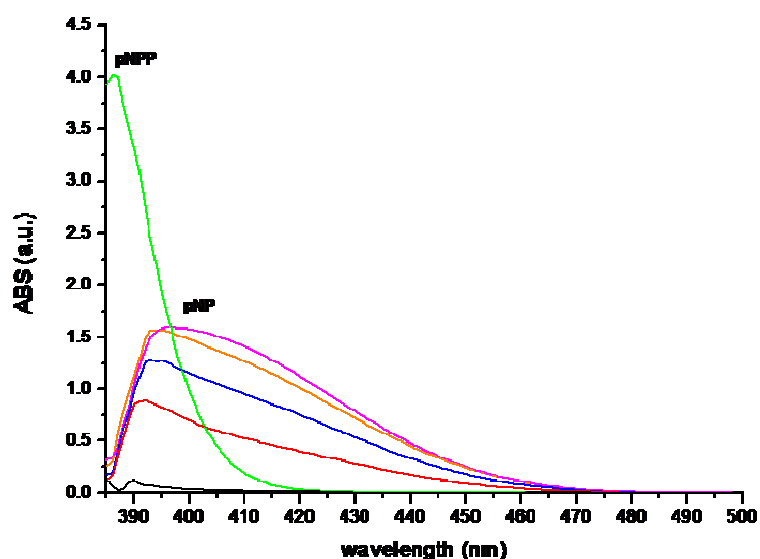


Figure 5.22 Absorbance spectra of pNPP and pNP. The spectrum of pNPP 20 mM (bright green line), of pNP produced at the start of the reaction (black line) and of pNP produced after 5 (red line), 10 (blue line), 15 (orange line) and 20 min (pink line) are shown.

In order to solve this problem, the possibility of using lower concentrations of pNPP was investigated. The substrate is in fact present in excess (in order to make the reaction independent from its concentration) and moreover, any eventual loss in sensitivity due to the lower concentration of the substrate would be compensated by the high sensitivity of TLS. Therefore absorbance spectra of pNPP at lower concentrations (0.625, 1.25, 2.5, 5, 10 mM in Tris buffer 40 mM) were recorded (Fig. 5.23) in order to find the optimal substrate concentration to be used.

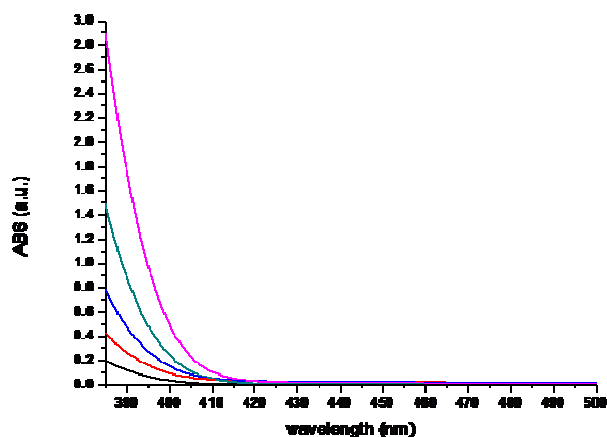


Figure 5.23 Absorbance spectra of different concentrations of pNPP. Spectra of pNPP 0.625 (black line), 1.25 (red line), 2.5 (blue line), 5 (green line) and 10 mM (pink line) are shown.

As it can be seen in figure 5.23, in the case of 10 mM pNPP the absorbance of the substrate around 407 nm was still high (0.17 a.u.), while between 1.25 and 5 mM the absorbances were ranging from 0.05 and 0.08 a.u. and at the lowest concentration i.e. 0.625 mM the measured absorbance dropped to 0.01 a.u.. Given the recorded absorbance spectra of pNPP and pNP, a substrate concentration equal to 1 mM was used to perform the enzymatic assay in a TL system. Assuming that the reaction rate is not affected by the decrease of substrate concentration, the relative contribution of pNPP to overall absorbance in detection of pNP after 10 minutes of reaction is not large (6.6% for 0.625 mM pNPP and 13.3% for 1.25 mM pNPP). Furthermore the enzymatic assay was developed in a TL system where the pump beam was provided by an Argon-ion laser operating at an excitation wavelength of 457.9 nm. As it can be seen from figure 5.22, at this wavelength pNP is still absorbing with a 0.1 a.u. recorded after 10 min. This absorbance allows obtaining a strong signal in a TL system. Moreover at this wavelength the contribution of pNPP to detected signal of pNP after 10 minutes is 2 and 5% for 0.625 and 1.25 mM pNPP, respectively.

5.2.2.2 Set up of the colorimetric reaction

The colorimetric reaction was performed first in a FIA-TLS system operating with an Argon-ion laser ($\lambda_{\text{exc}}=457.9$ nm, $P=124$ mW). Two different enzyme solutions (200 μL of PP2A 1 $\mu\text{U}/\mu\text{L}$ i.e. 0.2 mU per injection) were injected into the system where the carrier buffer 1 was running at a flow rate of 0.5 mL/min. The first solution was prepared by diluting the enzyme in enzyme buffer and injected immediately, i.e. 1 minute after preparation (the time required for filling the syringe with the sample and injecting it into the system). In this case the reaction time was 9 minutes. Under the given experimental conditions no peak was observed, but the baseline signal was highly noisy. Since in a FIA-TLS system the differences in the composition of the carrier and the sample buffer can affect the TL signal (due to perturbations caused by mixing of the different buffers), a second solution was prepared diluting the enzyme in the carrier buffer 1.

The solution was injected 1 minute after preparation and with 9 minutes retention in the system, the total reaction time was 10 minutes, indeed, the reaction started immediately after the preparation of the solution (being the enzyme diluted in the carrier buffer 1, containing pNPP). After injecting the second solution a small peak was observed (0.59 mV) but the noise was still high (Fig. 5.24) with a signal to noise ratio equal to 12.7. In order to obtain a higher TL signal the reaction time was increased by injecting the second solution after 21 minutes from preparation (with a resulting reaction time of 30 minutes). In this case a higher (1.68 mV) and better shaped peak was observed but the baseline was still noisy (Fig. 5.24) with a signal to noise ratio equal to 35.7. In order to obtain a signal which, at a given background noise, enables observations of 10% inhibition of the enzyme, for the given case the minimum detectable difference in peaks heights was 8% while for the signal to noise ratio of 12.7, as obtained with 9 minutes reaction time, the minimum detectable difference in peak height and corresponding inhibition of the enzyme, because of background noise, was 23%.

Results showed that the detection of the reaction product in the FIA-TLS system was possible even at a concentration of pNPP 20 times lower than the one used for the colorimetric reaction in the 96 multiwell plate. Moreover, despite the absence of the antioxidant DTT in the carrier buffer 1, the enzyme showed to be active.

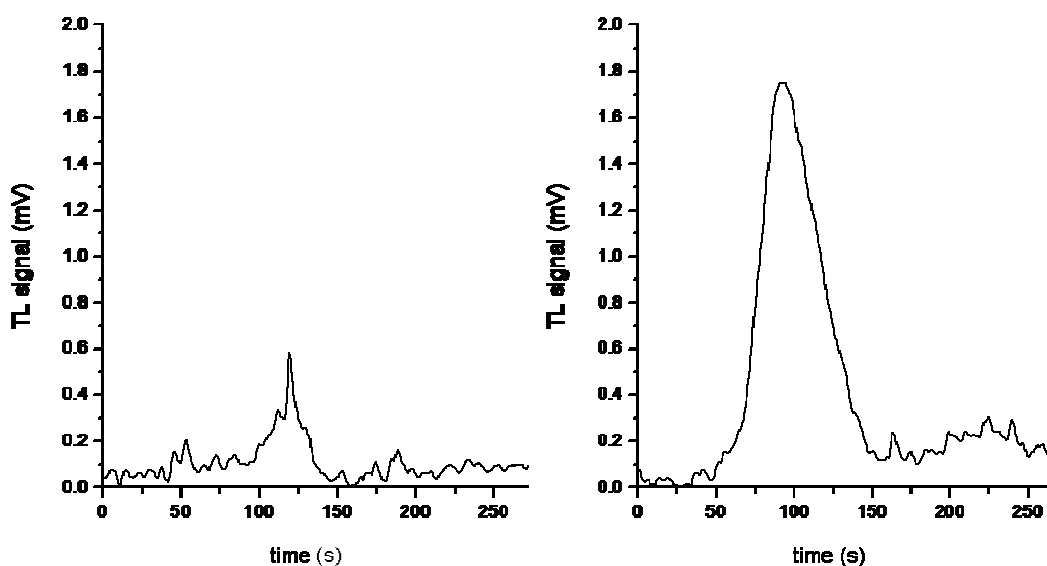


Figure 5.24 TL signal of pNP after the injection of the second solution. Reaction time of 10 min (left) and 30 min (right)

5.2.2.3 Effects of increased concentrations of reagents and decreased flow rate on the colorimetric reaction in the FIA-TLS system

In order to improve the performance of the FIA-TLS system a second set of experiments was carried out at a lower flow rate (0.3 mL/min) and at a slightly higher concentration of enzyme (1.33 $\mu\text{U}/\mu\text{L}$ i.e. final 0.27 mU in the solution) and pNPP (3 mM) in order to promote the formation of a larger amount of product and hence to obtain a stronger TL signal. The enzyme was diluted in the carrier buffer 2 and the enzyme solution (200 μL) was injected 21 min after preparation (32 min of reaction time). A second experiment was performed after reducing the reaction time by injecting the enzyme solution 6 min after preparation (17 min of reaction time). Figure 5.25 shows that, under the given experimental conditions, reproducible peaks were obtained in both cases. The TLS signal obtained after 17 min was 17% lower than the one obtained after 32 min but it was 35 times higher than the signal obtained in the previous 30 min experiment i.e. 59.2 mV versus 1.68 mV, with a corresponding signal to noise ratio in the order of 10^3 i.e. 3 orders of magnitude higher. With the achieved increase in the strength of the signal, the 17% lower sensitivity was considered a reasonable compromise for the shorter reaction time and

all further experiments were carried out by injecting the enzyme solutions 6 min after preparation.

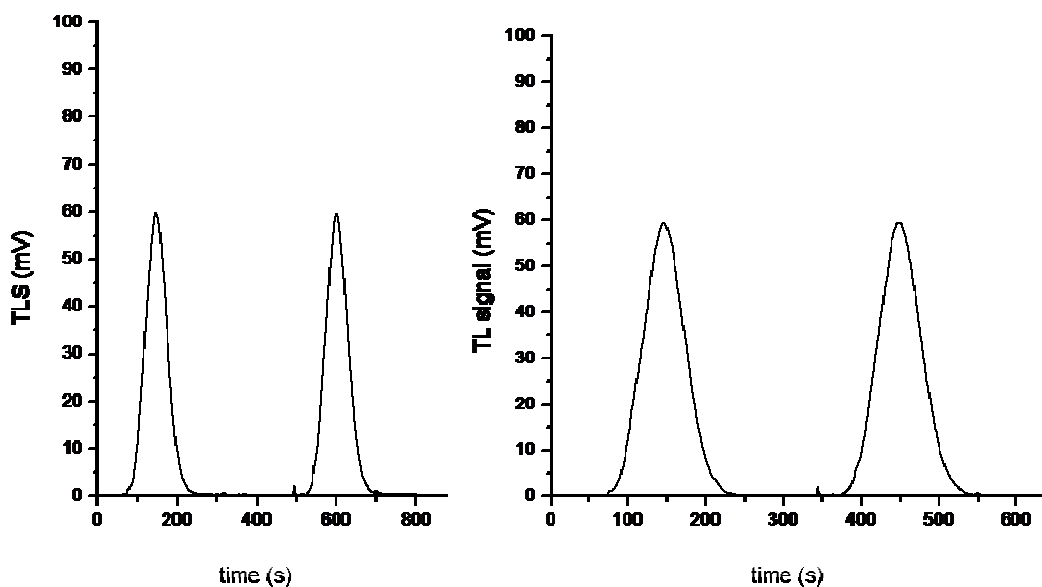


Figure 5.25 TL signal of pNP. Left: 32 minutes reaction time. Right: 17 minutes reaction time.

5.2.2.4 Effect of sample volumes and flow rates on the colorimetric reaction in the FIA-TLS system

Further adjustments of the colorimetric reaction were carried out by the reduction of the amount of reagents, injection volumes and time of analysis. The measurements were repeated by injecting 100 and 50 μL of two different solutions of PP2A (containing a total amount of 0.27 and 0.1 mU) in the system. As in the previous experiment the enzyme was diluted in the carrier buffer 2. Furthermore the flow rate was increased back to 0.5 mL/min in order to get sharper peaks. Figure 5.26 shows that under the given experimental conditions peaks were observed even when injecting the smallest volume of the PP2A with the lowest concentration. Moreover at this flow rate the time required for the measurements was reduced to 15 min (6 min before injection plus 9 min in the system). The signal was 4.5 times weaker than the one obtained in the previous 17 min experiment i.e 13 mV versus 59.2 mV with a corresponding signal to noise ratio in the order of 10^2 i.e. 1 order of magnitude lower, but still strong enough for the foreseen development of the assay.

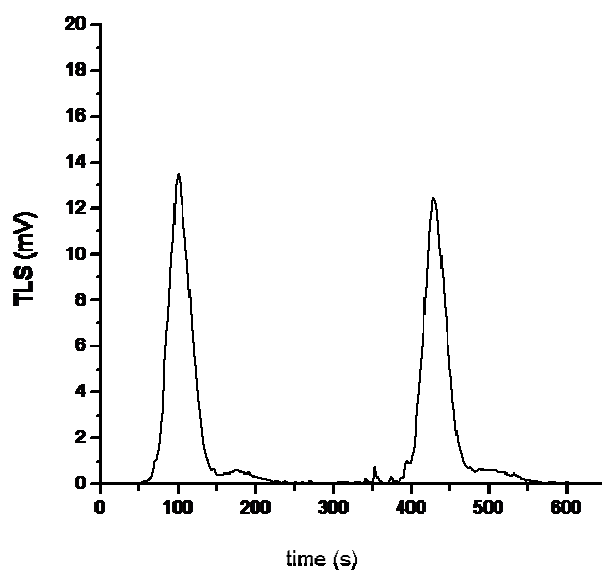


Figure 5.26 TL signal of pNP after the injection of 0.1 mU PP2A.

5.2.2.5 Development of the PPIA in a FIA-TLS system

Once demonstrated that pNP could be successfully detected in a TL system the possibility to perform the PPIA in the same experimental conditions was investigated. The inhibiting effect of two different concentrations of microcystin solutions (1 and 0.7 $\mu\text{g/L}$) on a 0.1 mU PP2A solution (0.2 mU/ μL , 50 μL injection) was tested. The enzyme solutions were prepared as in the previous experiment adding MC-LR just prior the injection (that is to say that the toxin was added 5 min after the start of the colorimetric reaction). As it can be seen in figure 5.27 reproducible peaks were obtained but only a small inhibiting effect was observed i.e. a decrease of the signal equal to 19%. Moreover no difference in the inhibition extent was observed between the two solutions of MC-LR which signal was equal to 11.7 mV in both cases.

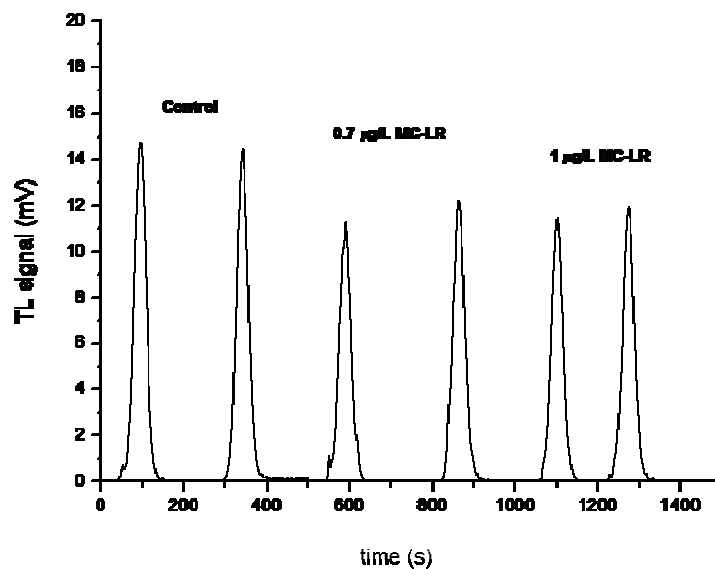


Figure 5.27 Inhibition of PP2A by MC-LR

5.2.2.6 Calibration curve and estimation of LOD for MC-LR

Further experiments were performed in order to obtain a calibration curve for MC-LR. The number of enzymatic units was decreased to 0.025 mU/injection (i.e. 0.5 $\mu\text{U}/\mu\text{L}$) in order to obtain a relatively larger inhibition for the same amount of toxin. The baseline noise was reduced by decreasing the laser power down to 10 mW but under these experimental conditions, in order to obtain reproducible signals, the pNPP concentration had to be increased back to 20 mM. The observed decrease in height TL signal was equal to 54.6%. Indeed, in the previous experiment the TL signal of para-nitrophenolate was equal to 14.55 mV while, in the given experimental conditions of this experiment, the signal was equal to 6.61 mV. The curve (Fig. 5.28) was obtained by incubating solutions of 0.025 mU PP2A diluted in the carrier buffer 3 with MC-LR solutions 1 and 5 $\mu\text{g}/\text{L}$ (final concentration). Solutions were prepared as follows: PP2A was first diluted in the carrier buffer 3 while MC-LR was added after 5 min. The solution was then injected after 6 minutes from MC-LR addition for a total reaction time of 20 min. The time required for the observation of the first signal is 20 min while the measurement of the signal itself requires 65 seconds. This means that, carrying out consecutive injections, the number of measurements that can be performed in 30 minutes is equal to 28. Under the given experimental conditions the extrapolated LOD for MC-LR was 0.64 $\mu\text{g}/\text{L}$, almost 2 times below the limit set by WHO for drinking water. These results are promising, indeed, in literature it can

be found that the time required to perform the PPIA assay in a microtiter plate varies between 1 hour¹⁹⁹ and 30 minutes¹⁹⁷. The protocol by Ikheara, in principle, allows to analyze a number of samples 3 times higher than the one of the TL system in the same time but the sample volumes required for the analysis are 2 times larger than the one required by the TL system. Moreover it is expected that the high sensitivity of the TL technique will allow using smaller injection volumes and lower concentrations of enzyme. Although the LOD reached with the FIA-PPIA-TLS system is higher in comparison to other techniques (Table 3.4), it has some advantages. Chromatographic techniques such as HPLC/UV and HPCE/UV have very low sample throughput with a required time for the chromatogram acquisition of around 15 minutes²⁰⁰ for each sample. The FIA-PPIA-TLS procedure requires smaller amount of reagents and it is simple while, usually, chromatographic and other biological techniques are more complex and require larger volumes of samples and pre concentration steps^{67,77} that are not required in a TL system. Regarding the commercial ELISA kits available for the detection of microcystins, the kit from Envirologix (*QuantiPlate™ Kit for Microcystins*, EP 022) has a LOD of 0.147 µg/L and the samples can be processed in 90 minutes. The kits from Abraxis (*Microcystins-DM ELISA kit*, 522015) and Enzo Life Sciences (*Microcystins (Adda Specific) ELISA kit*, ALX-850-319) can detect 0.1 µg/L of microcystins in approximately 120 and 90 minutes, respectively. The LOD obtained with TLS is already comparable to the LODs achieved by the three commercial ELISA kits and to the Abraxis *Myrocystins/Nodularins PP2A, Microtiter Plate* kit (520032) that can detect 0.25 µg/L in approximately 30 minutes.

Additional experiments such as tests for the optimization of the reagents concentrations and for a better temperature control of the FIA-PPIA-TLS system are still to be carried out; enzymes from different companies should be tested as well. Furthermore the FIA-PPIA-TLS assay can be downscaled to a TLM-microfluidic system where the inhibition of PP2A by MC-LR is expected to occur at a faster rate and where the volumes required for the assay are smaller.

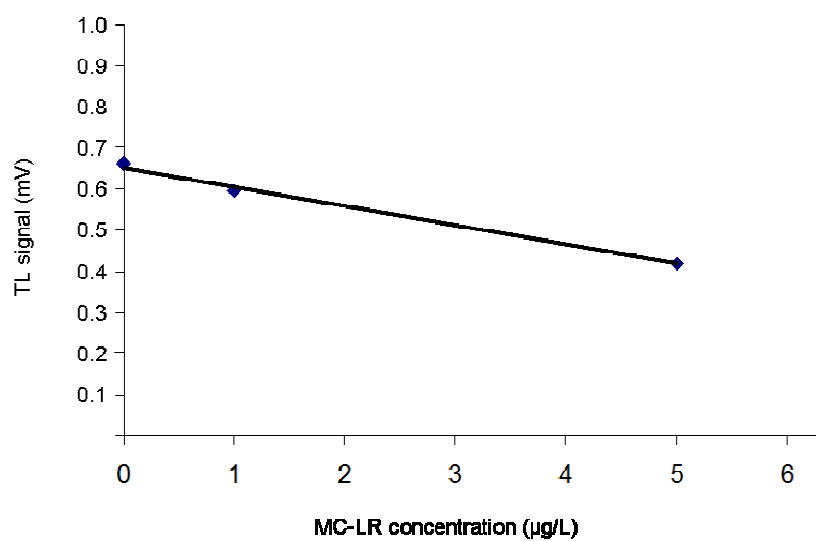


Figure 5.28 Calibration curve of MC-LR in a FIA-PPIA-TLS system

Table 5.3 summarizes the analytical performances obtained in this work with TL techniques together with the best analytical performances found in literature for the same analytes. As previously discussed, the LODs obtained with the TL techniques are higher than the one obtained with other techniques, but the TL systems can still be improved.

Table 5.3 Comparison of analytical performances obtained in this work and in literature

Analyte	Detection Method	LOD	Linearity range	Time of analysis	Reference
Cr-PE	FIA-TLS	13 µg/L (in 0.1 M KPi)	0.05-20 µg/mL	30 sec (1 sample)	This work § 5.1.4.1
		22 µg/L (in 40% ethanol)	0.05-10 µg/mL	30 sec (1 sample)	This work § 5.1.4.2
	FIA-TLM	119 µg/L (in 0.1 M KPi)	0.5-10 µg/mL	30 sec (1 sample)	This work § 5.1.5.2
		51 µg/L (in 30% ethanol)	0.5-10 µg/mL	30 sec (1 sample)	This work § 5.1.5.2
	Fluorescence spectroscopy	1 µg/L	0.001-0.5 µg/mL	not stated	Sobiechowska et al. ⁴⁴
MC-LR	PPIA-FIA-TLS	0.64 µg/L (in KPi 0.1 M)	0-5 µg/mL	30 min (28 samples)	This work § 5.2.2.6
	ELISA	0.1 µg/L	0.15-5 µg/L	90 min (90 samples)	Enzo Microcystins (Adda Specific) ELISA kit
	PP2A multiwell	0.25 µg/L	0.25-2.5 µg/L	30 min (90 samples)	Abraxis Mycrocystins/Nodularis PP2A, Microtiter Plate kit
		0.005 µg/L	0.005-5 µg/L	30 min (90 samples)	Ikehara et al. ¹⁹⁷
	Immuno-electrode	0.01 ng/L	0.0001-1 µg/L	37 min (1 sample)	Lebogang et al. ⁷⁵

5.3 REMOVAL OF MC-LR BY ADSORPTION ON COMPOSITE MATERIALS

5.3.1 Preliminary experiments

Preliminary experiments were performed in order to assess if the MC-LR was adsorbed on the available composite materials and to find the optimal experimental conditions.

5.3.1.1 Screening of the adsorption of MC-LR on the chitosan-tricyclodextrins composite materials

A first set of experiments was carried out on materials composed by tricyclodextrins and chitosan. In particular [100% CS] and [50% CS -50% TCD] films were tested. Absorbance measurements were performed on 3 mL of two solutions of microcystin (0.37 mg/L) in deionised water at pH 7. Absorbances were recorded every 5 minutes for the first 95 minutes and every 10 minutes till the absorbance reached a plateau. In both cases a decrease in the absorbance was observed thus indicating that the MC-LR was adsorbed on both materials (Fig. 5.29).

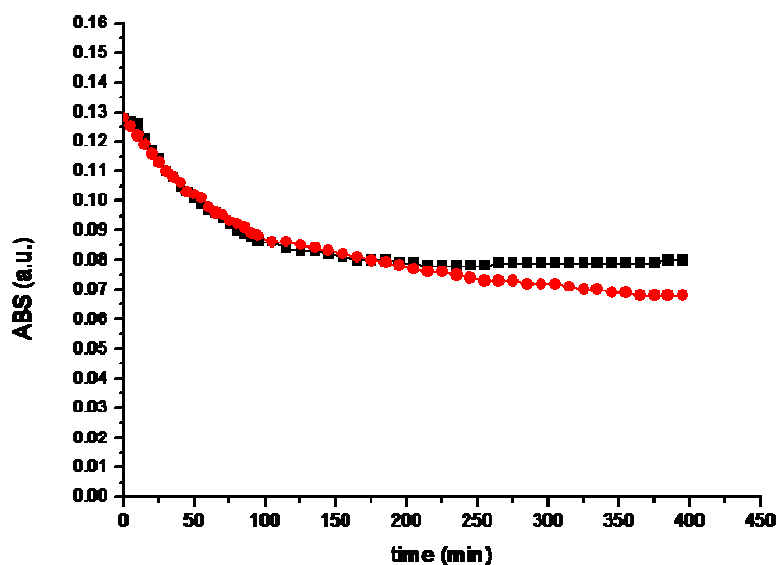


Figure 5.29 Absorbance measurements of solutions of MC-LR in the presence of a 100% CS (black squares) and a 50% CS-50%TCD composite material (red dots)

5.3.1.2 Screening of the adsorption of MC-LR on the cellulose-tricyclodextrins composite materials

A second set of experiments was performed on materials composed of cellulose and tricyclodextrins. The films were put in 2.7 mL of a 0.37 mg/L MC-LR solution that was stirred for the entire measurement span. Figure 5.30 shows that no adsorption was observed in both cases [50% CEL-50% TCD] (red plot) and [75% CEL-25% TCD] (green plot) of composite materials. Also in the case of the [100% CEL] material no adsorption was observed as it can be seen in figure 5.31. The [50% CS-50% CEL] material instead shows to adsorb the toxin (Fig. 5.32).

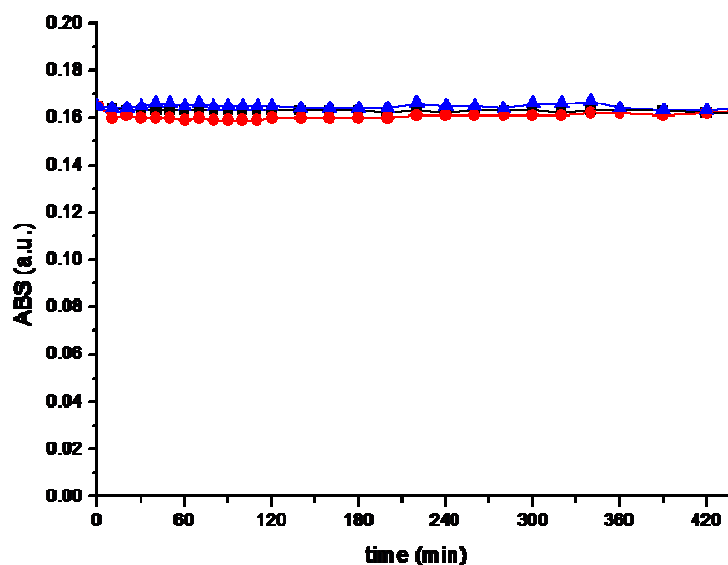


Figure 5.30 Absorbance measurements of MC-LR solutions in the absence (black squares) and in the presence of 50%CEL-50% TCD (red dots) and 75%-CEL-25% TCD composite materials (blue triangles)

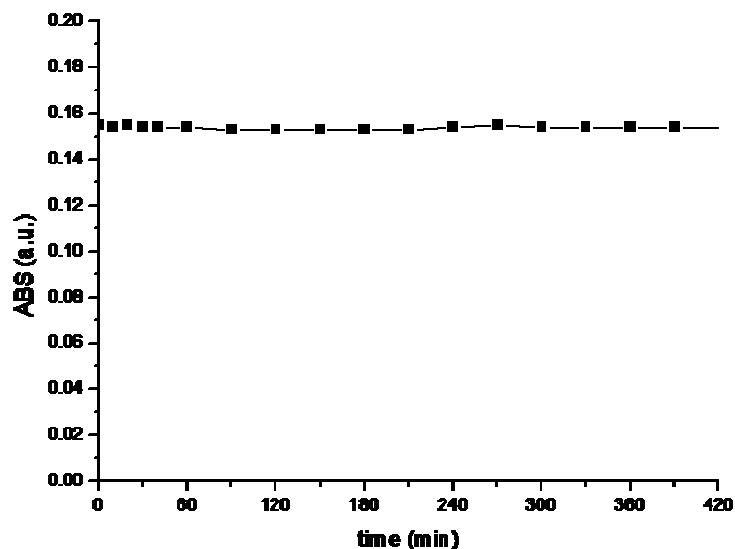


Figure 5.31 Absorbance measurements of a solution of MC-LR in the presence of a 100% CEL composite material

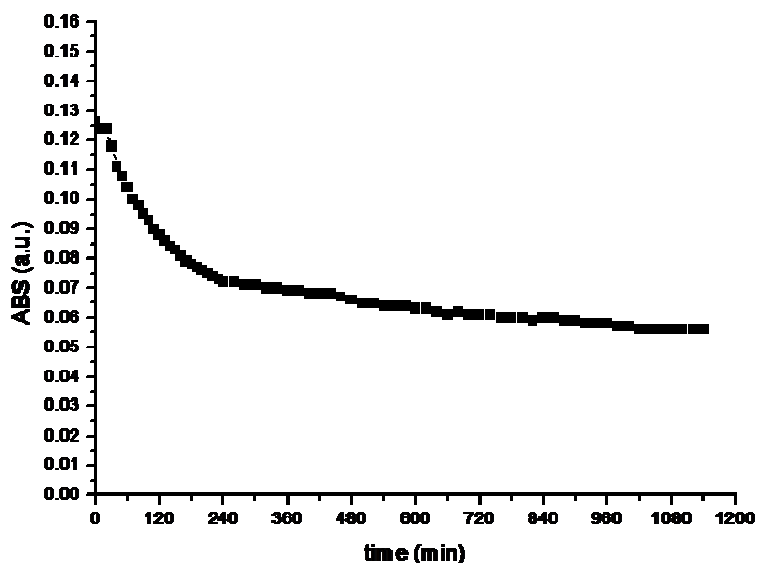


Figure 5.32 Absorbance measurements of a MC-LR solution in the presence of a 50%CS-50%CEL composite material

5.3.1.3 Adsorption of MC-LR on the chitosan-cellulose composite materials

From the results of MC-LR removal obtained with chitosan-tricyclodextrins and cellulose-tricyclodextrins composite films it could be stated that the material that was involved in the adsorption of MC-LR was chitosan. In fact all the composite materials that were made in part or completely by chitosan namely [50% CS-50% TCD], [50% CS-50% CEL] and [100% CS] showed to adsorb the toxin. None of the

composite materials made in part or completely by cellulose i.e. [50% CEL-50%TCD], [50% CEL- 50% DB18C6], [75% CEL- 25% TCD] and [100% CEL] showed to adsorb MC-LR.

5.3.1.4 Influence of the pH on the adsorption of MC-LR on composite materials

In literature it is reported that the adsorption efficiency of MC-LR is higher working in acidic conditions^{201, 202}. For this reason, experiments at pH 5 were carried out in order to investigate if under such experimental conditions it was possible to improve the efficiency of toxin adsorption on the composite materials.

The experiments on the [100% CS] and [50% CS -50% TCD] materials were repeated diluting the MC-LR in double deionised water brought to pH 5. All the other experimental conditions were the same as in the experiment at pH 7. Under the given experimental conditions no increase in the adsorption efficiency was observed. Moreover in the case of the [100% CS] film, the plateau was reached in 6 hours and an half i.e. twice as long as in the solution at pH 7 that reached the plateau in 3 hours (Fig. 5.33). Experiments performed at pH 5 did not show increased adsorption efficiency of the materials hence all the further experiments were performed at pH 7.

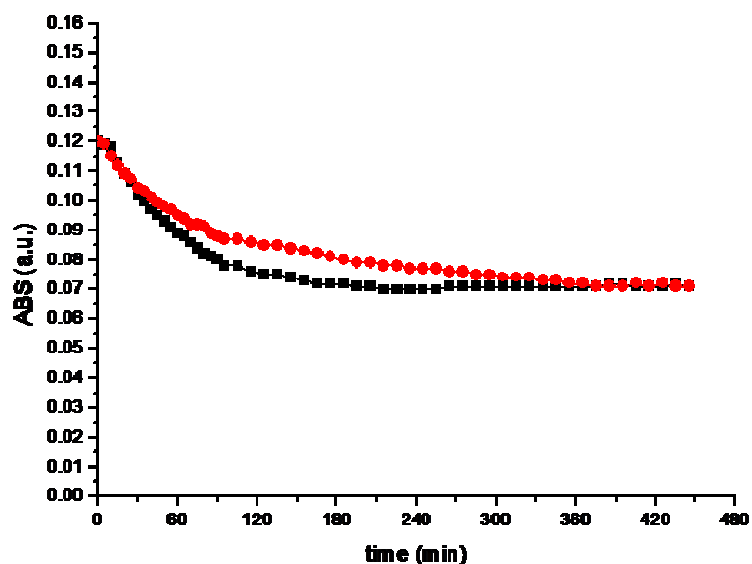


Figure 5.33 Absorbance measurements of a 100% CS material at pH 5 (red dots) and pH 7 (black squares)

5.3.2 Mechanism of adsorption

In order to understand the mechanism of adsorption of MC-LR, experiments were carried out on composite materials with different ratios of [CS-CEL]. In particular kinetic measurements were performed on composite materials made by 67,50,40,29 and 20% chitosan. Experiments were carried out under the same conditions as the previous one and for each material the measurement were taken in triplicates. The kinetic data were then fitted to the pseudo-first order and pseudo-second order models in order to determine which was the most appropriate²⁰³.

The pseudo-first and pseudo-second order models are based on the following equations respectively:

$$\ln(q_e - q_t) = \ln q_e - k_1 t \quad (1)$$

$$\frac{t}{q_t} = \frac{1}{(k_2 q_e^2)} + \frac{t}{q_e} \quad (2)$$

where k_1 and k_2 are pseudo-first order (min^{-1}) and pseudo-second order rate constant of sorption [$\text{g}/(\text{mg min})$], q_e is the amount of analyte adsorbed at equilibrium (mg/g), q_t is the amount of analyte or the sorbent at any time t (mg/g).

If the initial adsorption rate is

$$h = k_2 q_e^2 \quad (3)$$

then the equation 2 can be rearranged:

$$\frac{t}{q_t} = \frac{1}{h} + \frac{1}{q_e} t \quad (4)$$

If $1/q_t$ is plotted against t a linear plot can be obtained and q_e can be then extrapolated from the slope while h can be extrapolated from the intercept. Once obtained q_e and h , k_2 can be calculated from the equation 2.

In figure 5.34 the plots of q_t as a function of time for the five materials composed by the different concentrations of chitosan are shown. From the plots it is evident that for increasing concentrations of chitosan there is a corresponding increase in the adsorption of MC-LR. The adsorption of MC-LR on the 100% chitosan film was found to be similar to the one containing 67% of chitosan showing that an adsorption plateau was reached. This can be explained by the fact that cellulose confers tensile strength to the composite material and prevents its swallowing and the consequent loss of adsorbed MC-LR¹⁷⁷.

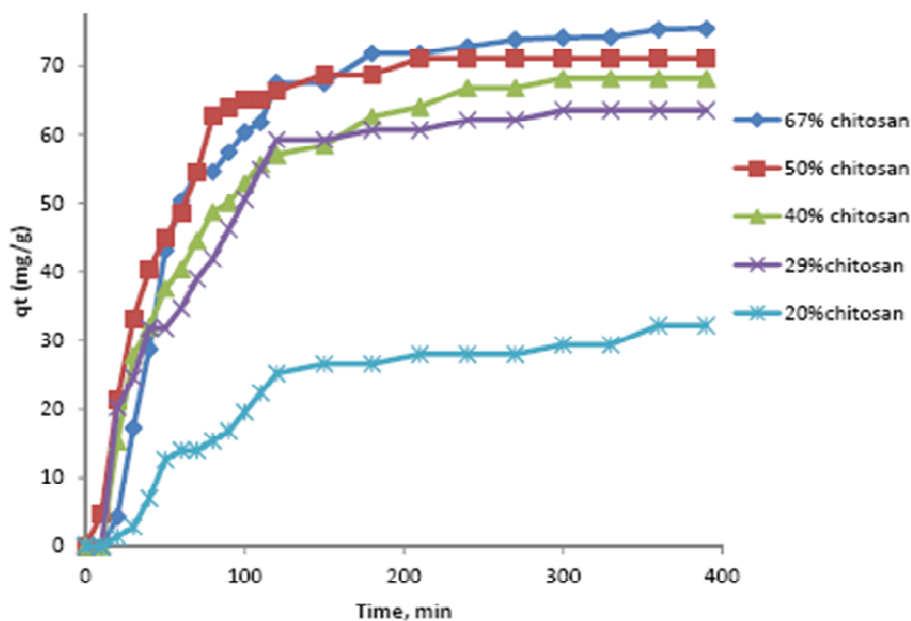


Figure 5.34 q_t as a function of time for different concentrations of chitosan in the composite material chitosan-cellulose.

Table 5.2 shows the results of the data fitting to both pseudo-first and pseudo-second order models for the five different [CS-CEL] composite materials.

Table 5.2 Fitting of the data to a pseudo first and to a pseudo second order models

Composite Material		Pseudo-First Order				Pseudo-Second Order			
% Chitosan	% Cellulose	Q_e (mg/g)	k_1 (min^{-1})	R^2	MSC	Q_e (mg/g)	$k_2 \cdot 10^4$ (g/mg. min)	R^2	MSC
67	33	94±8	0.020±0.001	0.9714	2.84	96±3	1.6±0.1	0.9894	4.18
50	50	72±1	0.02±0.01	0.9794	3.86	79±2	5±3	0.9953	5.46
40	60	52±1	0.010±0.007	0.9370	2.72	73±9	3±1	0.9965	5.66
29	71	44±1	0.01±0.02	0.9419	2.73	71±2	5±2	0.9987	6.52
20	80	31±5	0.007±0.001	0.7254	1.98	42±4	1.9±0.3	0.9932	5.00

The MSC represents the information content of a model therefore a better model will be the one giving higher MSC. From the relatively higher values of both R^2 and MSC, in the case of a pseudo second order compared to the pseudo first order it is clear that the adsorption of MC-LR by the chitosan-cellulose composite material follows a pseudo second order model. The adsorption of microcystin is dependent on the concentration of chitosan in the composite material i.e. at higher concentrations of chitosan an increased adsorption efficiency is achieved. This is in accordance with the previous experiments that showed that cellulose does not adsorb microcystin. These results showed that [CS-CEL] composite materials have much higher adsorption efficiency than other common adsorbents used for the removal of MC-LR. In table 5.3 some of the adsorbents already developed for the removal of this toxin are listed.

Table 5.3 Adsorbent materials already developed for the removal of MC-LR

Adsorber	mg of adsorbed MC-LR /g adsorber	Reference
Iron Oxide Nanoparticles	0.15	Gao et al. 2012 ²⁰⁴
Fe ₃ O ₄ @copper silicate nanotube microspheres	0.5	Chen et al. 2009 ²⁰⁵
Powdered activated carbon (PAC)	0.75	Newcombe et al. 2004 ²⁰⁶
Bamboo/Chitosan	1	Zhang et al. 2011 ²⁰⁷
Natural clay particles	4.6	Morris et al. 2000 ²⁰⁸
Carbon nanotubes	5.9	Yan et al. 2006 ²⁰⁹
Suspended Particulate Matter (SPM)	6,5	Liu et al. 2008 ²⁰²
PAC/UF (membrane ultrafiltration)	9.9	Lee et al. 2006 ²¹⁰
Activated carbon fibers (ACF)	17	Pyo et al. 2005 ²¹¹
Fe ₃ O ₄ @SiO ₂ magnetic microspheres	20	Deng et al. 2008 ²¹²
[CS-CEL] composites	96	Tran et al. 2013 ^{<sup>177</sup>}

As it can be seen from the table the best adsorbent reported are Fe₃O₄@SiO₂ magnetic microspheres that can adsorb up to 20 mg of microcystin per gram of

adsorbent. This value is 4.8 times lower than the one obtained with a [67% CS- 33% CEL] composite material i.e. 96 mg of microcystin-LR per g of material.

The adsorption of MC-LR on [CS-CEL] composite materials is highly efficient and reaches 96 mg of MC-LR per g of film, which is the highest in comparison to the other data found in literature. These data are very promising, indeed the adsorption efficiency, which is already higher than other adsorbents, could be further improved by varying the experimental conditions for example using microparticles instead of a film in order to increase the surface area. Furthermore the method of preparation of the [CS-CEL] composite materials is completely green. Chitosan and cellulose are biodegradable and the ionic liquid used as a solvent for the preparation of the film can be washed away with water and recovered by distillation.

6-Conclusions

Cyanobacteria harmful algal blooms represent a threat for environment and human health due to their release of toxic compounds that can contaminate even drinking water. In this work novel methods for a) the detection of cyanopigments as early warning systems b) for the detection of MC-LR and c) for the removal of MC-LR from fresh water are presented.

In the first part of this thesis it was demonstrated that TLS and TLM techniques can be successfully employed for the detection of cyanopigments. Moreover it was demonstrated that the sensitivity of these systems and the achieved LODs can be improved by the use of quenchers, by changing the thermo-optical properties of the samples and by coupling TL detection techniques with FIA. CL-APC and Cr-PE were detected in a conventional TLS system that was further optimized for the detection of Cr-PE. A 1.8 times improvement in the sensitivity of the system was obtained by quenching Cr-PE fluorescence with KI. However the calculated LODs in the absence and in the presence of KI were almost the same i.e. 57 $\mu\text{g/L}$ and 56 $\mu\text{g/L}$. Based on these results, it can be concluded that the sensitivity of the system is enhanced by fluorescence quenching of Cr-PE, however no significant improvement in LOD was achieved by the use of KI which, under the given experimental conditions, was shown to contribute to the increase of the background signal and related signal noise. Nevertheless it is expected that modifications in the system, such as pressure decrease, purification of the quencher, or the use of other quenchers, will improve the performance of the described TLS method. The modification of thermo-optical properties of the sample by addition of 10% ethanol allowed to decrease the Cr-PE LOD to 43 $\mu\text{g/L}$ while coupling TLS with FIA lead to an even lower LOD, i.e. 13 $\mu\text{g/L}$. However, when 40% ethanol was used in a FIA-TLS system, despite a 3 times relative increase in sensitivity, the extrapolated LOD was 22 $\mu\text{g/L}$ showing that also in this case the change of the buffer caused an important increase of the noise. The expected improvements in sensitivity due to the introduction of organic solvents into the samples were confirmed. Moreover, a further improvement of the LOD, attributed to reduced photodegradation, was achieved in FIA mode. As for the case of KI, it is expected that the background noise

in the FIA-TLS system observed in the presence of ethanol could be decreased by modifying experimental conditions, for example optimizing flow rates and the internal pressure or by using different organic solvents. The achieved LOD of 13 $\mu\text{g/L}$ is not far from the value of 3.16 $\mu\text{g/L}$ that was estimated to correspond to the presence of 1 $\mu\text{g/L}$ of MC-LR, as calculated for one half of the maximum possible content of phycoerythrin in cyanobacteria. These results indicate that TLS represents a powerful tool for the detection of cyanobacteria pigments which can be used as indicators of early onsets of massive HABs in natural waters.

Cr-PE was successfully detected also in a TLM-gravity-driven flow system. In this case, in the presence of 30% ethanol a 3 times increase in sensitivity was achieved compared to the one in KPi while the LODs in the absence and in the presence of the solvent were 119 $\mu\text{g/L}$ and 51 $\mu\text{g/L}$ respectively, showing that the change in the buffer was affecting this system less than the TLS one. Also for TLM systems further improvements can be achieved by noise reduction, use of different solvents and appropriate quenchers. It is therefore expected that these ameliorations will make the developed systems favorably comparable to other methods reported as early warning systems for MC-LR, based on cyanopigments detection. Furthermore, it can be expected that the constant developments of laser and microfluidic technologies will allow in the future to develop a portable system that could be use on field.

It is worth to mention that the TLS and TLM methods have been developed using standard aqueous solutions, therefore interferences in case of real samples, due to the presence of other absorbing compounds, should be expected. Different matrixes can affect the system as well but in the case of marine samples a positive contribution is expected, indeed, the presence of sodium chloride enhances the sensitivity of the TL technique²¹³.

In the second part of this thesis a FIA-PPIA-TLS system for the detection of MC-LR was developed. The LOD of MC-LR obtained is equal to 0.64 $\mu\text{g/L}$ and therefore below the limit of 1 $\mu\text{g/L}$ defined by WHO for drinking water and already competitive with the MC-LR detection kits commercially available. Although this LOD is higher than the one obtained with other techniques, it has the advantage of being simple, to require low amounts of reagents and to have a higher throughput. Moreover, improvements are expected to be achieved by optimizing the experimental conditions and by downscaling the FIA-PPIA-TLS to a microfluidic system.

In the third part of this thesis a novel method for the removal of MC-LR based on the adsorption on chitosan-cellulose composite materials is presented. After the screening of different composite materials, it was demonstrated that MC-LR is efficiently adsorbed on chitosan-cellulose films. Chitosan was found to be the adsorbent component while cellulose plays a role in the strengthening of the film. Indeed, in the case of [CS-CEL] materials, increasing concentrations of chitosan correspond to higher efficiencies of adsorption. Cellulose, alone or in combination with materials other than chitosan, does not show to adsorb the toxin. Furthermore, it was demonstrated that MC-LR adsorption follows a pseudo-second order kinetics and that the [CS-CEL] films, under the given experimental conditions, can adsorb up to 96 mg of MC-LR per g of film. This value, as far as found in literature, is 4.8 times higher than the highest achieved adsorption with other adsorbents. These results are really promising, in fact the already highly adsorption efficiency of these composite materials could be further improved by modifying their geometry in order to increase the surface area for example preparing microparticles instead of films. Moreover, the [CS-CEL] composite materials have the great advantage of being completely biocompatible and biodegradable. Furthermore, their preparation method is completely green indeed, the ionic liquid used to prepare the films can be washed away and recovered by distillation. In addition, it was demonstrated by additional experiments performed after this work was concluded that the adsorbed toxin can be removed from the composite material that can be then recycled without losing its adsorbing property¹⁸⁶.

7- REFERENCES

1. Paerl, H. W. & Huisman, J. Climate change: a catalyst for global expansion of harmful cyanobacterial blooms. *Environ. Microbiol. Rep.* **1**, 27–37 (2009).
2. Vasconcelos, V. Eutrophication , toxic cyanobacteria and cyanotoxins : when ecosystems cry for help. *Limnetica* **25**, 425–432 (2006).
3. Doblin, M. a., Coyne, K. J., Rinta-Kanto, J. M., Wilhelm, S. W. & Dobbs, F. C. Dynamics and short-term survival of toxic cyanobacteria species in ballast water from NOBOB vessels transiting the Great Lakes—implications for HAB invasions. *Harmful Algae* **6**, 519–530 (2007).
4. De Figueiredo, D. R., Reboleira, A. S. S. P., Antunes, S. C., Abrantes, N., Azeiteiro, U., Gonçalves, F. & Pereira, M. J. The effect of environmental parameters and cyanobacterial blooms on phytoplankton dynamics of a Portuguese temperate Lake. *Hydrobiologia* **568**, 145–157 (2006).
5. Stewart, I., Seawright, A. a & Shaw, G. R. Cyanobacterial poisoning in livestock, wild mammals and birds--an overview. *Adv. Exp. Med. Biol.* **619**, 613–37 (2008).
6. Briand, J. B., Jaquet, S. J., Bernard, C. B. & Humbert, J.-F. Review article Health hazards for terrestrial vertebrates from toxic cyanobacteria in surface water ecosystems. *Vet. Res.* **34**, 361–377 (2003).
7. Mulvenna, V. *et al.* Health risk assessment for cyanobacterial toxins in seafood. *Int. J. Environ. Res. Public Health* **9**, 807–20 (2012).
8. Crush, J. R., Briggs, L. R., Sprosen, J. M. & Nichols, S. N. Effect of Irrigation with Lake Water Containing Microcystins on Microcystin Content and Growth of Ryegrass , Clover , Rape , and Lettuce. *Environ. Toxicol.* **23**, 246–252 (2008).
9. Saker, M. L. & Eaglesham, G. K. The accumulation of cylindrospermopsin from the cyanobacterium *Cylindrospermopsis raciborskii* in tissues of the Redclaw crayfish *Cherax quadricarinatus*. *Toxicon* **37**, 1065–77 (1999).
10. WHO. *Guidelines for drinking-water quality*, 4th ed., 178. World Health Organization, Geneva, Switzerland (2011).
11. Ince, P. G. & Codd, G. A. Return of the cycad hypothesis - does the amyotrophic lateral sclerosis/parkinsonism dementia complex (ALS/PDC) of Guam have new implications for global health? *Neuropathol. Appl. Neurobiol.* **31**, 345–53 (2005).

12. Pablo, J., Banack, S. A., Cox, P. A., Johnson, T. E., Papapetropoulos, S., Bradley, W. G., Buck, A. & Mash, D. C. Cyanobacterial neurotoxin BMAA in ALS and Alzheimer's disease. *Acta Neurol. Scand.* **120**, 216–25 (2009).
13. Li, G., Cai, F., Yan, W., Li, C. & Wang, J. A Proteomic Analysis of MCLR-Induced Neurotoxicity: Implications for Alzheimer's disease. 1–39 (2012).
14. Tokeshi, M., Uchida, M., Hibara, a, Sawada, T. & Kitamori, T. Determination of subyoctomole amounts of nonfluorescent molecules using a thermal lens microscope: subsingle-molecule determination. *Anal. Chem.* **73**, 2112–6 (2001).
15. Awramik, S. M. The oldest records of photosynthesis. *Photosynth. Res.* **33**, 75–89 (1992).
16. Michalak, A. M., Anderson, A. J., Beletesky, D., Boland, S., Bosch, N. S., Bridgeman, T. B., Chaffin, J. D., Cho, K., Confesor, R., Daloğlu, I., DePinto, J. V., Evans, M. A., Fannestier, G. L., He, L., Ho, J. C., Jenkins, L., Johengen, T. H., Kuok, C., LaPorte, E., Liu, X., McWilliams, M. R., Posselt, D. J., Richards, R. P., Scavia, D., Steiner, A. L., Verhamme, E., Wright, D. M. & Zagorski, M. A. Record-setting algal bloom in Lake Erie caused by agricultural and meteorological trends consistent with expected future conditions. *Proc. Natl. Acad. Sci. U. S. A.* **110**, 6448–52 (2013).
17. McGregor, G. B., Stewart, I., Sendall, B. C., Sadler, R., Reardon, K., Carter, S., Wruck, D. & Wickramasinghe, W. First report of a toxic *Nodularia spumigena* (Nostocales/ Cyanobacteria) bloom in sub-tropical Australia. I. Phycological and public health investigations. *Int. J. Environ. Res. Public Health* **9**, 2396–411 (2012).
18. Chislok, M. F., Doster, E., Zitomer, R. A. & Wilson, A. E. Eutrophication : Causes , Consequences , and Controls in Aquatic Ecosystems. *Nat. Educ. Knowl.* **4(4):10**, (2013).
19. Paerl, H. W. & Paul, V. J. Climate change: links to global expansion of harmful cyanobacteria. *Water Res.* **46**, 1349–63 (2012).
20. Naidenko, O. V., Cox, C. & Bruzelius, N. Troubled Waters. Farm Pollution Threatens Drinking Water. *Environ. Work. Gr.* <http://www.ewg.org/report/troubledwaters> **April**, (2012).
21. Valiela, I., Mcclelland, J., Hauxwell, J., Behr, P. J. & Hersh, D. Macroalgal blooms in shallow estuaries : Controls and ecophysiological and ecosystem consequences. *Limnol. Oceanogr.* **42**, 1105–1118 (1997).
22. Visser, P. M., Ibelings, B. W., Van der Veer, B., Koedood, J. & Mur, L. R. Artificial mixing prevents nuisance blooms of the cyanobacterium *Microcystis* in Lake Nieuwe Meer , the Netherlands. *Freshw. Biol.* **36**, 435–450 (1996).

23. Jöhnk, K. D., Huisman, J., Sharples, J., Sommeijer, B., Visser, P. M. & Stroom, J. M. Summer heatwaves promote blooms of harmful cyanobacteria. *Glob. Chang. Biol.* **14**, 495–512 (2008).
24. Bailey-Watts, A. E., Wise, E. J. & Kirika, A. An experiment in phytoplankton ecology and applied fishery management : effects of artificial aeration on troublesome algal blooms in a small eutrophic loch. *Aquac. Fish. Manag.* **18**, 259–275 (1987).
25. Lawson, R. & Anderson, M. a. Stratification and mixing in Lake Elsinore, California: an assessment of axial flow pumps for improving water quality in a shallow eutrophic lake. *Water Res.* **41**, 4457–67 (2007).
26. Fan, J., Hobson, P., Ho, L., Daly, R. & Brookes, J. The effects of various control and water treatment processes on the membrane integrity and toxin fate of cyanobacteria. *J. Hazard. Mater.* **264**, 313–22 (2014).
27. Kenefick, S. L., Hrudey, S. E., Peterson, H. G. & Prepas, E. E. Toxin Release from *Microcystis Aeruginosa* after Chemical Treatment. *Water Sci. Technol.* **27**, 433–440 (1993).
28. Touchette, B. W., Edwards, C. T. & Alexander, J. in *Cyanobacterial Algal Bloom. State Sci. Res. needs* (ed. Hudnell, K. H.) **619**, 314–315 (Springer, 2008).
29. Shapiro, J., Lamarra, V. & Lynch, M. *Biomanipulation: an ecosystem approach to lake restoration*. 85–96 (1975).
30. Ke, Z.-X., Xie, P. & Guo, L. G. Impacts of two biomanipulation fishes stocked in a large pen on the plankton abundance and water quality during a period of phytoplankton seasonal succession. *Ecol. Eng.* **35**, 1610–1618 (2009).
31. Meijer, M., Boois, I. De, Scheffer, M., Portielje, R. & Hoser, H. Biomanipulation in shallow lakes in The Netherlands : an evaluation of 18 case studies. *Hydrobiologia* **408/409**, 13–30 (1999).
32. Wilson, A. E. & Chislok, M. F. in *Cyanobacteria Ecol. Toxicol. Manag.* (ed. Da S. Ferrao-Filho, A.) 213–221 (Nova Science Publishers, 2013).
33. Jeppesen, E., Meerhoff, M., Davidson, T. A., Trolle, D., Søndergaard, M., Lauridsen, T. L., Beklioglu, M., Brucet, S., Volta, P., González-Bergonzoni, I. & Nielsen, A. Climate change impacts on lakes: an integrated ecological perspective based on a multi-faceted approach, with special focus on shallow lakes. *J. Limnol.* **73**, 84–107 (2014).
34. Søndergaard, M., Jensen, J. P. & Jeppesen, E. Role of sediment and internal loading of phosphorus in shallow lakes. *Hydrobiologia* **506-509**, 135–145 (2003).

35. Health Canada. hc-sc.gc.ca http://www.hc-sc.gc.ca/ewh-semt/pubs/water-eau/cyanobacterial_toxins/index-eng.php#s1 (last accessed November 6, 2014)
36. NHMRC & NRMCC. Fact Sheets - Microcystin in *Australian Drinking Water Guidelines Paper 6 National Water Quality Management Strategy*. National Health and Medical Research Council, National Resource Management Ministerial Council, Commonwealth of Australia, Canberra (2011). [nhmrc.gov.au/](http://www.nhmrc.gov.au/)
http://www.nhmrc.gov.au/_files_nhmrc/publications/attachments/eh34_adwg_11_06.pdf (last accessed November 6, 2014)
37. WHO. Algae and cyanobacteria in fresh water in *Guidelines for safe recreational water environments*, Vol 1: Coastal and fresh waters, 136-158. World Health Organization, Geneva, Switzerland (2003). [who.int/en/](http://www.who.int/en/)
<http://whqlibdoc.who.int/publications/2003/9241545801.pdf> (last accessed November 6, 2014)
38. NHMRC, Cyanobacteria and algae in freshwater in *Guidelines for Managing Risks in Recreational Water*, 91-117. National Health and Medical Research Council, Commonwealth of Australia, Canberra (2008). [nhmrc.gov.au](http://www.nhmrc.gov.au/)
https://www.nhmrc.gov.au/_files_nhmrc/publications/attachments/eh38.pdf (last accessed November 6, 2014)
39. Burch, M. D. Effective doses, guidelines & regulations. *Adv. Exp. Med. Biol.* **619**, 831–53 (2008).
40. Guidelines for Canadian Drinking Water Quality Summary Table. (2010).
41. Lucentini, L. & Ottaviani, M. *Cianobatteri in acque destinate al consumo umano. Stato delle conoscenze per la valutazione del rischio. Volume 1.* (2011).
42. *Drinking-water Standards for New Zealand 2005 (Revised 2008). 2005*, (Ministry of Health, Wellington, New Zealand, 2008).
43. Gregor, J., Marsálek, B. & Sípková, H. Detection and estimation of potentially toxic cyanobacteria in raw water at the drinking water treatment plant by in vivo fluorescence method. *Water Res.* **41**, 228–34 (2007).
44. Sobiechowska-Sasim, M., Stoń-Egiert, J. & Kosakowska, A. Quantitative analysis of extracted phycobilin pigments in cyanobacteria—an assessment of spectrophotometric and spectrofluorometric methods. *J. Appl. Phycol.* (2014). doi:10.1007/s10811-014-0244-3
45. Schmidt, W., Petzoldt, H., Bornmann, K., Imhof, L. & Moldaenke, C. Use of cyanopigment determination as an indicator of cyanotoxins in drinking water. *Water Sci. Technol.* **59**, 1531–40 (2009).

46. Bogorad, L. Phycobiliprotein: complementary chromatic adaptation. *Ann. Rev. Plant Physiol.* **26**, 369–401 (1975).
47. Vincent, W. F. Cyanobacterial Dominance in the Polar Regions in *The Ecology of Cyanobacteria Their Diversity in Time and Space*, eds. Whitton, B. A. & Potts, M., Chapter 12, 321–340. Kulwer Academy Publishers, Dordrecht, The Netherlands (2002).
48. Samsonoff, W. & MacColl, R. Biliproteins and phycobilisomes from cyanobacteria and red algae at the extremes of habitat. *Arch. Microbiol.* **176**, 400–405 (2001).
49. Jüttner, F. & Lüthi, H. Topology and enhanced toxicity of bound microcystins in *Microcystis* PCC 7806. *Toxicon* **51**, 388–97 (2008).
50. Sivonen, K. & Jones, G. Cyanobacterial Toxins in *Toxic Cyanobacteria in Water. A guideline to their public health consequences, monitoring and management*, eds. Chorus, I. & Bartram, J., chapter 3. WHO, Geneva, Switzerland (1999).
51. Van Apeldoorn, M. E., van Egmond, H. P., Speijers, G. J. a & Bakker, G. J. I. Toxins of cyanobacteria. *Mol. Nutr. Food Res.* **51**, 7–60 (2007).
52. Gupta, N., Pant, S. C., Vijayaraghavan, R. & Rao, P. V. L. Comparative toxicity evaluation of cyanobacterial cyclic peptide toxin microcystin variants (LR, RR, YR) in mice. *Toxicology* **188**, 285–296 (2003).
53. Giannuzzi, L., Sedan, D., Echenique, R. & Andrinolo, D. An acute case of intoxication with cyanobacteria and cyanotoxins in recreational water in Salto Grande Dam, Argentina. *Mar. Drugs* **9**, 2164–75 (2011).
54. Monks, N. R., Liu, S., Xu, Y., Yu, H., Bendelow, A. S, & Moscow, J. A. Potent cytotoxicity of the phosphatase inhibitor microcystin LR and microcystin analogues in OATP1B1- and OATP1B3-expressing HeLa cells. *Mol. Cancer Ther.* **6**, 587–98 (2007).
55. Yoshizawa, S., Matsushima, R., Watanabe, M. F., Harada, K., Ichiara, A., Carmichael, W. W. & Fujiki, H.. Inhibition of protein phosphatases by microcystin and nodularin associated with hepatotoxicity. *J. Cancer Res. Clin. Oncol.* **116**, 609–614 (1990).
56. Eriksson, J. E., Toivola, D., Meriluoto, J. A. O., Karaki, H., Han, Y. & Hartshorne, D.. Hepatocyte deformation induced by cyanobacterial toxins reflects inhibition of protein phosphatases. *Biochem. Biophys. Res. Commun.* **173**, 1347–53 (1990).
57. Nishiwaka-Matsushima, R., Nishiwaki, S., Ohta, T., Yoshizawa, S., Suganuma, M., Harada, K., Watanabe, MF. & Fujiki, H. Structure-Function Relationships of Microcystins, Liver Tumor Promoters, in Interaction with Protein Phosphatase. *Jpn. J. Cancer Res* **82**, 993–996 (1991).

58. Dawson, R. M. The toxicology of microcystins. *Toxicon* **36**, 953–962 (1998).
59. Pouria, S., de Andreade, A., Barbosa, J., Cavalcanti, R. L., Varreto, V. T. S., Ward, C. J., Preisen, W., Poon, G. K., Neild, G. H. & Codd, G. A. Early reports Fatal microcystin intoxication in haemodialysis unit in Caruaru , Brazil. *Lancet* **352**, 21–26 (1998).
60. WHO & IARC. Ingested Nitrate and Nitrite, and Cyanobacterial Peptide Toxins in *IARC Monographs on the Evaluation of Carcinogenic Risks to Humans*, **94**, 412. WHO, Geneva, Switzerland (2010). <http://monographs.iarc.fr/ENG/Monographs/vol94/mono94.pdf> (last accessed November 6, 2014)
61. Ueno, Y., Nagata, S., Tsutsumi, T., Hasegawa, A., Watanabe, M. F., Park, H. D., Chen, G. C., Chen, G and Yu, S. Z. Detection of microcystins, a blue-green algal hepatotoxin, in drinking water sampled in Haimen and Fusui, endemic areas of primary liver cancer in China, by highly sensitive immunoassay. *Carcinogenesis* **17**, 1317–21 (1996).
62. Ward, C. J., Beattie, K. A, Lee, E. Y. & Codd, G. A. Colorimetric protein phosphatase inhibition assay of laboratory strains and natural blooms of cyanobacteria: comparisons with high-performance liquid chromatographic analysis for microcystins. *FEMS Microbiol. Lett.* **153**, 465–73 (1997).
63. Spoof, L., Vesterkvist, P., Lindholm, T. & Meriluoto, J. Screening for cyanobacterial hepatotoxins, microcystins and nodularin in environmental water samples by reversed-phase liquid chromatography–electrospray ionisation mass spectrometry. *J. Chromatogr. A* **1020**, 105–119 (2003).
64. Lawton, L. A, Edwards, C. & Codd, G. A. Extraction and high-performance liquid chromatographic method for the determination of microcystins in raw and treated waters. *Analyst* **119**, 1525–30 (1994).
65. Yuan, M. & Carmichael, W. W. Detection and analysis of the cyanobacterial peptide hepatotoxins microcystin and nodularin using SELDI-TOF mass spectrometry. *Toxicon* **44**, 561–70 (2004).
66. Pelander, A., Ojanperä, I., Lahti, K., Niinivaara, K. & Vuori, E. Visual detection of cyanobacterial hepatotoxins by thin-layer chromatography and application to water analysis. *Water Res.* **34**, 2643–2652 (2000).
67. Wang, J., Pang, X., Ge, F. & Ma, Z. An ultra-performance liquid chromatography-tandem mass spectrometry method for determination of microcystins occurrence in surface water in Zhejiang Province, China. *Toxicon* **49**, 1120–8 (2007).
68. Yu, T., Xie, P., Dai, M. & Liang, G. Determinations of MC-LR and [Dha(7)] MC-LR concentrations and physicochemical properties by liquid chromatography-tandem mass spectrometry. *Bull. Environ. Contam. Toxicol.* **83**, 757–60 (2009).

69. Zhang, T., Kiyonami, R., Wang, L. & Jiang, G and Thermo Fisher Scientific. Identification and Quantitation of Microcystins by Targeted Full-Scan LC-MS / MS. [thermoscientific.com](http://www.thermoscientific.com/content/dam/tfs/ATG/CMD/CMD%20Documents/AN-569-Identification-Quantitation-Microcystins-Targeted-Full-Scan-AN63631-E.pdf)
<http://www.thermoscientific.com/content/dam/tfs/ATG/CMD/CMD%20Documents/AN-569-Identification-Quantitation-Microcystins-Targeted-Full-Scan-AN63631-E.pdf> (last accessed November 6, 2014)
70. Roy-Lachapelle, A., Fayad, P. B., Sinotte, M., Deblois, C. & Sauvé, S. Total microcystins analysis in water using laser diode thermal desorption-atmospheric pressure chemical ionization-tandem mass spectrometry. *Anal. Chim. Acta* **820**, 76–83 (2014).
71. Devlin, S., Meneely, J. P., Green, B., Campbell, K., Vasconcelos, V. & Elliott, C. T. Production of a broad specificity antibody for the development and validation of an optical SPR screening method for free and intracellular microcystins and nodularin in cyanobacteria cultures. *Talanta* **122**, 8–15 (2014).
72. Roegner, A. F., Schirmer, M. P., Puschner, B., Brena, B. & Gonzalez-Sapienza, G. Rapid quantitative analysis of microcystins in raw surface waters with MALDI MS utilizing easily synthesized internal standards. *Toxicon* **78**, 94–102 (2014).
73. Feng, L., Zhu, A., Wang, H. & Shi, H. A nanosensor based on quantum-dot haptens for rapid, on-site immunoassay of cyanotoxin in environmental water. *Biosens. Bioelectron.* **53**, 1–4 (2014).
74. Lei, L. M., Wu, Y. S., Gan, N. Q. & Song, L. R. An ELISA-like time-resolved fluorescence immunoassay for microcystin detection. *Clin. Chim. Acta.* **348**, 177–80 (2004).
75. Lebogang, L., Mattiasson, B. & Hedström, M. Capacitive sensing of microcystin variants of *Microcystis aeruginosa* using a gold immunoelectrode modified with antibodies, gold nanoparticles and polytyramine. *Microchim. Acta* **181**, 1009-1017 (2014).
76. Tian, J., Zhao, H., Quan, X., Zhang, Y., Yu, H & Chen, S. Fabrication of graphene quantum dots/silicon nanowires nanohybrids for photoelectrochemical detection of microcystin-LR. *Sensors Actuators B Chem.* **196**, 532–538 (2014).
77. Zhou, X., Liu, L., Xu, W, Son, B., Sheng, J., He, M. & Shi, H. An evanescent wave multi-channel immunosensor system for the highly sensitive detection of small analytes in water samples. *Sensors Actuators B Chem.* **198**, 150–156 (2014).
78. Fortin, N., Aranda-Rodriguez, R., Jing, H., Pick, F., Bird, D. & Greer, C. W. Detection of microcystin-producing cyanobacteria in Missisquoi Bay, Quebec, Canada, using quantitative PCR. *Appl. Environ. Microbiol.* **76**, 5105–12 (2010).

79. Metcalf, J. S., Bell, S. G. & Codd, G. A. Colorimetric Immuno-Protein Phosphatase Inhibition Assay for Specific Detection of Microcystins and Nodularins of Cyanobacteria Colorimetric Immuno-Protein Phosphatase Inhibition Assay for Specific Detection of Microcystins and Nodularins of Cyanobacteria. *Appl. Environ. Microbiol.* **67**, 904–909 (2001).
80. Franko, M. Thermal Lens Spectrometric Detection in Flow Injection Analysis and Separation Techniques. *Appl. Spectrosc. Rev.* **43**, 358–388 (2008).
81. Franko, M., Sarakha, M., Čibej, A., Boškin, A., Bavcon, M. & Trebse, P. Photodegradation of pesticides and application of bioanalytical methods for their detection. *Pure Appl. Chem.* **77**, (2005).
82. Passamonti, S., Terdoslavich, M., Margon, A., Cocolo, A., Medic, N., Micali, F., Decorti, G & M. Franko. Uptake of bilirubin into HepG2 cells assayed by thermal lens spectroscopy. Function of bilitranslocase. *FEBS J.* **272**, 5522–35 (2005).
83. Margon, A., Terdoslavich, M., Cocolo, A., Decorti, G., Passamonti, S. & Franko, M. Determination of bilirubin by thermal lens spectrometry and studies of its transport into hepatic cells. *J. Phys. IV* **125**, 717–720 (2014).
84. Martelanc, M., Žiberna, L., Passamonti, S. & Franko, M. Direct determination of free bilirubin in serum at sub-nanomolar levels. *Anal. Chim. Acta* **809**, 174–82 (2014).
85. Shokoufi, N., Atrabi, R. J. & Kargosha, K. Laser-induced thermal lens spectrometry after cloud point extraction for trace analysis of mercury in water and dry samples. *JAST* **5**:39 (2014). <http://www.jast-journal.com/content/pdf/s40543-014-0039-9.pdf>
86. Luterotti, S., Marković, K., Franko, M., Bicanic, D., Madžgalj, A. & KljaK, K. Comparison of spectrophotometric and HPLC methods for the determination of carotenoids in foods. *Food Chem.* **140**, 390–397 (2013).
87. Saavedra, R., Soto, C., Gómez, R. & Muñoz, A. Determination of lead(II) by thermal lens spectroscopy (TLS) using 2-(2'-thiazolylazo)-p-cresol (TAC) as chromophore reagent. *Microchem. J.* **110**, 308–313 (2013).
88. Herculano, L. S., Malacarne, L. C., Zanuto, V. S., Lukasiewicz, G. V., Capeloto, O. A. & Astrath, N. G. Investigation of the photobleaching process of eosin Y in aqueous solution by thermal lens spectroscopy. *J. Phys. Chem. B* **117**, 1932–7 (2013).
89. Cevdek, A. & Franko, M. Comparison of CIM discs and CPG glass as solid supports for bioanalytical columns used in allergen detection. *Anal. Bioanal. Chem.* **398**, 555–62 (2010).

90. Kobylinska, D. K., Bruzzoniti, M. C., Sarzanini, C. & Franko, M. Determination of colloid silver in drinking water by flow injection analysis with TLS spectrometric UV detection. *J. Phys. Conf. Ser.* **214**, 012119 (2010).
91. Bruzzoniti, M. C., Kobylinska, D. K., Franko, M. & Sarzanini, C. Flow injection method for the determination of silver concentration in drinking water for spacecrafts. *Anal. Chim. Acta* **665**, 69–73 (2010).
92. Boškin, A., Tran, C. D. & Franko, M. Oxidation of organophosphorus pesticides with chloroperoxidase enzyme in the presence of an ionic liquid as co-solvent. *Environ. Chem. Lett.* **7**, 267–270 (2008).
93. Lima, S. M., Figueiredo, M. S., Andrade, L. H., Caíres, A. R., Oliveira, S. L. & Aristone, F. Effects of residue and antioxidant on thermo-optical properties of biodiesel. *Appl. Opt.* **48**, 5728–32 (2009).
94. Jiménez-Pérez, J. L., Cruz-Orea, a., Lomelí Mejia, P. & Gutierrez-Fuentes, R. Monitoring the Thermal Parameters of Different Edible Oils by Using Thermal Lens Spectrometry. *Int. J. Thermophys.* **30**, 1396–1399 (2009).
95. Uchiyama, K., Hibara, A., Kimura, H., Sawada, T. & Kitamori, T. Thermal Lens Microscope. *Jpn. J. Appl. Phys.* **39**, 5316–5322 (2000).
96. Kitamori, T., Tokeshi, M., Hibara, A. & Sato, K. Thermal Lens Microscopy and Microchip Chemistry. *Anal. Chem.* 53A–60A (2004).
97. Nge, P. N., Rogers, C. I. & Woolley, A. T. Advances in Microfluidics Materials, Functions, Integration and applications. *Chem. Rev.* **113**, 2550–2583 (2014).
98. Rahmanian, O. & DeVoe, D. L. Pen microfluidics: rapid desktop manufacturing of sealed thermoplastic microchannels. *Lab Chip* **13**, 1102–8 (2013).
99. Martinez-QuiJada, J., Caverhill-Godkewitsch, S., Reynolds, M., Gutierrez-Rivera, L., Johnstone, R. W., Elliott, D. G., Samesoto, D. & Backhouse, C. J. Fabrication and characterization of aluminum thin film heaters and temperature sensors on a photopolymer for lab-on-chip systems. *Sensors Actuators A Phys.* **193**, 6–7 (2013).
100. Abgrall, P. & Gué, a-M. Lab-on-chip technologies: making a microfluidic network and coupling it into a complete microsystem—a review. *J. Micromechanics Microengineering* **17**, R15–R49 (2007).
101. Wan, C., Chen, C., Hwang, K., Lay, Y., Luo, L., Liu, P. & Fan, L. Development and automation of microelectromechanical systems-based biochip platform for protein assay. *Sensors Actuators B Chem.* **193**, 53–61 (2014).

102. Benz, C., Retzbach, H., Nagl, S. & Belder, D. Protein-protein interaction analysis in single microfluidic droplets using FRET and fluorescence lifetime detection. *Lab Chip* **13**, 2808–14 (2013).
103. Pereira, a T., Novo, P., Prazeres, D. M. F., Chu, V. & Conde, J. P. Heterogeneous immunoassays in microfluidic format using fluorescence detection with integrated amorphous silicon photodiodes. *Biomicrofluidics* **5**, 14102 (2011).
104. Ryu, G., Huang, J., Hofmann, O., Walshe, C. A., Sze, J. Y. Y., McClean, G. D., Mosley, A., Rattle, S. J., deMello, J. C., deMello, A. J. & Bradley, D. D. C. Highly sensitive fluorescence detection system for microfluidic lab-on-a-chip. *Lab Chip* **11**, 1664–70 (2011).
105. McIntosh, D., Zhou, Q., Lara, F. J., Landers, J. & Campbell, J. C. Fluorescence Detection 400–480 nm Using Microfluidic System Integrated GaP Photodiodes. *Adv. Optoelectron.* **2011**, 1–4 (2011).
106. Dongre, C., Dekker, R., Hoeckstra, H. J. W. M., Pollnau, M., Martinez-Vazquez, R., Osellame, R., Cerullo, G., Ramponi, R., van Weeghel, R., Besselink, G. A. J. & van den Vlekert, H. H. Fluorescence monitoring of microchip capillary electrophoresis separation with monolithically integrated waveguides. *Opt. Lett.* **33**, 2503–5 (2008).
107. Medina-Sánchez, M., Miserere, S., Morales-Narváez, E. & Merkoçi, A. On-chip magneto-immunoassay for Alzheimer's biomarker electrochemical detection by using quantum dots as labels. *Biosens. Bioelectron.* **54**, 279–84 (2014).
108. Noiphung, J., Sonjaroen, T., Dungcha, W., Henry, C. S., Chailapakul, O. & Laiwattanapaisal, W. Electrochemical detection of glucose from whole blood using paper-based microfluidic devices. *Anal. Chim. Acta* **788**, 39–45 (2013).
109. Frago, A., Latta, D., Laburia, N., Von Germar, F., Hansen-Hagge, T. E., Kemmer, W., Gärtner, C., Klemm, R., Drese, K. S. & O'Sullivan, C. K. Integrated microfluidic platform for the electrochemical detection of breast cancer markers in patient serum samples. *Lab Chip* **11**, 625–31 (2011).
110. Franciosi, L., Gonorukhina, F., Fusetti, F., Poolman, D., Ludewijk, M.E., Timens, W., ten Hacken, N. & Bischoff, R. Proteomic analysis of human epithelial lining fluid by microfluidics-based nanoLC-MS/MS: a feasibility study. *Electrophoresis* **34**, 2683–94 (2013).
111. Tsao, C. W., Tao, S., Chen, C. F., Liu, J. & DeVoe, D. L. Interfacing microfluidics to LDI-MS by automatic robotic spotting. *Microfluid. Nanofluidics* **8**, 777–787 (2010).
112. Sato, K., Tokeshi, M., Odake, T., Kimura, H., Ooi, T., Nakao, M. & Kitamori, T. Integration of an immunosorbent assay system: analysis of secretory human

- immunoglobulin A on polystyrene beads in a microchip. *Anal. Chem.* **72**, 1144–7 (2000).
113. Tsukahara, T., Hotokezaka, H., Harada, M., Kikutani, Y., Tokeshi, M. & Ikeda, Y. Highly efficient electrochemical valence control of uranium using microfluidic chip equipped with microelectrodes. *Microfluid. Nanofluidics* **14**, 989–994 (2012).
 114. Ohashi, T., Mawatari, K. & Kitamori, T. On-chip antibody immobilization for on-demand and rapid immunoassay on a microfluidic chip. *Biomicrofluidics* **4**, 32207 (2010).
 115. Islam, K. N., Ihara, M., Dong, J., Kasagi, N., Mori, T. & Ueda, H. Micro open-sandwich ELISA to rapidly evaluate thyroid hormone concentration from serum samples. *Bioanalysis* **2**, 1683–7 (2010).
 116. Kitagawa, F., Akimoto, Y. & Otsuka, K. Label-free detection of amino acids using gold nanoparticles in electrokinetic chromatography-thermal lens microscopy. *J. Chromatogr. A* **1216**, 2943–6 (2009).
 117. Smirnova, A., Shimura, K., Hibara, A., Proskurnin, M. a & Kitamori, T. Pesticide analysis by MEKC on a microchip with hydrodynamic injection from organic extract. *J. Sep. Sci.* **31**, 904–8 (2008).
 118. Henares, T. G. Funano, S., Terabe, S., Mizutani, F., Sekizawa, R. & Hisamoto, H. Multiple enzyme linked immunosorbent assay system on a capillary-assembled microchip integrating valving and immuno-reaction functions. *Anal. Chim. Acta* **589**, 173–9 (2007).
 119. Mawatari, K., Tokeshi, M. & Kitamori, T. Quantitative detection and fixation of single and multiple gold nanoparticles on a microfluidic chip by thermal lens microscope. *Anal. Sci.* **22**, 781–4 (2006).
 120. Tamaki, E., Sato, K., Tokeshi, M., Sato, K., Aihara, M. & Kitamori, T. Single-cell analysis by a scanning thermal lens microscope with a microchip: direct monitoring of cytochrome c distribution during apoptosis process. *Anal. Chem.* **74**, 1560–4 (2002).
 121. Minagawa, T., Tokeshi, M. & Kitamori, T. Integration of a wet analysis system on a glass chip : determination of Co (ii) as 2-nitroso-1-naphthol chelates by solvent extraction and thermal lens microscopy . *Lab Chip* **1**, 72–5 (2001).
 122. Maya, F., Estela, J. M. & Cerdà, V. Flow analysis techniques as effective tools for the improved environmental analysis of organic compounds expressed as total indices. *Talanta* **81**, 1–8 (2010).
 123. Brocenschi, R. F., Rocha-Filho, R. C., Duran, B. & Swain, G. M. The analysis of estrogenic compounds by flow injection analysis with amperometric detection using a boron-doped diamond electrode. *Talanta* **126**, 12–9 (2014).

124. Ma, L., Sun, Y., Kang, X. & Wan, Y. Development of nanobody-based flow injection chemiluminescence immunoassay for sensitive detection of human prealbumin. *Biosens. Bioelectron.* **61**, 165–71 (2014).
125. Mol, H. G. J. & van Dam, R. C. J. Rapid detection of pesticides not amenable to multi-residue methods by flow injection-tandem mass spectrometry. *Anal. Bioanal. Chem.* (2014). doi:10.1007/s00216-014-7644-8
126. Radulescu, M. C., Bucur, B., Bucur, M. P. & Radu, G. L. Bionzymatic biosensor for rapid detection of aspartame by flow injection analysis. *Sensors (Basel)*. **14**, 1028–38 (2014).
127. Thangaraj, R., Nellaiappan, S., Sudhakaran, R. & Kumar, A. S. A flow injection analysis coupled dual electrochemical detector for selective and simultaneous detection of guanine and adenine. *Electrochim. Acta* **123**, 485–493 (2014).
128. Kishikawa, N., Kondo, N., Amponsaa-Karikari, A., Kodamatani, H., Ohiyama, K., Nakashima, K., Yamazaki, S. & Kuroda, N. Rapid determination of isoamyl nitrite in pharmaceutical preparations by flow injection analysis with on-line UV irradiation and luminol chemiluminescence detection. *Luminescence* **29**, 8–12 (2014).
129. Liang, Q. & Li, Y. A rapid and accurate method for determining protein content in dairy products based on asynchronous-injection alternating merging zone flow-injection spectrophotometry. *Food Chem.* **141**, 2479–85 (2013).
130. Nanita, S. C. & Padivitage, N. L. T. Ammonium chloride salting out extraction/cleanup for trace-level quantitative analysis in food and biological matrices by flow injection tandem mass spectrometry. *Anal. Chim. Acta* **768**, 1–11 (2013).
131. Ramdzan, A. N., Mornane, P. J., McCullough, M. J., Mazurek, W. & Kolev, S. D. Determination of acetaldehyde in saliva by gas-diffusion flow injection analysis. *Anal. Chim. Acta* **786**, 70–7 (2013).
132. Vahl, K., Kahlert, K., von Mülhen, L., Albrecht, A., Meyer, G. & Behnert, J. Determination of the titratable acidity and the pH of wine based on potentiometric flow injection analysis. *Talanta* **111**, 134–9 (2013).
133. Madžgalj, A., Baesso, M. L. & Franko, M. Flow injection thermal lens spectrometric detection of hexavalent chromium. *Eur. Phys. J. Spec. Top.* **153**, 503–506 (2008).
134. Alvarez-Romero, G., Rojas-Hernández, A., Morales-Peréz, A. & Ramirez-Silva, M. T. Determination of β -D-glucose using flow injection analysis and composite-type amperometric tubular biosensors. *Biosens. Bioelectron.* **19**, 1057–1065 (2014).

135. Pei, Y., Eom, S., Park, D.-H., Jae-Min, O. & Choy, J.-H. Removal of Cyanobacteria *Anabaena flos- aquae* Through Montmorillonite Clays. *Energy Environ. Focus* **3**, 60–63(4) (2014).
136. Teixeira, M. R., Sousa, V. & Rosa, M. J. Investigating dissolved air flotation performance with cyanobacterial cells and filaments. *Water Res.* **44**, 3337–44 (2010).
137. Sorlini, S., Gialdini, F. & Collivignarelli, C. Removal of cyanobacterial cells and Microcystin-LR from drinking water using a hollow fiber microfiltration pilot plant. *Desalination* **309**, 106–112 (2013).
138. Campinas, M. & Rosa, M. J. Evaluation of cyanobacterial cells removal and lysis by ultrafiltration. *Sep. Purif. Technol.* **70**, 345–353 (2010).
139. Delgado, L. F., Charles, P., Glucina, K. & Morlay, C. The removal of endocrine disrupting compounds, pharmaceutically activated compounds and cyanobacterial toxins during drinking water preparation using activated carbon--a review. *Sci. Total Environ.* **435-436**, 509–25 (2012).
140. Song, W., de la Cruz, A. a, Rein, K. & O’Shea, K. E. Ultrasonically induced degradation of microcystin-LR and -RR: identification of products, effect of pH, formation and destruction of peroxides. *Environ. Sci. Technol.* **40**, 3941–6 (2006).
141. Yuan, B., Li, Y., Huang, X., Liu, H. & Qu, J. Fe(VI)-assisted photocatalytic degradating of microcystin-LR using titanium dioxide. *J. Photochem. Photobiol. A Chem.* **178**, 106–111 (2006).
142. Brooke, S., Newcombe, G., Nicholson, B. & Klass, G. Decrease in toxicity of microcystins LA and LR in drinking water by ozonation. *Toxicol.* **48**, 1054–9 (2006).
143. Daly, R. I., Ho, L. & Brookes, J. D. Effect of chlorination on *Microcystis aeruginosa* cell integrity and subsequent microcystin release and degradation. *Environ. Sci. Technol.* **41**, 4447–53 (2007).
144. Zhou, S., Shao, Y., Gao, N., Li, L., Deng, J., Zhu, M. & Zhu, S. Effect of chlorine dioxide on cyanobacterial cell integrity, toxin degradation and disinfection by-product formation. *Sci. Total Environ.* **482-483**, 208–13 (2014).
145. USEPA. *Cyanobacteria and Cyanotoxins : Information for Drinking Water Systems.* (2012).
146. Šimkovic, I. What could be greener than composites made from polysaccharides? *Carbohydr. Polym.* **74**, 759–762 (2008).

147. Das, H. & Singh, S. K. Useful byproducts from cellulosic wastes of agriculture and food industry--a critical appraisal. *Crit. Rev. Food Sci. Nutr.* **44**, 77–89 (2004).
148. Dautzenberg, H., Shuldt, U., Grasnack, G., Karle, P., Müller, P., Löhr, M., Pelegrin, M., Piechaczyk, M., Rombs, K. V., Günzburg, W. H., Salmons, B. & Saller, R. M. Development of Cellulose Sulfate-based Polyelectrolyte Complex Microcapsules for Medical Applications. *Ann. N. Y. Acad. Sci.* **875**, 46–63 (1999).
149. Czaja, W., Krystynowicz, A., Bielecki, S. & Brown, R. M. Microbial cellulose - the natural power to heal wounds. *Biomaterials* **27**, 145–51 (2006).
150. Czaja, W. K., Young, D. J., Kawecki, M. & Brown, R. M. The future prospects of microbial cellulose in biomedical applications. *Biomacromolecules* **8**, 1–12 (2007).
151. Gericke, M., Trygg, J. & Fardim, P. Functional cellulose beads: preparation, characterization, and applications. *Chem. Rev.* **113**, 4812–36 (2013).
152. Wyman, C. E., Decker, S. R., Himmel, M. E., Brady, J. W. & Skopec, C. E. in *Polysaccharides Struct. Divers. Funct. Versatility, Second Ed.* (ed. Dumitriu, S.) **27**, (CRC Press 2004, 2004).
153. Rosenau, T., Potthast, A., Sixta, H. & Kosma, P. The chemistry of side reactions and byproduct formation in the system NMMO/cellulose (Lyocell process). *Prog. Polym. Sci.* **26**, 1763–1837 (2001).
154. Rabea, E. I., Badawy, M. E.-T., Stevens, C. V, Smagghe, G. & Steurbaut, W. Chitosan as antimicrobial agent: applications and mode of action. *Biomacromolecules* **4**, 1457–65 (2003).
155. Dai, T., Tanaka, M., Huang, Y.-Y. & Hamblin, M. R. Chitosan preparations for wounds and burns: antimicrobial and wound-healing effects. *Expert Rev. Anti. Infect. Ther.* **9**, 857–79 (2011).
156. Araki, J., Yamanaka, Y. & Ohkawa, K. Chitin-chitosan nanocomposite gels: reinforcement of chitosan hydrogels with rod-like chitin nanowhiskers. *Polym. J.* **44**, 713–717 (2012).
157. Zhao, Q. S., Ji, Q. X., Cheng, X. J., Sun, G. Z., Ran, C., Zhao, B. & Chen, X. G. Preparation of alginate coated chitosan hydrogel beads by thermosensitive internal gelation technique. *J. Sol-Gel Sci. Technol.* **54**, 232–237 (2010).
158. Hilmi, A. B. M., Halim, A. S., Hassan, A., Lim, C. K., Noorsal, K. & Zainol, I. In vitro characterization of a chitosan skin regenerating template as a scaffold for cells cultivation. *Springerplus* **2**, 79 (2013).
159. González-Campos, J. B., Mota-Morales, J. D., Kumar, S., Zaraté-Triviño, D., Hernández-Iturriaga, M., Prokhorov, Y., Lepe, M. V., Garcia-Carvajal, Z. Y.,

- Sanchez, I. C. & Luna-Bárceñas, G. New insights into the bactericidal activity of chitosan-Ag bionanocomposite: The role of the electrical conductivity. *Colloids Surf. B. Biointerfaces* **111C**, 741–746 (2013).
160. Tikhonov, V. E., Stepnova, E. A., Babak, V. G., Yamskov, I. A., Palma.Guerrero, J., Jansson, H. B., Lopez-Llorca, L. V., Salinas, J., Gerasimenko, D. V., Avdienko, I. D. & Varlamov, V.P. Bactericidal and antifungal activities of a low molecular weight chitosan and its N-(2-(3-(dodec-2-enyl)succinoyl)-derivatives. *Carbohydr. Polym.* **64**, 66–72 (2006).
 161. Chou, C. P., Wang, Y. C., Chang, S. J., Liu, P. H. & Kuo, S. M. Evaluation of the Effects of Chitosan Hemostasis Dressings on Hemorrhage Caused by Breast Biopsy. *Breast Care (Basel)*. **7**, 220–224 (2012).
 162. Pozza, M. & Millner, R. W. J. Celox (chitosan) for haemostasis in massive traumatic bleeding: experience in Afghanistan. *Eur. J. Emerg. Med.* **18**, 31–3 (2011).
 163. Elsayed, A., Al-Remawi, M., Qinna, N., Farouk, A., Al-Sou'od, K. A., & Badwan, A. A. Chitosan-sodium lauryl sulfate nanoparticles as a carrier system for the in vivo delivery of oral insulin. *AAPS PharmSciTech* **12**, 958–64 (2011).
 164. Hamman, J. H. Chitosan based polyelectrolyte complexes as potential carrier materials in drug delivery systems. *Mar. Drugs* **8**, 1305–22 (2010).
 165. Ren, X., Yan, T., Zhang, S., Zhang, X., Gao, P., Wu, D., Du, B. & Wei, Q. Ultrasensitive dual amplification sandwich immunosensor for breast cancer susceptibility gene based on sheet materials. *Analyst* **139**, 3061–3068 (2014).
 166. Lee, S., Khang, S. W., Ryu, J. H., Na, J. H., Lee, D. E., Han, S. J., Kang, C. M., Choe, Y. S., Lee, K. C., Leary, J. F., Choi, K., Lee, K. H. & Kim, K. Tumor-homing glycol chitosan-based optical/PET dual imaging nanoprobe for cancer diagnosis. *Bioconjug. Chem.* **25**, 601–10 (2014).
 167. Chen, Y. L., Wang, C. Y., Yang, F. Y., Wang, B. S., Chen, J. Y., Lin, L. T., Leu, J. D., Chiu, S. J., Chen, F. D., Lee, Y. J. & Chen, W. R. Synergistic effects of glycosylated chitosan with high-intensity focused ultrasound on suppression of metastases in a syngeneic breast tumor model. *Cell Death Dis.* **5**, e1178 (2014).
 168. Xu, C., Lei, C., Meng, L., Wang, C. & Song, Y. Chitosan as a barrier membrane material in periodontal tissue regeneration. *J. Biomed. Mater. Res. B. Appl. Biomater.* **100**, 1435–43 (2012).
 169. Abarrategi, A., Lopiz-Morales, Y., Ramos, V., Civantos, A., Lopez-Duran, L., Marco, F., Lopez-Lacomba, J., L. Chitosan scaffolds for osteochondral tissue regeneration. *J. Biomed. Mater. Res. A* **95**, 1132–41 (2010).

170. El Hadrami, A., Adam, L. R., El Hadrami, I. & Daayf, F. Chitosan in plant protection. *Mar. Drugs* **8**, 968–87 (2010).
171. Coimbra Rodrigues da Silva, M. A., Cordero.Nunes, C. S., Oliveira-Marucato, E. S., Viera da Cunha, A. M. M., Barroso, S. A. & Lopes da Silva, J. A. Winemaking method without the admixture of sulphur dioxide, using chitosan-based films. (2013).
172. Jianglian, D. & Shaoying, Z. Application of Chitosan Based Coating in Fruit and Vegetable Preservation: A Review. *J. Food Process. Technol.* **04**, 5–8 (2013).
173. Mohanasrinivasan, V., Mishra, M., Paliwal, J. S., Singh, S. K., Selvarajan, E., Suganthi, V. & Devi, C. S. Studies on heavy metal removal efficiency and antibacterial activity of chitosan prepared from shrimp shell waste. *3 Biotech* **4**, 167–175 (2013).
174. Mahmoodi, N. M., Salehi, R., Arami, M. & Bahrami, H. Dye removal from colored textile wastewater using chitosan in binary systems. *Desalination* **267**, 64–72 (2011).
175. Crini, G. & Badot, P. M. Application of chitosan, a natural aminopolysaccharide, for dye removal from aqueous solutions by adsorption processes using batch studies: A review of recent literature. *Prog. Polym. Sci.* **33**, 399–447 (2008).
176. Chen, D., Hu, B. & Huang, C. Chitosan modified ordered mesoporous silica as micro-column packing materials for on-line flow injection-inductively coupled plasma optical emission spectrometry determination of trace heavy metals in environmental water samples. *Talanta* **78**, 491–7 (2009).
177. W U, Q. L., Chen, Z. D., X U, W. & Shao, R. Study of Chitosan Modified Attapulgit to the Flocculation and Harvest of Chlorella. *Polym. Bulletin* **1**, (2013).
178. Zou, H., Pan, G., Chen, H. & Yuan, X. Removal of cyanobacterial blooms in Taihu Lake using local soils II. Effective removal of *Mycrocystis aeruginosa* using local soils and sediments modified by chitosan. *Environ. Pollut.* **141**, 201–5 (2006).
179. Dutta, P. K., Dutta, J. & Tripathi, V. S. Chitin and chitosan : Chemistry , properties and applications. *J. Sci. Ind. Res.* **63**, 20–31 (2004).
180. Pillai, C. K. S., Paul, W. & Sharma, C. P. Chitin and chitosan polymers: Chemistry, solubility and fiber formation. *Prog. Polym. Sci.* **34**, 641–678 (2009).
181. Zhang, S., Sun, N., He, X., Lu, X. & Zhang, X. Physical Properties of Ionic Liquids: Database and Evaluation. *J. Phys. Chem. Ref. Data* **35**, 1475 (2006).

182. Xie, H., Zhang, S. & Li, S. Chitin and chitosan dissolved in ionic liquids as reversible sorbents of CO₂. *Green Chem.* **8**, 630 (2006).
183. Johnson, K. E. What' s an Ionic Liquid ? “ T. *Interface* 38–41 (2007).
184. Earle, M. J. & Seddon, K. R. Ionic liquids. Green solvents for the future. *Pure Appl. Chem.* **72**, 1391–1398 (2000).
185. Dyson, P. J. & Geldbach, T. J. Applications of Ionic Liquids in Synthesis and Catalysis. 50–53
186. Tran, C. D., Duri, S., Delneri, A. & Franko, M. Chitosan-cellulose composite materials: Preparation, Characterization and application for removal of microcystin. *J. Hazard. Mater.* **252-253**, 355–366 (2013).
187. Dean, R. B. & Dixon, W.J. Simplified statistics for small numbers of observations. *Anal. Chem.* **23**:4 (1951).
188. ICH. International Conference on Harmonisation of Technical Requirements for Registration of Pharmaceuticals for Human Use, ICH Harmonised Tripartite Guideline, Validation of Analytical Procedures: Text and Methodology Q2(R1). [ich.org](http://www.ich.org)
http://www.ich.org/fileadmin/Public_Web_Site/ICH_Products/Guidelines/Quality/Q2_R1/Step4/Q2_R1__Guideline.pdf (last accessed November 6, 2014)
189. Miyaishi, K., Imasaka, T. & Ishidashi, N. Thermal lensing spectrophotometric analysis with ion-pair solvent extraction. *Anal. Chim. Acta* **124**, 381–389 (1981).
190. Georges, J. Advantages and limitations of thermal lens spectrometry over conventional spectrophotometry for absorbance measurements. *Talanta* **48**, 501–9 (1999).
191. Senthilkumar, N., Kurinijmalar, C, Thangam, R, Suresh, V., Kavitha, G., Gunasekaran, P. & RengasamY, R. Further studies and biological activities of macromolecular protein R-Phycoerythrin from *Portieria hornemannii*. *Int. J. Biol. Macromol.* **62**, 107–16 (2013).
192. Miroliaei, M. & Nemat-Gorgani, M. Effect of organic solvents on stability and activity of two related alcohol dehydrogenases: a comparative study. *Int. J. Biochem. Cell Biol.* **34**, 169–75 (2002).
193. Hoogenboezem, W., Wagenvoort, A. J. & Blaauboer, K. The occurrence of toxic cyanobacteria in some Dutch surface waters used for the production of drinking water. *Rhine Water Work.* Nieuwegein, Riwa (2004)
194. Rodriguez, H., Rivas, J., Guerrero, M. G. & Losada, M. Nitrogen-fixing cyanobacterium with a high phycoerythrin content. *Appl. Environ. Microbiol.* **55**, 758–60 (1989).

195. Mahlmann, D. M., Jahnke, J. & Loosen, P. Rapid determination of the dry weight of single, living cyanobacterial cells using the Mach-Zehnder double-beam interference microscope. *Eur. J. Phycol.* **43**, 355–364 (2008).
196. Tubaro, A., Florio, C., Luxich, E., Sosa, S., Della Loggia, R. & T. Yasumoto. A protein phosphatase 2A inhibition assay for a fast and sensitive assessment of okadaic acid contamination in mussels. *Toxicon* **34**, 743–752 (1996).
197. Ikehara, T., Imamura, S., Oshiro, N., Ikehara, S., Shinjo, F. & Yasumoto, T. A protein phosphatase 2A (PP2A) inhibition assay using a recombinant enzyme for rapid detection of microcystins. *Toxicon* **51**, 1368–73 (2008).
198. Bouaïcha, N., Maatouk, I., Vincent, G. & Levi, Y. A colorimetric and fluorometric microplate assay for the detection of microcystin-LR in drinking water without preconcentration. *Food Chem. Toxicol.* **40**, 1677–83 (2002).
199. Sassolas, A., Catanante, G., Fournier, D. & Marty, J. Development of a colorimetric inhibition assay for microcystin-LR detection : comparison of the sensitivity of different protein phosphatases. *Talanta* **85**, 2498–503
200. Aguete, E. C., Gago-Martinez, A., Leão, J. M., Rodriguez-Vasquez, J. A., Menard, C. & Lawrence, J. F. HPLC and HPCE analysis of microcystins RR, LR and YR present in cyanobacteria and water by using immunoaffinity extraction. *Talanta* **59**, 697–705 (2003).
201. Zhang, H., Huang, Q., Ke, Z., Yang, L., Wang, X. & Yu, Z. Degradation of microcystin-LR in water by glow discharge plasma oxidation at the gas-solution interface and its safety evaluation. *Water Res.* **46**, 6554–62 (2012).
202. Liu, G., Qian, Y., Dai, S. & Feng, N. Adsorption of Microcystin LR and LW on Suspended Particulate Matter (SPM) at Different pH. *Water. Air. Soil Pollut.* **192**, 67–76 (2008).
203. Kumar, K. V. & Sivanesan, S. Pseudo second order kinetics and pseudo isotherms for malachite green onto activated carbon: comparison of linear and non-linear regression methods. *J. Hazard. Mater.* **136**, 721–6 (2006).
204. Gao, Y., Gao, N. Y., Deng, Y., Gu, J. S., Shen, Y. C. & Wang, S. X., Adsorption of Microcystin-LR from Water with Iron Oxide Nanoparticles. *Water Environ. Res.* **84**, 562–568 (2012).
205. Chen, H., Lu, X., Deng, C. & Yan, X. Facile Synthesis of Uniform Microspheres Composed of a Magnetite Core and Copper Silicate Nanotube Shell for Removal of Microcystins in Water. *J. Phys. Chem. C* **113**, 21068–21073 (2009).
206. Newcombe, G. & Nicholson, B. Water treatment options for dissolved cyanotoxins. *J. Water Suppl. Res. Technol.* **534**, 227–239 (2004).

207. Zhang, H., Zhu, G., Jia, X., Ding, Y. & Zhang, M. Removal of microcystin-LR from drinking water using bamboo-based charcoal adsorbent modified with chitosan. *J. Environ. Sci.* **23**, 1983–1988 (2011).
208. Morris, R. J., Williams, D. E., Luu, H. A., Holmes, C. F. B., Anderson, R. J. & Calvert, S. E. The adsorption of microcystin-LR by natural clay particles. *Toxicon* **38**, 303–8 (2000).
209. Yan, H., Gong, A., He, H., Zhou, J., Wei, Y. & Lv, L. Adsorption of microcystins by carbon nanotubes. *Chemosphere* **62**, 142–8 (2006).
210. Lee, J. & Walker, H. W. Effect of process variables and natural organic matter on removal of microcystin-LR by PAC-UF. *Environ. Sci. Technol.* **40**, 7336–42 (2006).
211. Pyo, D. & Moon, D. Adsorption of Microcystin LR by Activated Carbon Fibers. *Bull. Korean Che. Soc.* **26**, 2089–2092 (2005).
212. Deng, Y., Qi, D., Deng, C., Zhang, X. & Zhao, D. Superparamagnetic high-magnetization microspheres with an Fe₃O₄@SiO₂ core and perpendicularly aligned mesoporous SiO₂ shell for removal of microcystins. *J. Am. Chem. Soc.* **130**, 28–9 (2008).
213. Phillips, C. M., Crouch, S. R. & Leroi, G. E. Matrix Effects in Thermal Lensing Spectrometry : Determination of Phosphate in Saline Solutions. **1964**, 1710–1714 (1986).